# ANALYSIS AND CLASSIFICATION OF RENAL ULTRASOUND IMAGES

A Dissertation submitted in fulfillment of the requirements for the Degree of

**MASTER OF ENGINEERING**

*in*

**Electronic Instrumentation & Control Engineering**


*Submitted by*

Komal
801451014

*Under the Guidance of*

Dr. Jitendra Virmani
Asst. Professor, EIED


**2016**


**Electrical and Instrumentation Engineering Department**
**Thapar University, Patiala**
***(Declared as Deemed-to-be-University u/s 3 of the UGC Act., 1956)***
**Post Bag No. 32, Patiala – 147004**
**Punjab (India)**

## DECLARATION

I hereby certify that the work which is presented in a dissertation entitled, "Analysis and Classification of Renal Ultrasound Images", in partial fulfillment of the requirements for the award of the degree of Master of Engineering in Electronic Instrumentation & Control, submitted to Electrical & Instrumentation Engineering Department of Thapar University, Patiala, is an authentic record of my work carried under the supervision of Dr. Jitendra Virmani. It refers other researcher's work which are duly listed in the reference section. The matter contained in this dissertation has not been submitted, neither in part nor in full to any other degree to any other university or institute except as reported in the text and references.

Place: TU, Patiala
Date: 30-7-2016

**(Komal)**
Roll No.: 801451014

It is certified that the above statement made by the student is correct to the best of my knowledge and belief.

Date: 30-7-2016

**(Dr. Jitendra Virmani)**
Asst. Prof., EIED
Electrical & Instrumentation Engineering Department
Thapar University, Patiala

***Countersigned by:***

**(Dr. Ravinder Agarwal)**
Professor and Head
Electrical & Instrumentation Engineering Department
Thapar University, Patiala

**(Dr. SS Bhatia)**
Dean (Academic Affairs)
Thapar University, Patiala

# Acknowledgement

I would like to express my heartfelt gratitude and respect to my supervisor Dr. Jitendra Virmani, Assistant Professor, Electrical and Instrumentation Engineering Department, Thapar University-Patiala for his able guidance, constructive criticism, indispensable support and constant encouragement. I am indebted to him for his patience in correcting the thesis as well as the manuscripts from every aspect of qualitative and effective presentation, which lead to the successful completion of this research work.

I owe my deepest thanks to M. B. Subramanya, research scholar, Biomedical Instrumentation Laboratory, Indian Institute of Technology Roorkee, Uttarakhand for providing the labelled renal ultrasound images.

I am obliged to Dr. Manju Saini (Department of Radiology, Himalayan Institute of Medical Sciences, HIHT University), Dr. Shruti Thakur (Department of Radiology, IGMC, Shimla) and Dr. Anmol Bhatia (Assistant Professor, Department of gastroenterology, PGIMER, Chandigarh) for helping us in understanding the sonographic appearance of renal ultrasound images.

I would like to thank Indrajeet Kumar and Kriti (research scholars working under Dr. Jitendra Virmani) who are part of our research group and have graciously helped me with their valuable suggestions.

I would like to extend my gratitude to the anonymous reviewers who helped me to improve the quality of my publications through their invaluable advices and constructive suggestions.

Last but not the least, I am is also thankful to Thapar University - Patiala, Punjab, for providing constant patronage and support.

I dedicate my dissertation work to my beloved parents Sh. Ashok Kumar and Smt. Sangeeta Sharma for they have always been the pillar of strength and support for me, and my sweet little brother Akshay whom I missed the most.

**(Komal, 801451014)**

# List of Abbreviations

| | |
|---|---|
| AML | Angiomyolipoma |
| ANFC | Adaptive neuro-fuzzy classifier |
| ANN | Artificial neural network |
| ARCKi | Generation of association rules with high confidence for kidney images |
| ASM | Angular second moment |
| B-mode | Brightness mode |
| CAC | Computer aided classification |
| CM | Confusion matrix |
| CT | Computerized tomography |
| DEFS | Differential evolution feature selection |
| DWT | Discrete wavelet transform |
| FFT | Fast Fourier transform |
| FFV | First order feature vector |
| FOS | First order statistics |
| FPGA | Field programmable gate array |
| FRL | Focal renal lesion |
| FV | Feature vector |
| GaAFV | Gabor absolute feature vector |
| GaCFV | Gabor combined feature vector |
| GaFV | Gabor feature vector |
| GAFV | GLCM additive feature vector |
| GaRFV | Gabor ratio feature vector |
| GA-SVM | Genetic algorithm support vector machine |

| | |
|---|---|
| GCFV | GLCM combined feature vector |
| GLCM | Gray-level co-occurrence matrix |
| GLRL | Grey-level run length |
| GMAFV | GLCM mean absolute feature vector |
| GMFV | GLCM mean feature vector |
| GMRFV | GLCM mean ratio feature vector |
| GRaFV | GLCM ratio feature vector |
| GRAFV | GLCM range absolute feature vector |
| GRCFV | GLCM range combined feature vector |
| GRFV | GLCM range feature vector |
| GRRFV | GLCM range ratio feature vector |
| GWT | Gabor wavelet transform |
| HFNN | Hybrid fuzzy-neural network |
| HFV | Higher order feature vector |
| HIHT | Himalayan institute hospital trust |
| HOS | Higher order statistics |
| ICA | Individual classification accuracy |
| IDM | Inverse difference moment |
| *k*NN | K-nearest neighbor |
| LMAFV3 | Laws' mask absolute feature vector computed using 1D filter of length 3 |
| LMAFV5 | Laws' mask absolute feature vector computed using 1D filter of length 5 |
| LMAFV7 | Laws' mask absolute feature vector computed using 1D filter of length 7 |
| LMAFV9 | Laws' mask absolute feature vector computed using 1D filter of length 9 |
| LMCFV7 | Laws' mask combined feature vector computed using 1D filter of length 7 |
| LMFV3 | Laws' mask feature vector computed using 1D filter of length 3 |

| | |
|---|---|
| LMFV5 | Laws' mask feature vector computed using 1D filter of length 5 |
| LMFV7 | Laws' mask feature vector computed using 1D filter of length 7 |
| LMFV9 | Laws' mask feature vector computed using 1D filter of length 9 |
| LMRFV3 | Laws' mask ratio feature vector computed using 1D filter of length 3 |
| LMRFV5 | Laws' mask ratio feature vector computed using 1D filter of length 5 |
| LMRFV7 | Laws' mask ratio feature vector computed using 1D filter of length 7 |
| LMRFV9 | Laws' mask ratio feature vector computed using 1D filter of length 9 |
| MATLAB | Matrix laboratory |
| MBPN | Multi-layer back propagation network |
| MI | Moment invariant |
| MLP | Multi-layer perceptron |
| MRD | Medical renal disease |
| MRI | Magnetic resonance imaging |
| MSDF | Multi-scale differential features |
| NOR | Normal |
| OCA | Overall classification accuracy |
| PCA | Principal component analysis |
| PreSAGe | Pre-processing solution for association rule generation |
| PROI | Parenchymal region of interest |
| RBAs | ROI based approaches |
| RCC | Renal cell carcinoma |
| RLM | Run length matrix |
| ROI | Region of interest |
| SBAs | Segmentation based approaches |
| SGLDM | Spacial gray-level dependence matrix |

| | |
|---|---|
| SROI | Sinus region of interest |
| SVM | Support vector machine |
| TEMs | Texture energy images |
| TI | Texture image |
| TRs | Rotationally invariant texture energy images |
| US | Ultrasound |

# List of Figures

# List of Tables

# Abstract

The present research work has been carried out with an aim to enhance the diagnostic potential of conventional B-Mode ultrasound (US) imaging modality for diagnosis of renal diseases. Accordingly, an efficient design of an interactive system for diagnosis of renal diseases using B-Mode renal US images is proposed in the present study. The research objectives for the present study were formulated keeping in view the needs of the radiologists, based on the practical difficulties faced by them in routine clinical practice.

The study has been conducted on a comprehensive image database of 35 B-Mode renal US images with representative cases from each image class i.e. normal, MRD and cyst. These images have been originally acquired from Department of Radio-diagnosis, Himalayan Institute of Hospital and Trust (HIHT), Dehradun, India, during the period from January 2012 to May 2013. The image database comprises of 11 Normal, 8 MRD and 16 Cyst images.

The proposed interactive system for diagnosis of renal diseases using B-Mode US images consists of four modules as shown in Fig. 1. The brief description of these modules is given below.

*Module 1: SVM based CAC system for diagnosis of renal diseases.*

A CAC system is designed to assist or provide second opinion to the radiologist for classification of renal US images into normal, MRD and cyst image class. It classifies renal US images into three classes namely, normal, MRD and cyst. The design of this module considers the features from renal parenchymal ROIs for normal and MRD classes as the nature of echogenicity of parenchyma region changes (becomes hyper-echoic as compared to normal) in case of MRD renal US image. For cyst class, ROIs are extracted from region inside lesion. These regions inside renal cyst exhibit anechoic appearance. This is equivalent to radiologists looking at the renal parenchyma region of normal and MRD image and region inside lesion for cyst US image class. The CAC system employs SVM (support vector machine) classifier for the classification task.

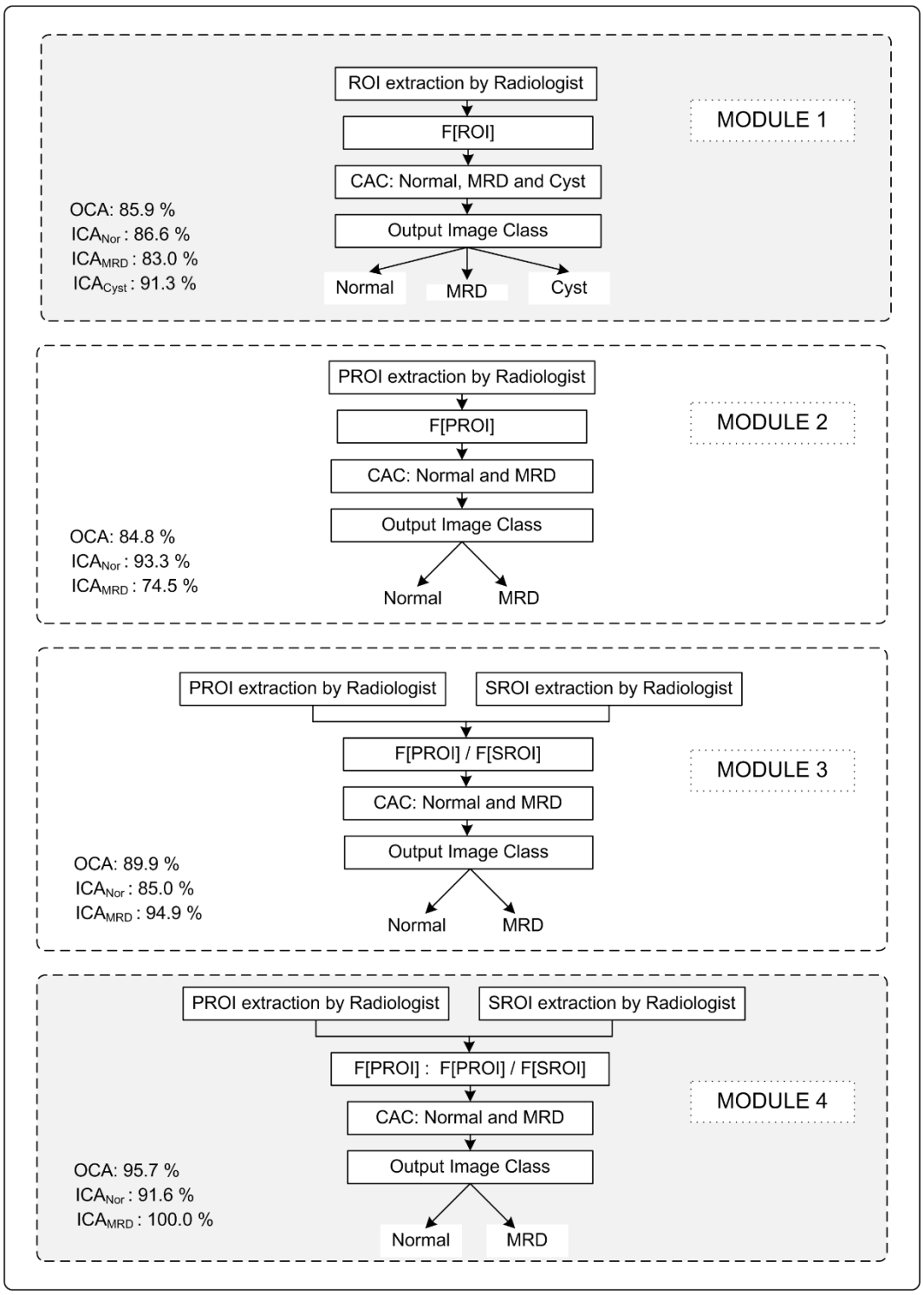


**Fig. 1** Block diagram of the proposed interactive system for diagnosis of renal diseases.
**Note:** PROIs: Parenchymal regions of interest; SROIs: Sinus regions of interest, CAC: Computer aided classification.

*Module 2: ANFC based CAC system for diagnosis of MRD using absolute texture features.*

The *Module 2* classifies renal US images into two classes namely, normal and MRD. The design of this module considers the absolute features from renal parenchyma PROIs for normal and MRD classification as the nature of echogenicity of parenchyma region changes (becomes hyper-echoic as compared to normal) in case of MRD renal US image. This is equivalent to radiologists looking at the renal parenchyma region of normal and MRD image. The proposed CAC System utilizes ANFC for the classification task. Accordingly, *Module 2* incorporates an ANFC based CAC system for diagnosis of Medical Renal Disease using absolute texture features.

*Module 3: ANFC based CAC system for diagnosis of MRD using ratio texture features.*

The *Module 3* classifies renal US images into two classes namely, normal and MRD. The design of this module utilizes echogenicity of renal parenchyma along with the echogenicity of renal sinus region. The renal sinus appears hyper-echoic with respect to renal parenchyma region in normal renal US image. But in MRD, the echogenicity of renal parenchyma increases and it becomes iso-echoic with respect to renal sinus. So, the classification is made on basis of the ratio texture features obtained from renal parenchyma PROIs and renal sinus SROIs, where renal sinus echogenicity remains same for normal and MRD image class, and the difference lies only in the echogenicity of renal parenchyma region. This is equivalent to radiologists looking at the renal parenchyma and renal sinus region of normal and MRD image. The proposed CAC System utilizes ANFC for the classification task. This classification is also compared with the classification performance by considering the PROIs from renal parenchyma region only (*Module 2*). Accordingly, *Module 3* incorporates an ANFC based CAC system for diagnosis of Medical Renal Disease using texture ratio features.

*Module 4: ANFC based CAC system for diagnosis of MRD using combined texture features.*

The *Module 4* classifies renal US images into two classes namely, normal and MRD. The design of this module aims to classify normal and MRD renal US images using the combination of the approaches used in above two modules. Here the texture ratio features obtained from PROIs and SROIs are considered along with the individual contribution of absolute features obtained from PROIs only, for differential diagnosis between normal and MRD renal US image class. This is equivalent to radiologists looking at the renal parenchyma

and renal sinus region of normal and MRD image. The proposed CAC system utilizes ANFC for the classification task. Accordingly, *Module 4* incorporates an ANFC based CAC system for diagnosis of Medical Renal Disease using combined texture features.

A brief comparison of classification performance obtained by *Module 1*, *Module 2*, *Module 3* and *Module 4* designs implemented for the proposed interactive system for diagnosis of renal diseases using B-Mode US images is depicted in Table 1.

**Table 1** Classification performance of module 1, 2, 3 and 4

| *CAC System Designs* | *Classes* | *OCA* | *ICA* |
|---|---|---|---|
| *Module 1*: SVM based CAC system for diagnosis of renal disease. | Normal<br>MRD<br>Cyst | 85.9 | 86.6<br>83.0<br>91.3 |
| *Module 2*: ANFC based CAC system for diagnosis of MRD using absolute texture features. | Normal<br>MRD | 84.8 | 93.3<br>74.5 |
| *Module 3*: ANFC based CAC system for diagnosis of MRD using ratio texture features. | Normal<br>MRD | 89.9 | 85.0<br>94.9 |
| *Module 4*: ANFC based CAC system for diagnosis of MRD using combined texture features. | Normal<br>MRD | 95.7 | 91.6<br>100 |

**Note:** MRD: Medical renal disease, SVM: Support vector machine, OCA: Overall classification accuracy, ICA: Individual class accuracy, The OCA and ICA values are expressed in percentage.

From Table 1, it can be observed that,

(a) *Module 1* yields the maximum OCA of 85.9 % along with ICA values of 86.6 %, 83.0 % and 91.3 % for normal, MRD and cyst classes respectively by using combined GLCM features for three class classification of renal diseases into **Normal, MRD** and **Cyst**. Therefore, the design of SVM based CAC system for diagnosis of renal diseases should be used for classification between normal, MRD and cyst renal US images.

(b) *Module 4* yields the best results with an OCA of 95.7 % along with ICA values of 91.6 % and 100 % for normal and MRD classes respectively, for characterization of **Normal** and **MRD** B-Mode renal US images . Therefore, the design of ANFC based CAC system for diagnosis of Medical Renal Disease using combined texture features should be used for classification between of normal and MRD renal US images.

# Contents

# Chapter 1

## Introduction

### 1.1 Motivation

Kidney is the organ that help in filtering of waste products from the blood. It performs many important roles for the normal functioning of human body such as (*a*) removing excess water, (*b*) retaining it when the body needs more, (*c*) adjusting the levels of other minerals and removing waste products such as urea, creatinine, (*d*) generating important chemicals called hormones which regulates blood pressure, production of red blood cells and calcium balance in the body. Kidneys are located at the upper back wall of the abdomen. One kidney is placed to the left and the other to the right of the backbone probably because of considerable space occupied by the liver. The lower rib cage protects the kidneys. A normal kidney measures 10-12 cm vertically and 4-6 cm transversely. Renal parenchyma which is the outer C-shaped structure includes cortex and renal medulla. The process of waste excretion takes place in renal parenchyma. Since renal medulla are in shape of pyramids, they are also called as renal pyramids. Each pyramid is surrounded by cortex which forms the outer layer of renal parenchyma region and consist of connective tissues. Centrally located renal sinus is mainly composed of renal fat, renal vessels, calices, nerve tissue, and lymphatic channels. The diagram of internal anatomy of kidney is given in Fig. 1.1.

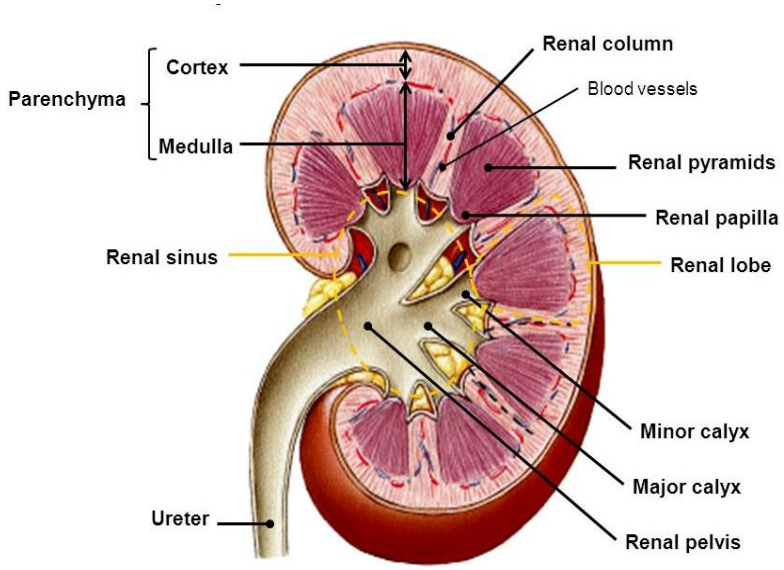


**Fig. 1.1** Internal anatomy of kidney.
**Note:** Image courtesy [1]

A million tiny structures called nephrons are present inside each kidney that filter blood and remove waste products. Most kidney diseases attack the nephrons. This damage may result in kidney failure. The timely clinical diagnosis of renal diseases is important, failing which it may lead to severe complications such as renal failures. Kidney diseases are broadly classified in two categories, i.e., *focal renal diseases* and *diffuse renal diseases*. The brief description of renal diseases and their types is shown in Fig 1.2.

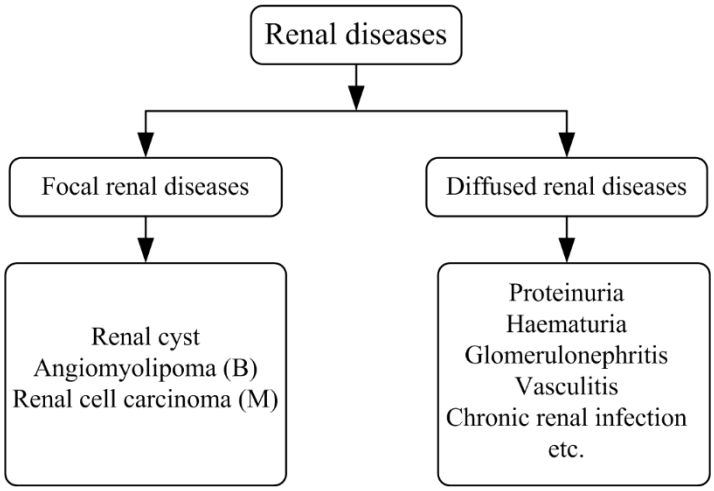


**Fig. 1.2** Brief description of types of renal diseases.
**Note:** B: Benign, M: Malignant.

### 1.1.1 Focal Renal Diseases

In focal renal diseases, the abnormality is focused in a small localized region of the kidney parenchyma which is often referred to as *focal renal lesion* (FRL). Renal cysts, Angiomyolipoma (AML, i.e., a primary benign FRL), Renal Cell Carcinoma (RCC, i.e., a primary malignant FRL), are some of the commonly occurring focal renal diseases.

#### 1.1.1.1 Renal Cyst

Renal cysts are sacs that are filled with fluid that can form on the kidney and are frequently observed on ultrasound (US). They are almost always benign but can lead to serious disorders that may impair kidney function. But usually, renal cysts are simple type of cysts i.e. noncancerous cysts occurring individually that cause rare problems whereas in polycystic kidney disease, many cysts are present. It is a progressive disease that can even lead to kidney failure_[2]. Usually, cysts are asymptomatic unless they are large enough to cause *mass effect* (i.e., compression and displacement of adjacent structures). *Typical renal cysts* appear with anechoic echotexture, well defined smooth thin lined capsule and posterior acoustic enhancement.

On the other hand, *atypical renal cysts* contain low level fine echoes which occur as a result of hemorrhage or infection and are outlined by thick irregular wall. Typical renal cysts can be easily diagnosed from their characteristic appearance on B-mode US. Atypical renal cysts always appear with internal echoes and thickened irregular walls [3, 4]. The sample US images of typical and atypical cyst, from image database is shown in Fig. 1.3.

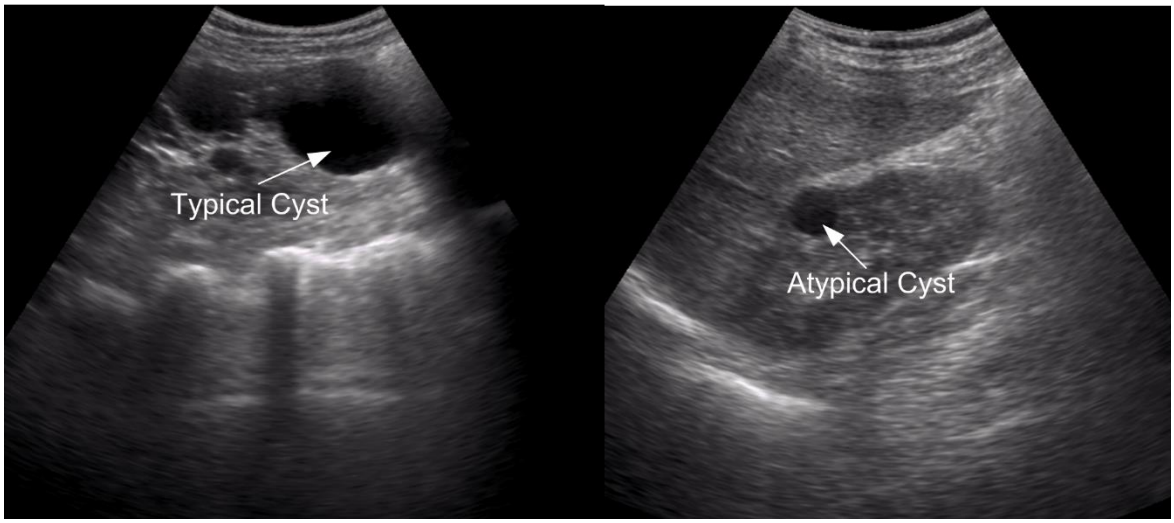


**Fig. 1.3** Sample US image of (*a*) typical renal cyst, (*b*) atypical renal cyst.

#### 1.1.1.2 Angiomyolipoma (AML)

Angiomyolipoma (AML) is a commonly occurring benign (non-cancerous) solid renal tumor made up of vascular, fatty and smooth muscle tissue and variable amounts of mature adipose tissue [5, 6]. Two types of renal AML exists which can be differentiated clinically. The first type is perceived in tuberous sclerosis patients, that develops bilaterally, and can have multiple centres with variable sizes. The sample US image of AML class is shown in Fig. 1.4.

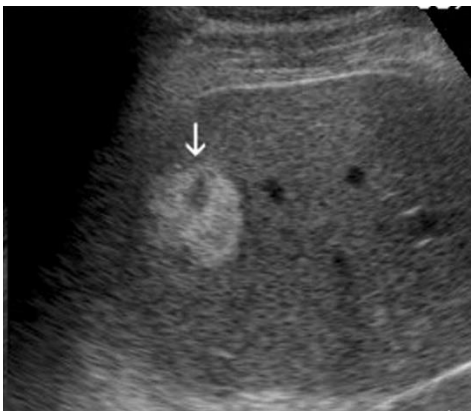

**Fig. 1.4** Sample US image of AML class.
**Note**: Image courtesy: [7]

The AML develops in 80.0 % of tuberous sclerosis cases which is a genetic disease. The second type is a mid-size solitary lesion with unilateral location. Its appearance in sonography depends on proportion of fat, vessels and bleeding.

#### 1.1.1.3 Renal Cell Carcinoma (RCC)

Renal Cell Carcinoma (RCC), also known as renal adenocarcinoma is most commonly occurring solid primary malignant (cancerous) lesion [8, 9]. The RCC originates in the lining of the proximal convoluted tubule which is a part of the very small tubes in the kidney used for transportation of waste molecules from the blood to the urine. The sample US image of RCC class is shown in Fig. 1.5.

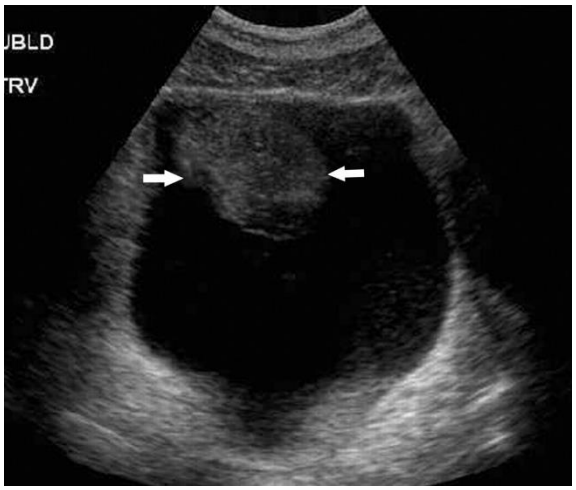


**Fig. 1.5** Sample US image of RCC class.
**Note**: Image courtesy: [10]

### 1.1.2 Diffuse Renal Diseases

In diffuse renal diseases, the abnormality is scattered throughout the renal parenchyma. The important functions performed by kidney that help in filtration of blood mainly involve parenchyma region of kidney. Renal parenchyma occupy most of the space of kidneys. It contains two layers. The outer layer is renal cortex, and the inner part is renal medulla, including glomeruli and renal tubules where filtration and urine formation occur. Disorders like proteinuria, hematuria etc. may have diseased glomerulus, blood vessels and nephrons in renal parenchyma. When these diseases occur in renal parenchyma, they are not exactly diagnosable and are referred as diffuse renal disease, also known as medical renal disease (MRD) [11-23].

Proteinuria occurs due to the abnormal secretion of excessive protein mainly albumin and globulin in the urine. This excessive amount of protein may cause significant damage to the glomeruli. This kidney disorder is characterized by a number of signs of disease like myeloma,

diabetes mellitus and amyloidosis. Interstitial nephritis, polycystic kidneys, and other tubular disorders are not associated with significant proteinuria [11, 12].

Haematuria is presence of red blood cells (erythrocytes) in urine. It is indicative of presence of kidney stone, infection, enlarged prostate gland or tumor in the urinary tract. Most often haematuria is diagnosed by medical history or urine analysis.

When the presence of red blood cells in the urine is detected, it is termed as gross haematuria. Microscopic examination or dipstick method is used for detection of microscopic haematuria [11, 13, 15, 16].

Glomerulonephritis is a condition wherein there is an attack on the filters of the kidney. Each nephron consist of a filter called the glomerulus from where the blood passes through and gets filtered. The waste products are removed through the tubes as urine.

Glomerulonephritis results in damage to the capillaries of the kidney. If glomeruli are damaged, the kidneys will stop working properly and it can lead into renal failure [11-16]. A wide variety of infections can trigger chronic glomerulonephritis including pneumonia, hepatitis, measles, malaria and syphilis.

Vasculitis is a medical term for inflammation of blood vessels. The white blood cells and antibodies (natural defenses) start damaging the body by mistake leading to vasculitis. Vasculitis is different from other medical renal diseases because in vasculitis, blood vessels in particular are damaged. It becomes difficult for the doctors to understand fully why this happens and the condition is quite rare [11, 12].

Chronic renal infection (pyelonephritis) is a particular urinary tract infection that generally begins in bladder and spreads up to the kidneys and thus requires immediate medical attention. It can involve high blood pressure (hypertension) and may lead to failure of kidney. Its progression rate is very slow, and sometimes patients experience kidney dysfunction for more than 20 years after onset.

If left untreated, the infection of kidney can permanently damage both the kidneys or the bacteria can spread through blood circulation causing life-threatening infection [11, 12, 20-23].

Thus, early diagnosis of MRD that hampers the normal functioning of parenchyma is clinically significant to avoid further complications such as renal cancer and other chronic kidney disease [16-23].

## 1.2 Ultrasound Imaging

In the past several years, ultrasonography has become a very popular tool for imaging physiological systems in the body. The US waves are sine waves of frequency greater than 20KHz (above the frequency of audible sound). Medical US uses very high frequency range of 1-20MHz. The higher frequency waves gives greater resolution but tissue penetration is reduced. An alternating electric field passed through crystals make them to vibrate and emit high frequency sine waves. When the current is switched off, the reflected sin waves or echoes cause the crystal to vibrate producing electricity. This electrical signal is processed by the ultrasound machine to produce an image. When the echoes are reflected from tissues of human kidney, they are displayed as a B-scan image that form a texture pattern because of the characteristics of the imaging system as well as the tissue. This suggests that the diagnosis of US kidney image is directly related with the analysis of texture patterns.

Texture is an image feature that provide important characteristics for surface and objects identification from the image. The US measures the size and appearance of the kidneys and also helps in detection of tumors, congenital anomalies, swelling, blockage of urine flow etc. Widely available US imaging modality helps in diagnosing the diseases of soft tissue organs such as kidney because of its real-time, inexpensive, non-radioactive & non-invasive properties.

The US imaging modality reliably differentiate solid masses from simple cysts which are most common, space occupying lesions in the kidneys [19, 24-30]. There are many advantages of US such as fast processing and more accurate procedures due to its real time capabilities. Numerous imaging modalities like US, computerized tomography (CT), X-ray, magnetic resonance imaging (MRI) etc. can be used for diagnosing renal abnormalities. However, CT which uses ionizing radiations, is harmful for human body [31-34]. On the other hand, US does not produce any known harmful effects on any of the tissues examined during clinical practice and therefore, is considered to be the best for diagnosis of various disorders. US is painless, safe and inexpensive. Other advantage of US is that it uses high frequency waves to generate moving images onto screen of the inside body including organs, soft tissues, bones etc. However, the disadvantages of US imaging are artifacts due to the movement of patients and equipment margins.

## 1.3 Sonographic Appearances of Different Renal Image Classes used in the Present Research Work

### 1.3.1 Echogenicity

The ability to bounce an echo is called echogenicity i.e. returning a signal in US examinations. In other words, echogenicity is higher when the tissue surface, bouncing the sound echo reflects increased sound waves.

The amplitude of an echo returning to the transducer is represented by the degree of brightness (i.e. echogenicity) of a dot on the display. Combination of all the dots forms the final image. Particular echogenicity is exhibited by each organ, such as liver, spleen or kidney in its normal state. In diseased state, the echogenicity of the tissue can exhibit a different nature, they become either more echogenic (hyperechoic) or less echogenic (hypoechoic) than usual. These observations based on echogenicity of US images can help the radiologist to categorize the type of disease process involved.

**Types of echogenicity-**

1. Hyperechoic: Tissues with higher echogenicity are called "hyperechoic" and are usually represented with brighter dots on US images e.g., diaphragm, gallstone, bone, pericardium.

2. Hypoechoic: Tissues with lower echogenicity are called "hypoechoic" and are usually represented with darker gray dots on US images e.g. solid organs. Also, the structures that are deeply located often appear hypoechoic due to attenuation that limits beam transmission, resulting in return of a weak echo and darker appearance.

3. Anechoic: Absence of reflections result in dark dots (anechoic) e.g. fluid and blood filled structures as the beam passes easily through these structures without any substantial reflection.

4. Isoechoic: Tissues which reflect same echogenicity as other tissue.

In the present work, three classes of renal ultrasound images namely, normal, MRD and cysts are considered for classification. The brief details of the sonographic appearances of these renal image classes are depicted below:

### 1.3.2 Sonographic Appearance of Normal Kidney

The sample US image of normal case taken out randomly from image database is shown in Fig. 1.6.

A normal bean-shaped kidney has a parenchyma region which is divided into renal cortex and renal medulla. The outer portion of the kidney is called renal cortex that lies between renal capsule and renal medullary pyramids.

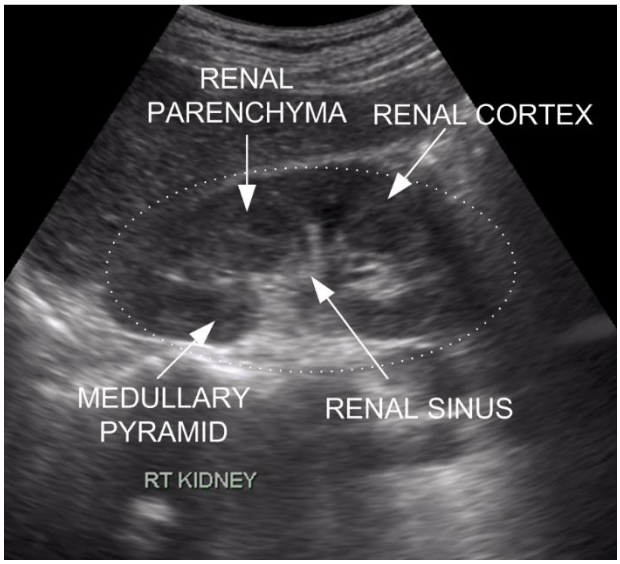


**Fig. 1.6** Sample US image of normal case.
**Note**: RT kidney: Right kidney, Renal sinus region exhibits more echogenicity in comparison to renal parenchyma. Cortico-medullary differentiation can also be made.

The centrally located hyperechoic region is termed as renal sinus which is mainly composed of renal fat, renal vessels, calices, nerve tissue, and lymphatic channels. The length of a kidneys lies between 9 and 13 cm. The mean normal value of parenchymal thickness varies between 1 to 1.5 cm, avoiding renal pyramids. The differentiation between renal sinus and parenchyma region can be made easily in case of normal class as renal sinus region exhibits more echogenicity (hyperechoic) in comparison to parenchyma region due to the presence of hilar adipose tissue with fibrous septae, blood vessels and lymphatics. Also, cortico-medullary differentiation can also be made as shown in Fig. 1.6.

### 1.3.3 Sonographic Appearance of MRD

The sample of US image of MRD case taken out randomly from image database is shown in Fig. 1.7. Any acquired renal disease may result in renal infection that leads to destruction of kidney tissues causing renal failure. Such disorders that may involve diseased glomerulus, nephrons and blood vessels of the parenchyma region, form the class of MRD. The echogenicity of renal cortex is correlated to severity of histological changes in renal parenchymal disease [11-13, 16-19, 22].

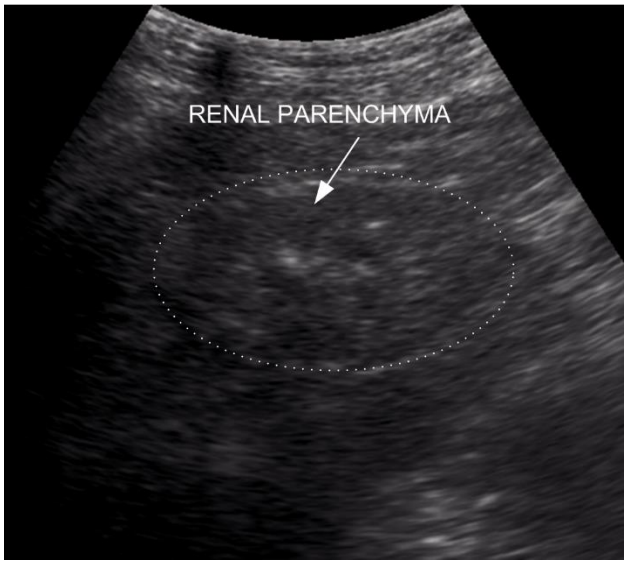


**Fig. 1.7** Sample US image of MRD case.
**Note**: Renal sinus and renal parenchyma appears to be iso-echoic (i.e. both become hyperechoic). Loss of cortico-medullary differentiation can also be observed.

In MRD image class, the texture of renal parenchyma region becomes hyperechoic and thus, the differentiation between renal sinus and renal parenchyma cannot be made as both become is-echoic with respect to each other. Also, loss of cortico-medullary differentiation takes place as shown in Fig. 1.7.

### 1.3.4 Sonographic Appearance of Renal Cyst

The sample US image of renal cyst is shown in Fig. 1.8.

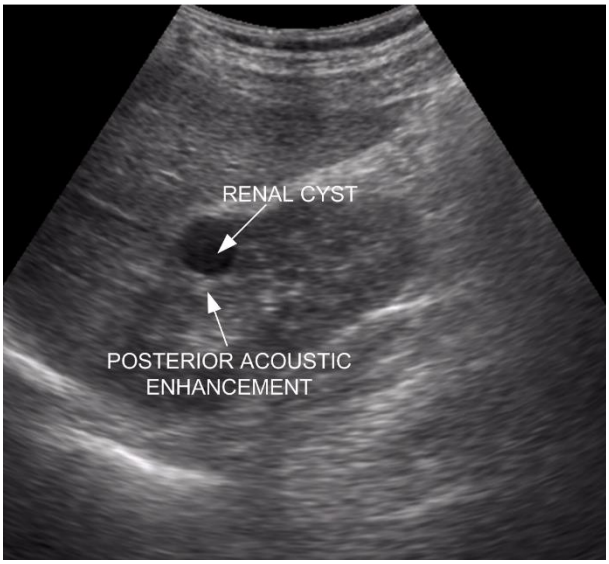


**Fig. 1.8** Sample US image of renal cyst.
**Note**: Anechoic appearance of renal cyst can be observed.

Renal cysts are thin walled, anechoic fluid-filled region in the kidney which exhibit posterior acoustic enhancement as shown in Fig. 1.8. A cyst found in kidney can be of any type like simple renal cyst, complex cyst or polycyst [2, 3].

## 1.4 Need for CAC Systems for Renal Diseases using B-Mode Ultrasound Images

Recently, the design of computer aided classification (CAC) systems has emerged as major research subjects in the field of medical imaging. The purpose of CAC is to provide a computer output to help radiologists and other health care professionals in image reading and understanding. The real time, inexpensive, non-radioactive, feasible and non-invasive nature of ultrasound (US) imaging modality are some of the significant advantages due to which it is considered as the primary examination for the imaging of soft tissues however there are certain associated disadvantages such as (*a*) inter and intra-observer variations associated with interpretation of ultrasound image, (*b*) motion artefacts and (*c*) equipment limitations [35-39]. These factors oppose the clarity of subjective diagnosis. Addressing these limitations is important for development of an efficient CAC system based on US imaging modality. Although MRI and CT scan offer high sensitivity for diagnosis of renal disease but they are costly and in CT the patient is also exposed to ionizing radiation and therefore it is necessary to address the limitations which are posed by US imaging modality [24-30, 36-39]. Hence, it is highly desired to design an efficient CAC system for characterization of renal diseases using ultrasound images [40-45].

## 1.5 Objectives of the Present Study

The main objective of the present research work is to enhance the potential of ultrasound scanner for differential diagnosis between renal diseases by designing efficient CAC system with comprehensive image database. The various research objectives formulated for the present research work are depicted here:

**(*i*) *Objective 1: The formulation of image assessment, data collection, ROI extraction and data bifurcation protocols***. To develop an efficient CAC system, it is necessary that the classifiers used in the classification module utilize an image database that contains the representative images and relevant information from each subclasses. The formulation of protocols for ROI extraction from the renal US images and their bifurcation into training and testing data sets is taken up as the first objective in the present work.

***(ii) Objective 2: To design a SVM based CAC system for diagnosis of renal diseases***.

Different types of features contribute in providing different relevant information for a particular image class. Thus, an attempt to evaluate the potential of features from statistical, signal processing and transform domain methods on renal ultrasound images for classification into normal, MRD and cyst renal US image class using SVM (support vector machine) classifier is taken up as the next objective.

***(iii) Objective 3: To design an ANFC based CAC system for diagnosis of MRD using absolute texture features.***

In normal renal US image, the texture of renal parenchyma region is hypoechoic along with visible cortico-medullary differentiation. But in case of MRD, the texture of renal parenchyma region becomes hyperechoic.

By utilizing this difference observed in the echogenicity of parenchyma in normal and MRD renal US image, the next objective of the present research work is to classify these image classes into normal and MRD by using absolute features. These features are obtained by considering renal parenchymal region of interest (PROIs) from normal and MRD renal US images that can provide a significant aid to the radiologist in early detection of medical renal disease. The ANFC is used for the classification task.

***(iv) Objective 4: To design an ANFC based CAC system for diagnosis of MRD using texture ratio features.***

In normal renal US image, the differentiation between renal sinus and renal parenchyma region can be made easily as renal sinus region exhibits more echogenicity in comparison to parenchyma region whereas in case of MRD renal US image class, the texture of renal parenchyma region becomes hyperechoic and thus, the differentiation between renal sinus and renal parenchyma cannot be made as both become iso-echoic with respect to each other.

By utilizing the difference observed in the echogenicity of renal sinus with respect to the renal parenchyma in case of normal and MRD renal US image class, the next objective of the present research work is to make a comparative study on the classification results obtained by considering the ratio of features from renal parenchymal regions of interest (PROIs), renal sinus regions of interest (SROIs), that can provide a significant aid to the radiologist in early detection of medical renal disease. ANFC is used for the classification task.

***(v) Objective 5: To design an ANFC based CAC system for diagnosis of MRD using combined texture features.***

The classification of normal and MRD renal US images is performed using two approaches viz. (*a*) by utilizing the absolute features from parenchyma region PROIs only and (*b*) by utilizing the ratio features from parenchyma region PROIs, renal sinus region SROIs. The combined contribution of above two approaches i.e. absolute and ratio features for classification into normal and MRD class is taken up as the last objective for the present work. ANFC is used for the classification task.

## 1.6 Organization of Thesis

This thesis report is organized into eight chapters, as described below:

(*i*) *Chapter* 1 titled **"*Introduction*"** lays the foundation as to why analysis and classification of B-mode renal ultrasound images is clinically significant. It focuses on the facts like why kidney? Types of renal diseases? Why renal diseases should be considered seriously? What is the affect on sonographic appearance as the disease progress? Why B-mode ultrasound? What is the need to develop efficient CAC systems for diagnosis of renal diseases? What are the objectives of the present research work? How these objectives were formulated? To conclude, the content documented in this chapter provides the basic motivation regarding the fact that an efficient design of CAC system for renal diseases can enhance the diagnostic potential of B-mode US imaging modality.

(*ii*) *Chapter* 2 titled **"*Literature review*"** presents a brief literature review of the other related studies for diagnosis of renal diseases using B-mode ultrasound images.

(*iii*) *Chapter* 3 titled "***Methodology***" explains the research methodology followed in the present work. It explains the various set of protocols followed i.e., the protocols followed for assessment of images, for selection of ROIs, for selection of ROI size, for bifurcation of dataset into training and testing dataset. Thus, the complete description of dataset used in the present research work is described in this chapter.

(*iv*) *Chapter* 4 titled **"*SVM based CAC system for diagnosis of renal disease*"** gives a detailed description of exhaustive experimentation carried out to design an SVM based CAC system for diagnosis of renal diseases using features from statistical, signal processing and transform domain methods.

(*v*) *Chapter* 5 titled **"*ANFC based CAC system for diagnosis of medical renal diseases using absolute texture features*"** gives a detailed description of exhaustive experimentation carried out to design an ANFC based CAC system for diagnosis of MRD using absolute texture features.

(*vi*) *Chapter* 6 titled **"*ANFC based CAC system for diagnosis of medical renal diseases using texture ratio features*"** gives a detailed description of exhaustive experimentation carried out to design an ANFC based CAC system for diagnosis of MRD using texture ratio features.

(*vi*) *Chapter* 7 titled **"*ANFC based CAC system for diagnosis of medical renal diseases using combined texture features*"** gives a detailed description of exhaustive experimentation carried out to design an ANFC based CAC system for diagnosis of MRD using combined texture features.

(*vi*) *Chapter* 8 titled **"*Conclusion and future scope*"** gives the brief conclusion of all the experiments conducted for the design of CAC system for classification of renal diseases. It also highlights the current limitations and future scope of how this work can be extended further.

# Chapter 2

# Literature Review

## 2.1 Introduction

Medical imaging has provided a significant contribution to medical health care, leading to healthier standard of living at reduced cost. The textural patterns exhibited by the body tissues are reflected on the images that are obtained by different modalities. The analysis of these textural patterns play a vital role in complexity detection without undergoing any pathological practice. Recently, development of CAC systems has piqued the interest of many researchers in the field of medical imaging.

The basic concept of CAC system is to provide a computerized output to the radiologists to them in image analysis and understanding [40-45]. The advantages of US imaging are that it is real time, inexpensive, non-radioactive, feasible and non-invasive in nature. Due to these advantages, US is considered to be the primary choice for the imaging of soft organs like kidney, however there are certain disadvantages associated with US such as (*a*) inter and intra-observer variations associated with interpretation of US image, (*b*) motion artefacts and (*c*) equipment limitations [35-40]. There are several bottlenecks associated with manual analysis such as time-consumption besides being susceptible to human-errors depending on one's expertise.

Therefore it is highly desired to minimize these limitations and design an efficient CAC system for characterization of renal diseases using US images that can provide significant aid to the radiologist in the clinical environment.

## 2.2 CAC System Designs for Renal US Image Classification

The studies in the literature for classification of renal diseases using US images are few and can be classified into two categories viz. (*a*) segmentation based approach (SBA) [46-54] and (*b*) ROI based approach (RBA) [40, 41, 55-57].

The brief overview of studies conducted for classification of renal diseases on US images is given in Fig. 2.1.

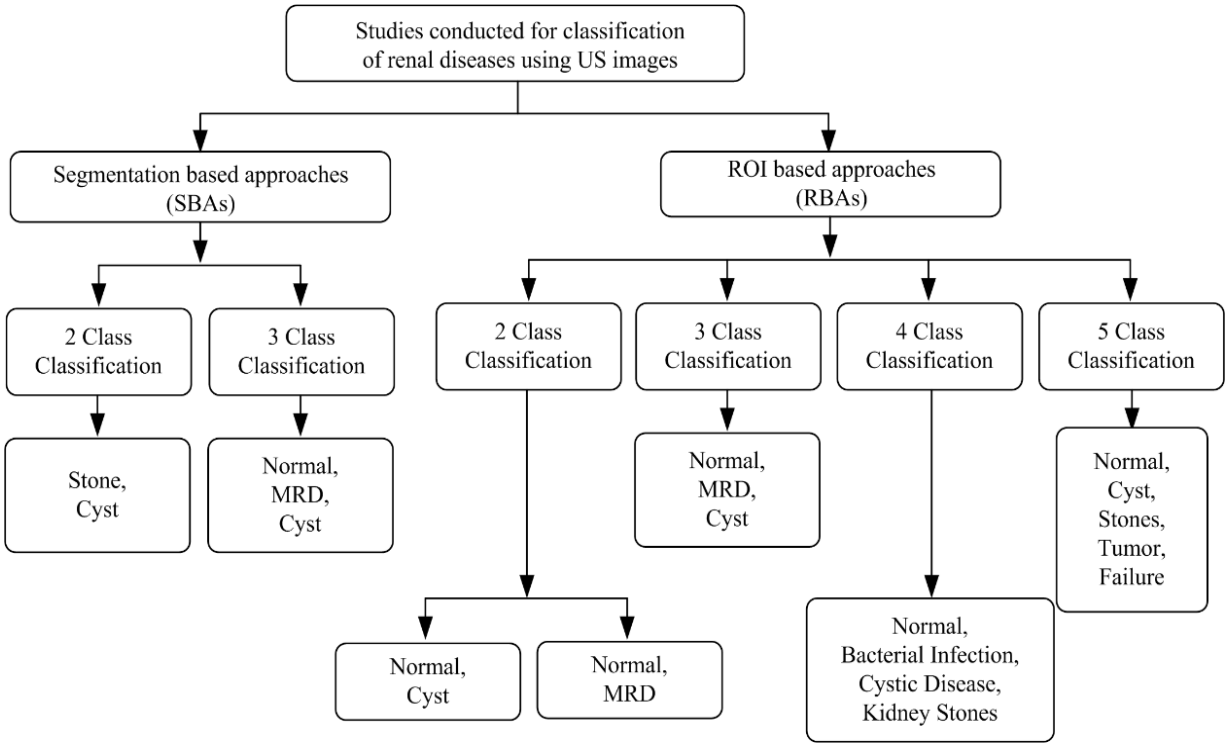


**Fig. 2.1** Brief description of studies conducted for classification of renal diseases on US images.

### 2.2.1 CAC System Designs based on Segmentation based Approaches (SBAs)

Various researchers in the past have developed different CAC systems for classifying the renal US images into various classes using segmentation based approaches (SBAs). In SBA, kidney region is first segmented and texture features are applied to the segmented kidney region. A brief description of these related studies is given in Table 2.1.

B. K. Raja et al. [46] reported classification of three kidney classes namely, normal, MRD and cyst using power spectral features.

B. K. Raja et al. [47] proposed a set of unconstrained features that are independent to kidney area for classification of renal US images into normal, MRD and cyst classes. Six different features viz. first order statistics (FOS), Multi-scale differential features (MSDF), spatial gray-level dependence matrix (SGLDM), features extracted using Fast Fourier Transform (FFT) and Gabor wavelet transform were used. The study revealed that the performance of fuzzy-neural system was superior as compared to Multi-layer back propagation network (MBPN). The individual classification accuracy achieved by fuzzy-neural system is 84.6 %, 80.7 % and 84.6 % for normal, MRD and cyst classes respectively.

B. K. Raja et al. [48] proposed classification of US images into 3 classes namely, normal, MRD and cyst using statistical texture analysis methods such as FOS, second-order gray level statistical features, multi scale and power spectral features.

B. K. Raja et al. [49] proposed an approach for the classification of three kidney classes namely, normal, MRD and cyst were considered for the classification using statistical texture methods and MI features.

**Table 2.1** Summary of studies carried out for renal US image classification using SBAs.

| Author | No. of Classes | No. of Images | Features | Classifiers | Acc. |
|---|---|---|---|---|---|
| B. K. Raja et al. [46] | 3 (Normal/ MRD/Cyst) | 150 | Power spectral features | - | - |
| B. K. Raja et al. [47] | 3 (Normal/ MRD/Cyst) | 150 | FOS, SGLDM, MI, MSDF, FFT, Gabor | MBPN and HFNN | 83.3 |
| B. K. Raja et al. [48] | 3 (Normal/ MRD/Cyst) | 150 | FOS, 2nd order gray level statistics, multi scale, power spectral features | ANN+ MBPN | 87.5 |
| B. K. Raja et al. [49] | 3 (Normal/ MRD/Cyst) | 150 | FOS, MI features | - | - |
| B. K. Raja et al. [50] | 3 (Normal/ MRD/Cyst) | 150 | FOS, 2nd order statistical features, MI, MSDF, power spectral, Gabor features | MBPN and HFNN | 94.8 |
| B. K. Raja et al. [51] | 3 (Normal/ MRD/Cyst) | 150 | Gabor wavelet features | *k*NN | 82.1 |
| K. Dhanalakshmi et al. [52] | 3 (Normal/ MRD/Cyst) | 150 | GLCM features | ARCKi | 93.0 |
| J. S. Jose, et al. [53] | 3 (Normal/ MRD/Cyst) | - | Fractal and histogram based features | Bayesian | - |
| K. D. Krishna et. al. [54] | 2 (Stone/Cyst) | 200 | Harlick's and histogram based features | SVM with MLP | 86.0 |

**Note:** SBAs: Segmentation based approaches, Acc.: Accuracy, MRD: Medical renal disease, FOS: First order statistics, ANN: Artificial neural network, MBPN: Multi-layer back propagation network, MI: Moment invariant, MSDF: Multi-scale differential features, FFT: Fast Fourier Transform, HFNN: Hybrid fuzzy-neural network, *k*NN: *k*-nearest neighbor, ARCKi: Generation of association rules with high confidence for kidney images, SGLDM : special gray-level dependence matrix, SVM: Support vector machine, MLP: Multi-Layer Perceptron, The value of accuracy is expressed in percentage.

B. K. Raja et al. [50] proposed an approach for automated diagnosis and classification of US kidney images into normal, MRD and cyst classes using statistical first and second order features, algebraic MI features, multi-scale differential features, spectral features estimated by Fast Fourier transform and dominant Gabor wavelet features. Higher order spline interpolated contour was used for segmentation of kidney region.

The classification efficiency obtained from fuzzy-neural system is 96.1 %, 92.3 % and 96.1 % for normal, MRD and cyst US image classes respectively. Also, it was found that ranking the features enhances the classification accuracy.

B. K. Raja et al. [51] proposed an approach for classification of US images into three classes namely, normal, MRD and cyst using dominant Gabor wavelet and k-nearest neighbor (*k*NN) classifier.

K. Dhanalakshmi et al. [52] classified US renal images into three classes namely normal, MRD and cyst by second order statistical features and feature selection by using a pre-processing solution for association rule generation (PreSAGe) algorithm which performs feature selection and discretization. Association rules with high confidence for kidney images (ARCKi), which is a new associative classifier is well suited to generate suggestions for diagnosis.

J. S. Jose et al. [53] presented an automated diagnosis and classification of renal US images into normal, MRD and cyst classes using fractal features, histogram-based features like mean, variance, kurtosis, skewness, energy, and entropy, FOS features like mean, dispersion, variance, average energy, skewness, kurtosis, median and mode and spatial gray level dependence (SGLDM) features and Bayesian classifier.

K. D. Krishna et al. [54] proposed a Field programmable gate array (FPGA) based CAC system for normal and abnormal classes of renal US images. Intensity histogram and Harlick's texture features were used for feature extraction from the segmented region of the kidney. Standard deviation of each metric was calculated for all images.

The classification was further extended to classify renal abnormal images into stone and cyst classes using SVM classifier with multi-layer perceptron (MLP) kernel that resulted in an accuracy of 86.0 %.

### 2.2.2 CAC System Designs using ROI based Approaches (RBAs)

Different CAC system designs have been proposed in the recent past for classifying the renal US images into different classes using ROI based approach. In this approach, the acquired images are manually cropped to extract regions of interest (ROIs) from the kidney.

A brief description of CAC system designs for classification of renal diseases using RBA is given in Table 2.2.

**Table 2.2** Summary of studies carried out for renal US image classification using RBAs.

| Author | No. of Classes | No. of Images [ROI size] | Features | Classifiers | Acc. |
|---|---|---|---|---|---|
| Prema T. Akkasaligar et al. [55] | 2 (Normal/ Cyst) | 52 [-] | GLCM, RLM | *k*NN | 84.0 |
| M. B. Subramanya et al. [41] | 2 (Normal/ MRD) | 35 [32 × 32] | FOS, MI, gradient, RLM, GLCM, Laws features | SVM | 85.8 |
| M. B. Subramanya et al. [40] | 3 (Normal/ MRD/Cyst) | 35 [32 × 32] | FOS, gradient, MI, GLCM, RLM features | SVM | 86.3 |
| W. M. Hafizah et al. [56] | 4 ( Normal/ Bacterial infection/ Cystic disease/ Kidney stones) | - [-] | Intensity histogram features, GLCM | - | - |
| M. W. Attia et. al. [57] | 5 (Normal/ Cyst/ Stone/ Tumor/Failure) | - [256 × 256] | DWT, GLCM | Neural network classifier | 97.0 |

**Note:** RBAs: ROI based approaches, Acc.: Accuracy, MRD: Medical renal disease, GLCM: Gray level co-occurrence matrix, RLM: Run length matrix, FOS: First order statistics, MI: Moment invariant, SVM: Support vector machine, *k*NN: k-nearest neighbor, DWT: Discrete wavelet transform. The value of accuracy is expressed in percentage.

Prema T. Akkasaligar et al. [55] proposed an approach that aimed at classifying the renal US images into two classes namely, normal and cyst using three different filters viz. Gaussian low pass, median filter and Weiner filter for pre-processing. Features from gray-level co-occurrence matrix (GLCM) and run length matrix (RLM) were extracted and *k*NN classifier was used for the classification task.

Results of the study indicated that Gaussian low pass filter was most suitable for removal of speckle noise and GLCM features were highly significant for the classification task. The overall classification accuracy of 84.0 % was obtained for classification between normal and cyst classes.

M. B. Subramanya et al. [41] presented a CAC system design for the classification of normal and MRD classes using B-mode US images and observed that an average classification accuracy of 85.8 % has been obtained using gradient and GLCM features together with SVM classifier.

M. B. Subramanya et al. [40] reported classification of US images into normal, MRD and cyst classes using texture analysis methods such as statistical features like first-order statistics (FOS), gradient based features, MI, GLCM, RLM and Laws' mask features have been computed by using SVM classifier.

On the basis of overall classification accuracy, few optimal feature sets were considered for the classification task by using Differential Evolution Feature Selection (DEFS) resulting in an average accuracy of 86.3 % using run-length matrix features.

W. M. Hafizah et al. [56] reported the classification of four classes of renal US images, namely, normal, bacterial infection, cystic disease and kidney stones using intensity histogram features and GLCM matrix features. The ROIs were cropped from images in order to remove complicated background.

After ROI cropping, contour detection was performed. Results of the study indicated that five texture features including kurtosis, mean, skewness, cluster shade and cluster prominence dominate over other texture features for classification task.

M. W. Attia et al. [57] proposed a method for automatic classification of renal US images into five classes namely, normal, cyst, stone, tumor and failure by using a set of statistical and multi-scale wavelet based features.

### 2.3 Concluding Remarks

From the above studies, it can be concluded that most of the researchers have used two types of approaches for renal disease classification i.e. (*a*) segmentation based approaches (SBAs) and (*b*) ROI based approaches (RBAs).

From the literature review of renal disease classification, few limitations of using SBAs were observed like (*i*) separate algorithm is required to segment the entire kidney tissue, (*ii*) there is no scope of excluding the centrally located renal sinus region (bearing similar echogenicity in normal as well as MRD class) for the purpose of feature extraction.

The RBAs not only eliminates the need of segmenting a kidney tissue, but also gives the flexibility of extracting the ROIs from parenchyma and renal sinus region. It is also observed that very few studies report CAC systems based on RBAs [40, 41, 55-57], in spite of various limitation involved in SBAs [46-54].

Therefore, the present study has been conducted using RBAs on normal, MRD and cyst renal US image classes with ROIs of size 25 × 25 pixels. The present study can be directly compared with the studies that use RBAs [40, 41, 55-57].

The description of classification of renal diseases using US images is given in Fig. 2.2. In this figure, the approaches and the studies taken up in the present work are shaded in gray background.

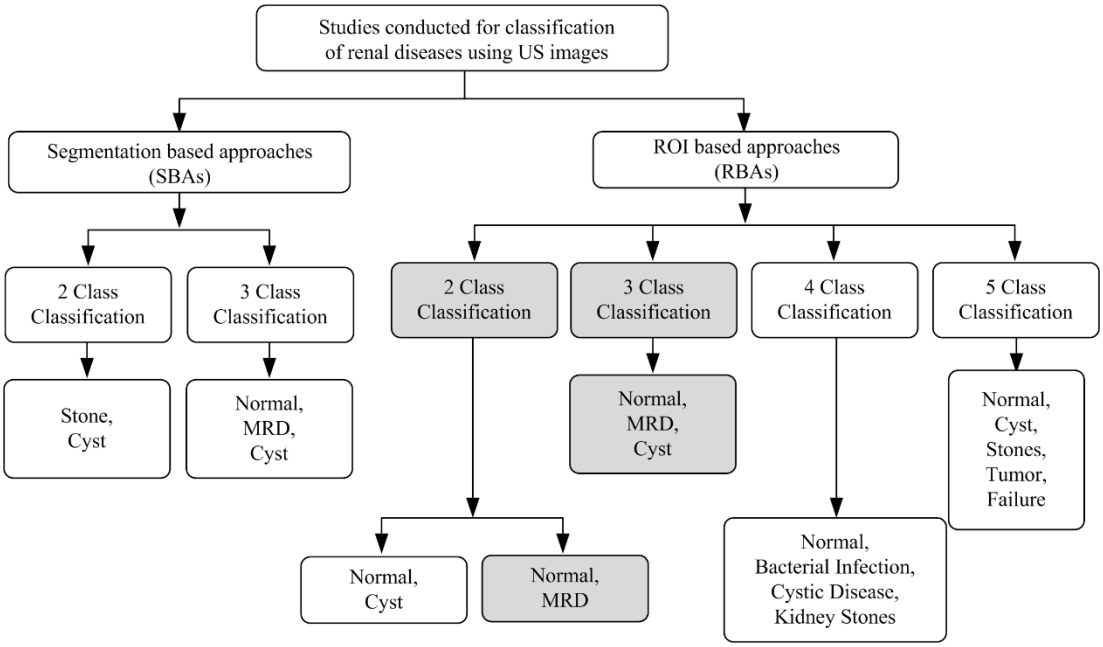


**Fig. 2.2** Brief description of classification of renal diseases using US images.
**Note**: The approaches and the studies taken up in the present work are shaded in gray background.

The methodology for different classification modules have been discussed in next chapter to give a brief overview of the proposed CAC systems for classification of renal diseases by using B-mode US images.

# Chapter 3

# Methodology

## 3.1 Introduction

Research is a scientific investigation that is carried out systematically for a deeper understanding of a specific topic. Formation of research objectives is crucial and first step to define the methodology of the research work undertaken. In the present work, the research objectives are framed by taking into consideration the relevant and important areas of sonographic images which can form the basis for attainment of optimum results.

This chapter gives a brief outline of the methodology followed in order to design an efficient interactive system for diagnosis of renal diseases by using B-mode renal US images.

The description of data sets used in present work is given in detail. The protocols for image assessment, data collection, ROI extraction, training and testing bifurcation for present work is also described.

## 3.2 Proposed Interactive System for Diagnosis of Renal Diseases

The block diagram of the proposed interactive system for diagnosis of renal diseases is shown in Fig. 3.1. This system consist of four modules.

### 3.2.1 Module 1: SVM based CAC system for diagnosis of renal diseases

This module classifies renal US images into three classes namely, normal, MRD and cyst. It is important to note that the nature of echogenicity of parenchyma region changes (becomes hyperechoic as compared to normal) in case of MRD renal US image.

Therefore, differentiation can be made between normal and MRD renal US image class by considering ROIs from renal parenchyma region. Hence, ROIs are extracted from parenchyma region for normal and MRD class. For renal cyst, ROIs from regions inside the renal lesion are considered as they exhibit anechoic appearance.

Accordingly, *Module 1* incorporates a CAC system for three class classification of renal US images into normal, MRD and cyst classes using SVM classifier.

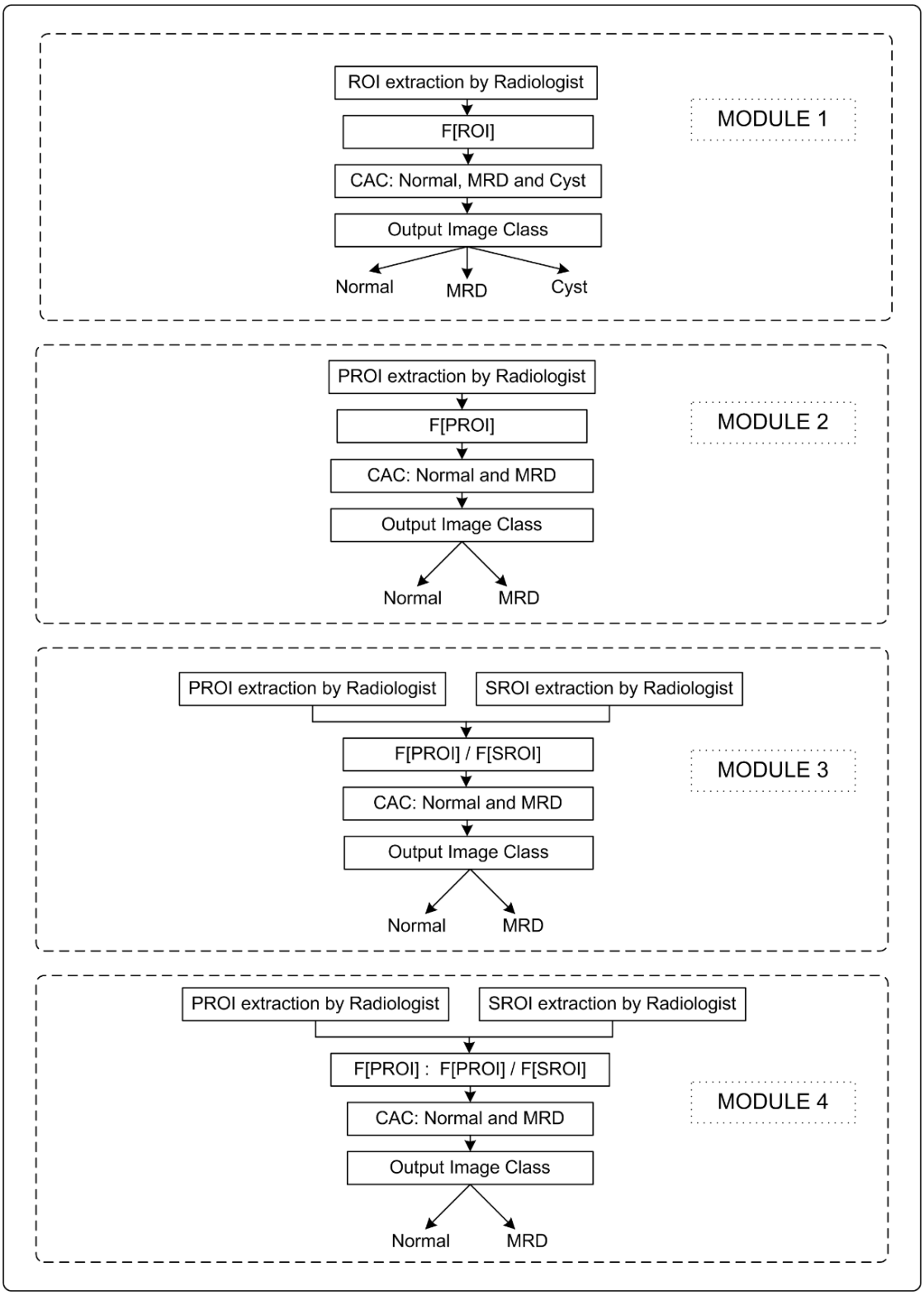


**Fig. 3.1** Block diagram of the proposed interactive system for diagnosis of renal diseases.
**Note**: ROI: Region of interest, PROI: Parenchyma region of interest, SROI: Sinus region of interest, MRD: Medical renal disease, CAC: Computer aided classification.

### 3.2.2 Module 2: ANFC based CAC system for diagnosis of MRD using absolute texture features

This module classifies renal US images into two classes namely, normal and MRD. The design of this module considers the parenchymal regions of interest (PROIs) extracted from renal parenchyma region as the nature of echogenicity of parenchyma region in MRD renal US image changes (becomes hyperechoic as compared to normal).

Accordingly, *Module 2* incorporates a CAC system for binary classification of renal US images into normal and MRD classes considering the absolute features extracted from PROIs only. The proposed CAC system design utilizes adaptive neuro-fuzzy classifier (ANFC) for the classification task.

### 3.2.3 Module 3: ANFC based CAC system for diagnosis of MRD using texture ratio features

This module classifies renal US images into two classes namely, normal and MRD. The design of this module utilizes echogenicity of renal parenchyma along with the echogenicity of renal sinus region. The renal sinus appears hyperechoic with respect to renal parenchyma region in normal renal US image. But in case of MRD, the echogenicity of renal parenchyma increases and therefore, renal parenchyma region becomes iso-echoic with respect to renal sinus [11, 12]. So, the classification is made on basis of the ratio of features extracted from renal parenchyma regions of interest (PROIs) and renal sinus regions of interest (SROIs), where renal sinus echogenicity remains same for normal and MRD image class, and the difference lies only in the echogenicity of renal parenchyma region. This classification is also compared with the classification performance by considering the PROIs from renal parenchyma region only (*Module 2*).

Accordingly, *Module 3* incorporates a CAC system for binary classification of renal images into normal and MRD classes considering the texture ratio features extracted from PROIs and SROIs. The proposed CAC system design utilizes ANFC for the classification task.

### 3.2.4 Module 4: ANFC based CAC system for diagnosis of MRD using combined texture features

This module classifies renal US images into two classes namely, normal and MRD. The design of this module uses the combination of the approaches used in above two modules (*Module 2 and Module 3*). Here the texture ratio features extracted from PROIs and SROIs are considered along with absolute features extracted from PROIs for diagnosis of MRD renal US image class.

Accordingly, *Module 4* incorporates a CAC system for binary classification of US renal images into normal and MRD classes considering the combined texture features from PROIs and SROIs. The proposed CAC system design utilizes ANFC for the classification task.

### 3.3 Image Assessment Protocol

The experienced participating radiologist ensured that all the images are free from artifacts, and confirmed the representativeness of each image class, i.e. normal, MRD and cyst class by visualization of sonographic appearance of normal, MRD and cystic kidney based on their knowledge and follow-up i.e. clinical history of the patient.

### 3.4 Dataset Description

For the present research work, a total of 35 B-mode renal US images consisting of 11 normal, 8 MRD and 16 cyst images, collected from Biomedical Instrumentation Laboratory, Indian Institute of Technology- Roorkee, Uttarakhand, India, have been used. The bifurcation of image dataset consisting of a total of 35 B-mode US images into different renal classes is shown in Fig. 3.2.

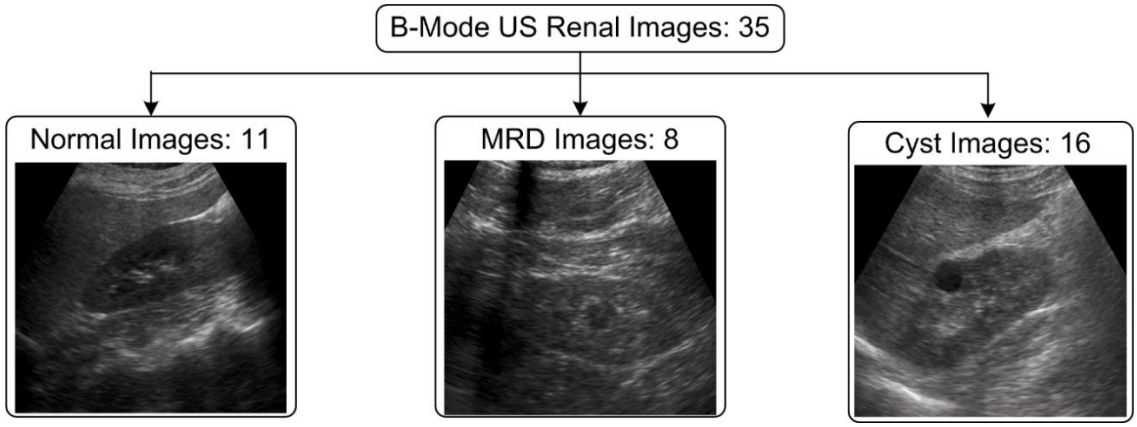


**Fig. 3.2** Data Set Description.
**Note**: MRD: Medical renal disease.

#### 3.4.1 Data Collection Protocols

The following protocols were followed for data collection.

(*i*) The images were recorded by Siemens ACUSON X300 ultrasound scanner

(*ii*) The images are acquired in longitudinal plane as the longitudinal cross section of either left or right kidney includes renal sinus, renal medulla and renal cortex region.

(*iii*) The cases of hydro-nephrotic kidney are excluded.

(*iv*) The images of the patients with only MRD and no other renal disorder are also included (cases of diabetic nephropathy are also in the exclusion criteria).

### 3.4.2 ROI Extraction Protocols

The protocols followed for extraction of ROIs and Selection of ROI size for design of different modules is explain in this section.

#### 3.4.2.1 Selection of ROIs

The following protocols were followed for cropping the ROIs from the image dataset:

(*i*) In the present work, ROIs of size 25 × 25 pixels are manually cropped from renal US images using MATLAB. Necrotic areas were avoided while cropping the ROIs.

(*ii*) *Module 1: SVM based CAC system for diagnosis of renal diseases.*

(*a*) Maximum non-overlapping ROIs were cropped from renal parenchyma region of kidney for normal renal US images, (*b*) Maximum non-overlapping ROIs were cropped from renal parenchyma region of kidney for MRD renal US images, (*c*) Maximum non-overlapping ROIs were cropped from the region inside the lesion for renal cyst US images, and (*d*) A total of 322 ROIs (120 from normal + 119 from MRD + 83 from cyst) were cropped from renal US images.

(*iii*) *Module 2: ANFC based CAC system for diagnosis of MRD using absolute texture features.*

(*a*) Maximum non-overlapping parenchymal ROIs (PROIs) were cropped from the renal parenchyma region of kidney from normal US images, (*b*) Maximum non-overlapping PROIs were cropped from the renal parenchyma region of kidney from MRD US images, (*c*) A total of 239 PROIs (120 from normal + 119 from MRD) were cropped from normal and MRD renal US images.

(*iv*) *Module 3: ANFC based CAC system for diagnosis of MRD using texture ratio features.*

(*a*) Two types of ROIs (i.e. PROIs and SROIs) were extracted, (*b*) Maximum non-overlapping PROIs are extracted from the parenchymal region of the kidney for both normal and MRD renal US images, (*c*) A single SROI is extracted from centrally located renal sinus region (which lies approximately towards the center of renal parenchyma of the kidney) for each of normal and MRD renal US images, (*d*) A total of 239 PROIs (120 from normal + 119 from

MRD) and 19 SROIs (11 from normal + 8 from MRD) were cropped in case of normal and MRD renal US images.

(*v*) *Module 4: ANFC based CAC system for diagnosis of MRD using combined texture features.* Same set of protocols are followed as given in section 3.4.2.1 (*iv*).

### 3.4.2.2 Selection of ROIs Size

Keeping in view the facts placed below ROI size of 25 × 25 pixels is considered appropriate for the present work.

(*i*) The image dataset of 35 B-mode renal US images is comparatively less for classification. Keeping this in mind the size of ROIs is kept small (25 × 25 pixels) so that number of cropped ROIs could be increased and significant analysis can be made.

(*ii*) The size of 25 × 25 pixels is also advantageous as it can easily extract renal sinus SROIs can be easily extracted without interfering in renal parenchyma region.

### 3.4.3 Dataset Bifurcation Protocol

The overall distribution of training and testing data for design of different modules is given here.

(*i*) *Module 1: SVM based CAC system for diagnosis of renal diseases.*

(*a*) Out of 120 normal ROIs, 60 ROIs were used for training and 60 ROIs were used for testing, (*b*) For MRD, out of 119 ROIs, 60 ROIs were used for training and 59 ROIs were used for testing, (*c*) Similarly, out of 83 cyst ROIs, 60 ROIs were used for training and rest 23 ROIs were used for testing.

(*ii*) *Module 2: ANFC based CAC system for diagnosis of MRD using absolute texture features*
(*a*) Out of 120 normal PROIs, 60 PROIs were used for training and 60 PROIs were used for testing. (*b*) For MRD, out of 119 PROIs, 60 PROIs were used for training and 59 PROIs were used for testing.

(*iii*) *Module 3: ANFC based CAC system for diagnosis of MRD using Texture Ratio Features*
(*a*) Out of 120 normal PROIs, 60 PROIs were used for training and 60 PROIs were used for testing, (*b*) Out of 11 normal SROIs, 5 SROIs were used for training and 6 SROIs were used for testing, (*c*) Out of 119 MRD PROIs, 60 PROIs were used for training and 59 PROIs were used for testing, (*d*) Out of 8 MRD SROIs, 4 SROIs were used for training and 4 SROIs were used for testing.

(*iv*) *Module 4: ANFC based CAC system for diagnosis of MRD using combined texture features*

Same set of protocols is followed as given in section 3.4.3 (*iii*).

The dataset bifurcation module for three class classification (normal, MRD and cyst) and two class classification (normal and MRD) is given in Fig. 3.3.

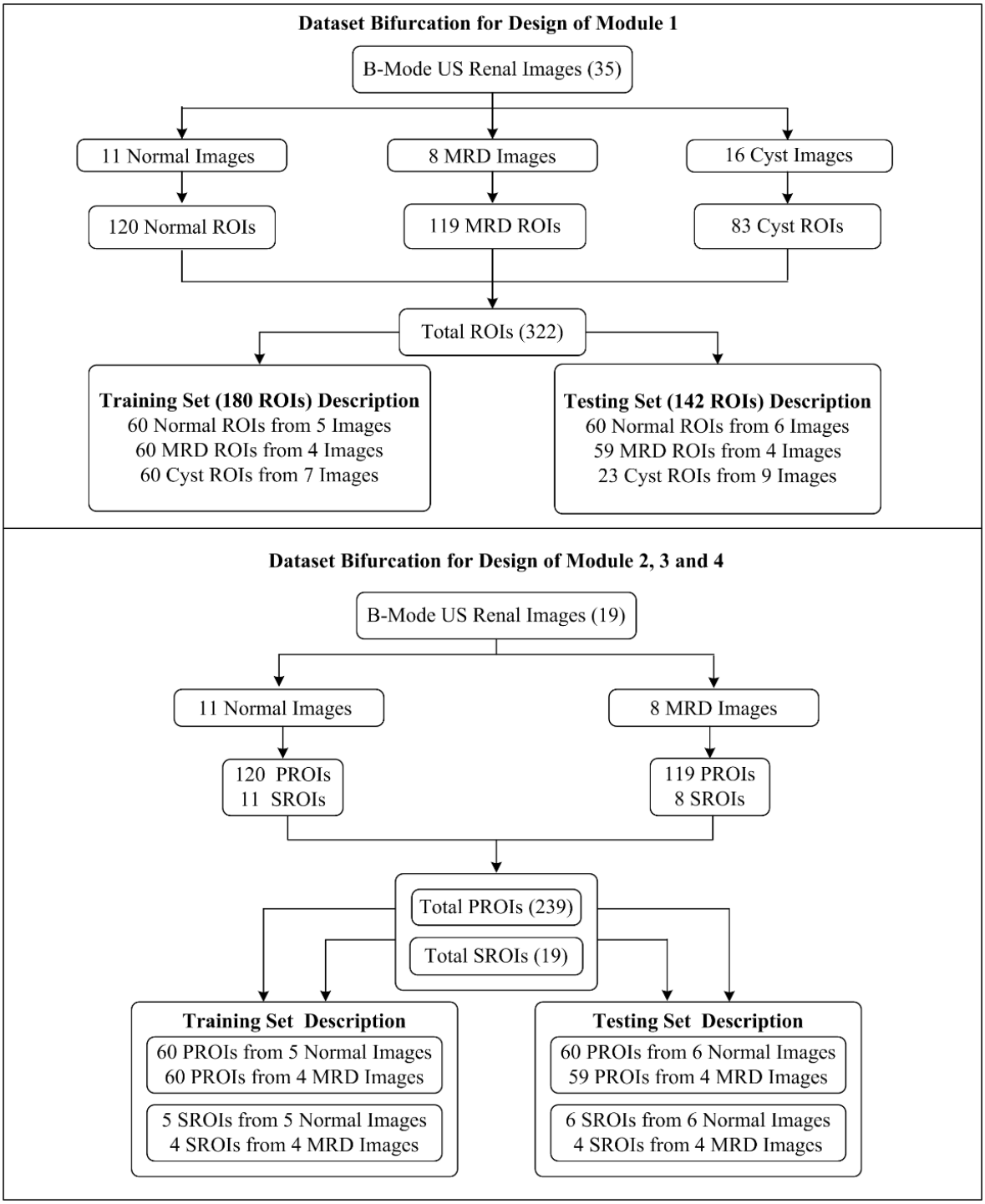


**Fig. 3.3** Dataset description and it's bifurcation into training and testing sets for three class (normal, MRD and cyst) and two class (normal and MRD) classification.
**Note:** ROIs: Regions of interest, PROIs: Parenchymal regions of interest, SROIs: Sinus regions of interest.

## 3.5 Brief Description of Experiments carried out in present work

The workflow diagram for generalized interactive system employed in the present work is shown in Fig 3.4.

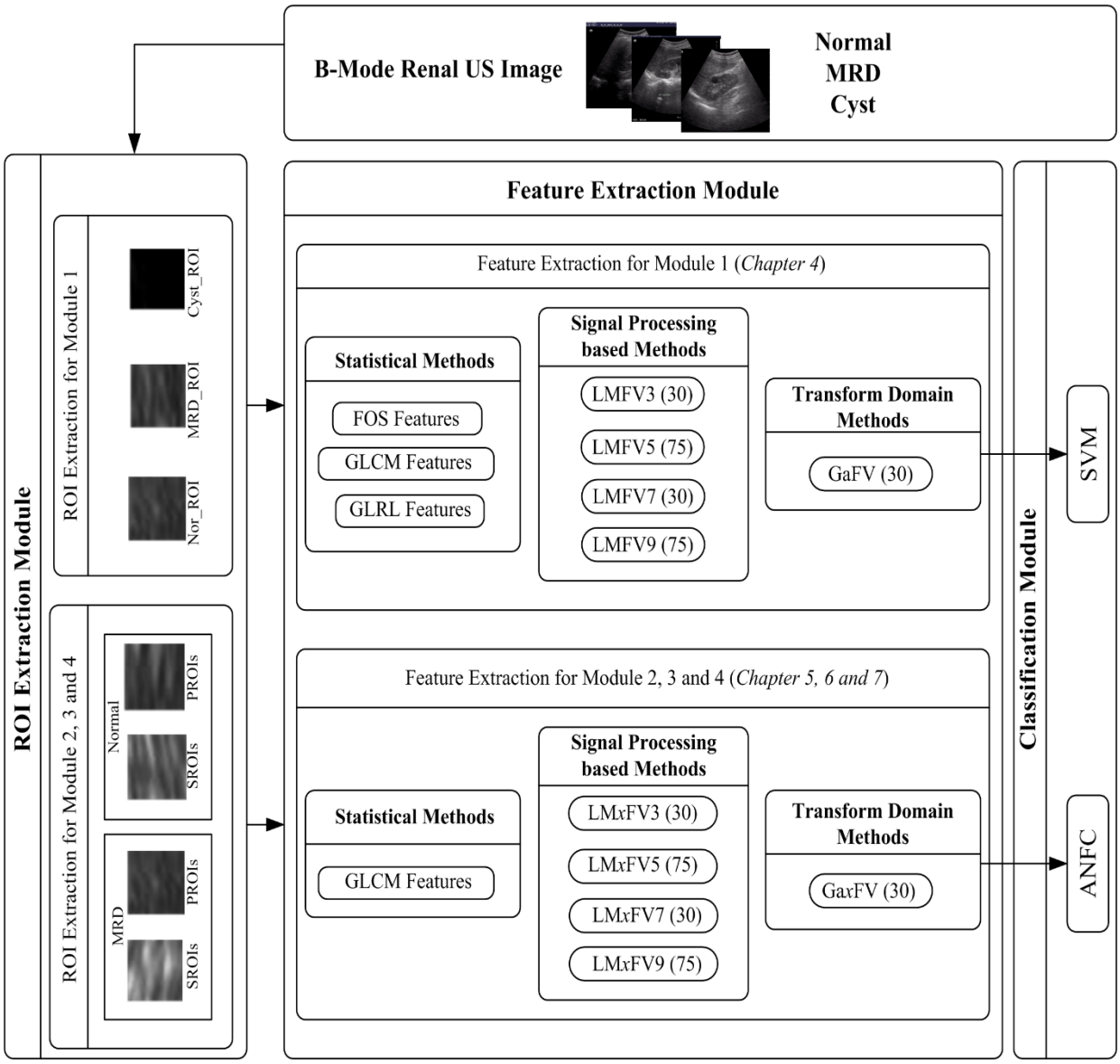


**Fig. 3.4** Workflow diagram for design of interactive system for diagnosis of renal diseases.
**Note**: FOS: First order statistics, GLCM: Gray level co-occurrence matrix, GLRL: Gray level run-length matrix, MRD: Medical renal disease, ROI: Region of interest, PROI: Parenchymal region of interest, SROI: Sinus region of interest, LMFV3: Laws' mask feature vector computed using 1D filter of length 3, LMFV5: Laws' mask feature vector computed using 1D filter of length 5, LMFV7: Laws' mask feature vector computed using 1D filter of length 7, LMFV9: Laws' mask feature vector computed using 1D filter of length 9, GaFV: Gabor feature vector, SVM: Support vector machine, ANFC: Absolute neuro-fuzzy classifier, *x*: absolute (A), ratio (R) and combined (C), *x*: absolute (A), ratio (R) and combined (C) for module 2, 3 and 4. For module 4, only LMCFV7 has been evaluated as Laws' mask filter of length 7 is yielding highest OCA among all Laws' mask feature vectors computed in module 2 and 3.

### 3.5.1 Module 1: SVM based CAC system for diagnosis of renal diseases

In this module, a CAC system to classify the renal US images into normal, MRD and cyst classes is proposed by exploring the potential of features extracted using statistical methods, signal processing based methods and transform domain methods. In statistical methods, the performance of FOS, GLCM method by varying the value of inter-pixel distance '*d'* from 1 to 10, and GLRL is evaluated.

In signal processing based methods, the performance of Laws' texture descriptors computed from Laws' mask 1D filters of lengths of 3, 5, 7 and 9 is evaluated. In transform domain methods, 2D Gabor features are computed by using 2D GWT considering 7 different orientations (22.5˚, 45˚, 67.5˚, 90˚, 112.5˚, 135˚, 157.5˚) and 3 scale values (0, 1, 2). The ROIs have been extracted from the renal parenchyma region of the kidney in case of normal and MRD classes and from regions inside the lesion for cyst image class. The SVM classifier is used for the classification task.

### 3.5.2 Module 2: ANFC based CAC system for diagnosis of MRD using absolute texture features

In this study, a CAC system to classify the renal US image into normal and MRD class is proposed by exploring the potential of features extracted using statistical methods, signal processing based methods and transform domain methods. In statistical methods, the performance of $GLCM_{mean}$ and $GLCM_{range}$ features at inter-pixel distance '*d'* = 1 is evaluated. In signal processing based methods, the performance of Laws' mask texture descriptors computed from Laws' mask 1D filters of lengths 3, 5, 7 and 9 is evaluated. In transform domain methods, 2D Gabor features are computed using Gabor wavelets obtained by using 7 different orientations (22.5˚, 45˚, 67.5˚, 90˚, 112.5˚, 135˚, 157.5˚) and 3 scale values (0, 1, 2). The PROIs have been extracted from the renal parenchyma region of the kidney for both normal and MRD renal US image classes. The ANFC is used for the classification task.

### 3.5.3 Module 3: ANFC based CAC system for diagnosis of MRD using texture ratio features

In this study, a CAC system to classify the renal US images into normal and MRD classes is proposed by exploring the potential of features extracted using statistical methods, signal processing based methods and transform domain methods. In statistical methods, the performance of $GLCM_{mean}$ and $GLCM_{range}$ features at inter-pixel distance '*d'* = 1 is evaluated.

In signal processing based methods, the performance of Laws' mask texture descriptors computed from Laws' 1D filters of lengths 3, 5, 7 and 9 is evaluated.

In transform domain methods, 2D Gabor features are computed using Gabor wavelets obtained by using 7 different orientations (22.5˚, 45˚, 67.5˚, 90˚, 112.5˚, 135˚, 157.5˚) and 3 scale values (0, 1, 2).

The PROIs have been extracted from the renal parenchyma region of the kidney and SROIs have been extracted from the renal sinus region (which lies approximately towards the center of renal parenchyma) for both normal and MRD renal US image classes. The ratio of features extracted from PROIs and SROIs is utilized for the classification task using ANFC.

### 3.5.4 Module 4: ANFC based CAC system for diagnosis of MRD using combined texture features

In this study, a CAC system to classify the renal US images into normal and MRD class is proposed by exploring the potential of features extracted using statistical methods, signal processing based methods and transform domain methods.

In statistical methods, the performance of $GLCM_{mean}$ and $GLCM_{range}$ features at inter-pixel distance '*d'* = 1 is evaluated. In signal processing methods, the performance of Laws' texture descriptors computed from Laws' mask 1D filters of length 7 is evaluated. In transform domain methods, 2D Gabor features are computed using Gabor wavelets obtained by using 7 different orientations (22.5˚, 45˚, 67.5˚, 90˚, 112.5˚, 135˚, 157.5˚) and 3 scale values (0, 1, 2).

The PROIs have been extracted from the renal parenchyma region of the kidney and SROIs have been extracted from the renal sinus region (which lies approximately towards the center of renal parenchyma) for both normal and MRD renal US image classes.

The combination of absolute texture features extracted from PROIs, and texture ratio features extracted from PROIs and SROIs is utilized for the classification task using ANFC.

## 3.6 Concluding Remarks

The chapter explained the methodology followed to design an efficient interactive system for classification of renal diseases. Various modules are defines for the design of different proposed CAC systems. The generalized block diagram of computer aided classification system for classification of renal diseases is given in Fig. 3.5.

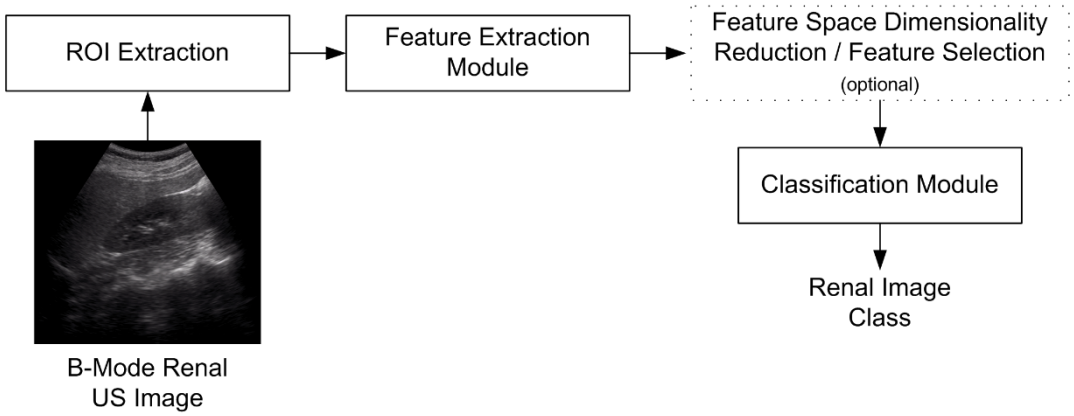


**Fig. 3.5** Generalized block diagram of computer aided classification system.

The ROIs extracted from image dataset are used as texture samples for feature extraction. The texture features extracted from ROIs are subjected to classification. The details of feature extraction and classification methods used in the experiments carried out in the present work, are discussed in detail in subsequent chapters.

# Chapter 4

# SVM based CAC System for Diagnosis of Renal Diseases

## 4.1 Introduction

Kidney performs important function of chemical regulation in human body which mainly involves parenchyma region. Thus, early diagnosis of renal diseases that hamper the normal functioning of kidney is clinically significant to avoid further complications such as renal cancer.

The real time, inexpensive, feasible, non-radioactive and non-invasive nature of ultrasound (US) imaging modality are some of the significant advantages due to which US is considered to be the primary choice for the imaging of soft organs however there are certain disadvantages associated with US such as (*a*) inter and intra-observer variability associated with interpretation of US image, (*b*) motion artefacts and (*c*) equipment limitations. These factors oppose the clarity of subjective diagnosis.

Addressing these limitations is important in order to develop an efficient CAC system based on US imaging modality. Although MRI and CT scan offer high sensitivity for diagnosis of renal diseases but they are costly and in CT the patient is also exposed to ionizing radiation and therefore, it is necessary to address the limitations which are posed by US imaging modality. Thus, the researchers have a keen interest in developing a system that provides possible objective aid to the radiologists to assist them in decision-making.

In the present work, an attempt has been made to design a CAC system for classification of renal US images into normal, MRD and cyst classes. The design of this system considers the ROIs extracted from renal parenchyma region for normal and MRD classes as the nature of echogenicity of parenchyma region changes (becomes hyperechoic as compared to normal) in case of MRD. For renal cyst, ROIs are extracted from region inside the renal lesion as they exhibit anechoic appearance.

The sample images of normal, MRD and cyst classes with ROIs marked are shown in Fig. 4.1. The SVM classifier is used for the classification task. Accordingly, in this chapter an efficient design of SVM based CAC system for diagnosis of renal diseases is proposed.

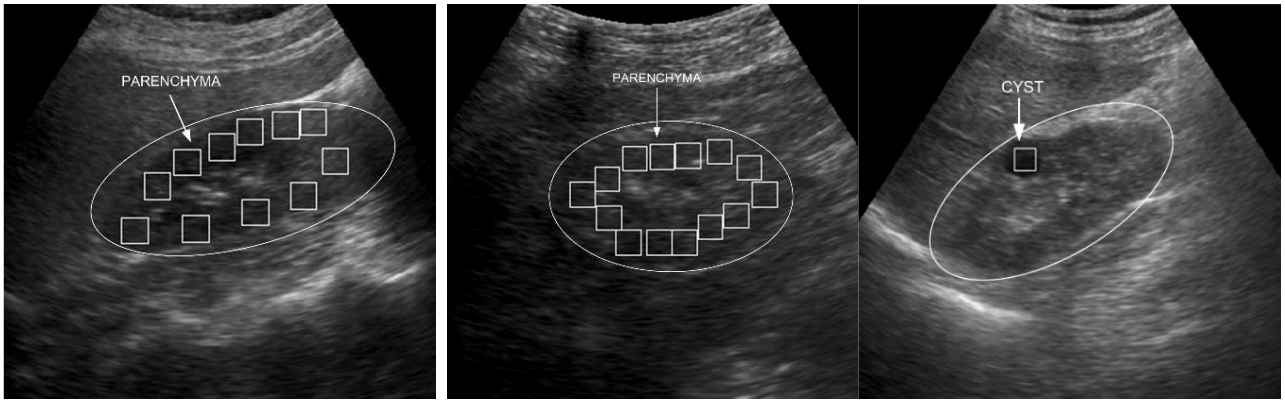


**Fig. 4.1** Sample US image of (*a*) normal, (*b*) MRD and (*c*) cyst with ROIs marked.
**Note**: ROI are extracted from renal parenchyma region in case of normal and MRD class, and region inside lesion for cyst class.

## 4.2 Dataset Description and its Bifurcation for Design of SVM based CAC System for Diagnosis of Renal Diseases

The present work has been carried out on 35 B-mode renal US images consisting of 11 normal, 8 MRD and 16 cyst images. The brief description of image assessment protocols and data collection protocols are defined in chapter 3, section 3.3 and 3.4.1 respectively.

The ROIs of size 25 × 25 pixels have been extracted from the parenchyma region of the kidney in case of normal and MRD classes and from region inside the lesion for cyst image class. The brief description of the ROI extraction protocols is given in chapter 3, section 3.4.2.1 (*ii*).

A total of 120 ROIs are extracted from 11 normal images, 119 ROIs are extracted from 8 MRD images and 83 ROIs are extracted from 16 cyst images. These ROIs are bifurcated to form training and testing data sets for classification purposes.

A brief description of dataset bifurcation protocol into training and testing sets is given in chapter 3, section 3.4.3 (*i*). Image dataset and its bifurcation into training and testing datasets for classification is depicted in Fig. 4.2. A total of 120 normal, 119 MRD and 83 cyst ROIs have been extracted from normal, MRD and cyst renal US image.

These ROIs are bifurcated into training and testing sets. A care is taken that ROIs of a particular image belongs to either of training or testing set for unbiased classification.

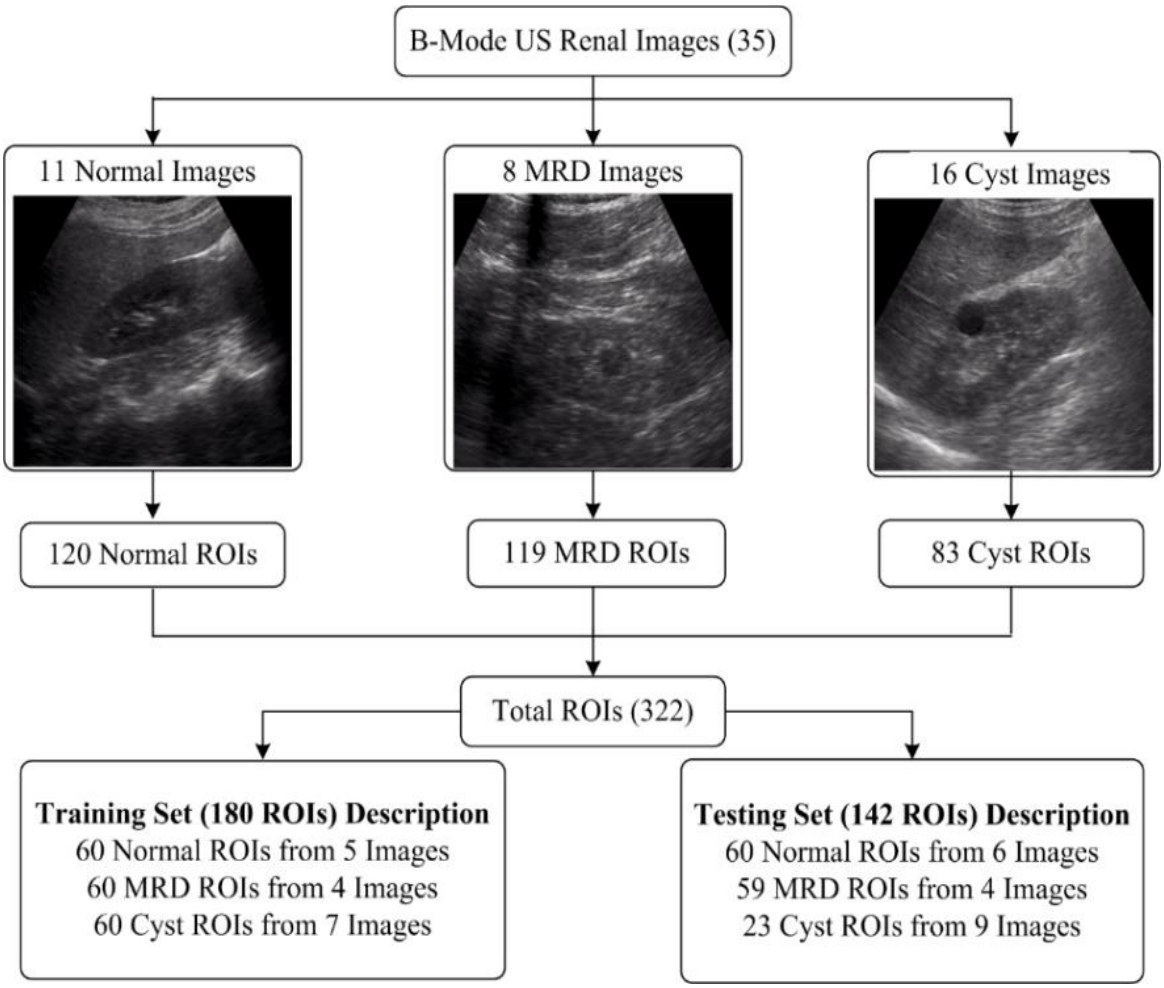


**Fig. 4.2** Dataset description and its bifurcation into training and testing sets.
**Note**: MRD: Medical renal disease, ROI: Region of interest.

## 4.3 Experimental Workflow for the Design of SVM based CAC System for Diagnosis of Renal Diseases

The block diagram of the experimental workflow adopted for design of SVM based CAC system for diagnosis of renal diseases is shown in Fig. 4.3. For evaluating the performance of the proposed CAC system, rigorous experimentation has been carried out for the classification of renal diseases.

The ROI extraction (as discussed above) is followed by feature extraction and classification. Feature extraction has been performed using statistical, signal processing and transform domain methods. Classification is performed using SVM classifier.

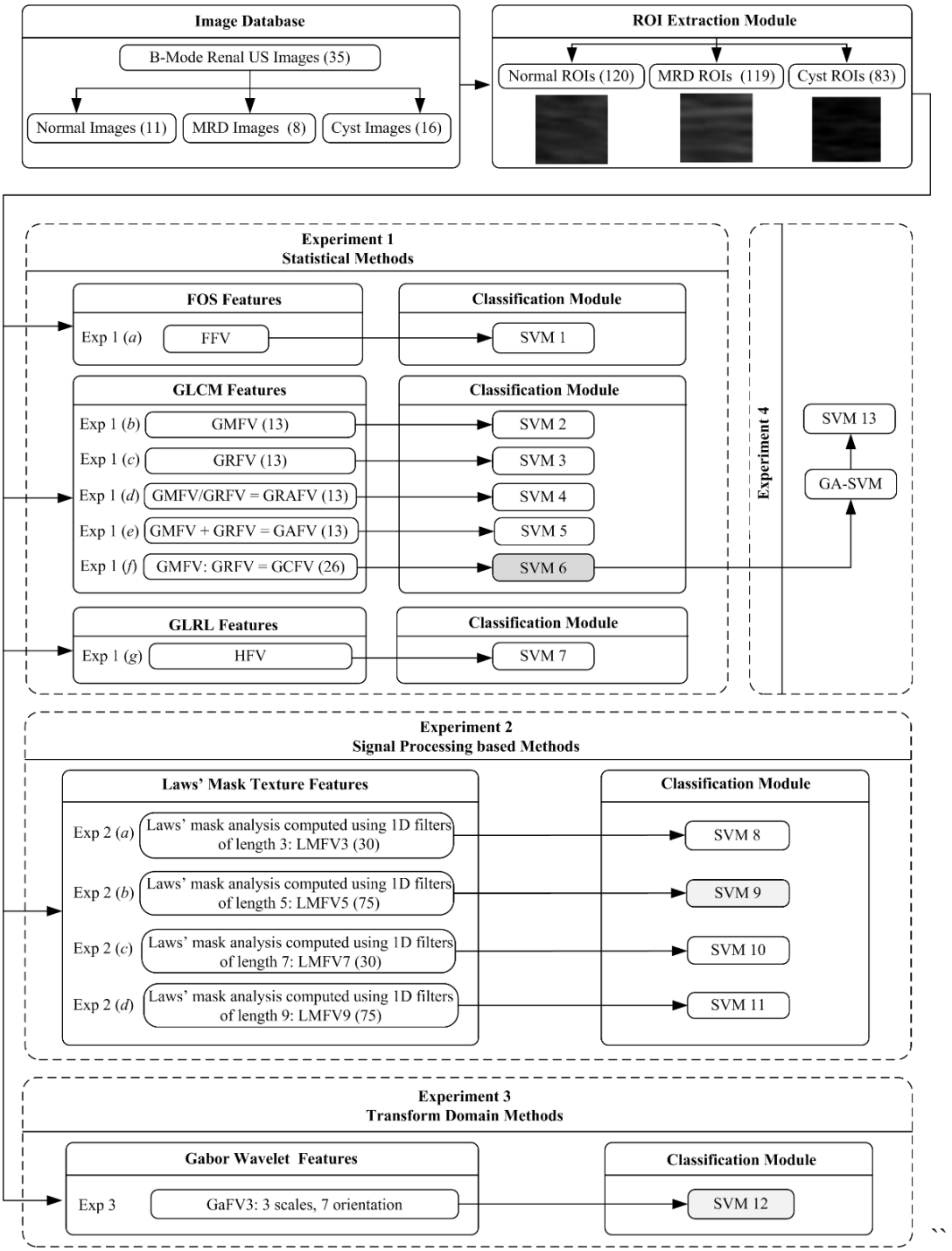


**Fig. 4.3** Experimental workflow for design of SVM based CAC system for diagnosis of renal disease.
**Note**: MRD: Medical renal disease, FOS: First order statistics, GLCM: Gray level co-occurrence matrix, GLRL: Gray level run length matrix, FFV: First order feature vector, HFV: Higher order feature vector, GMFV: $GLCM_{mean}$ feature vector, GRFV: $GLCM_{range}$ feature vector, GRaFV: GLCM ratio feature vector, GAFV: GLCM additive feature vector, GCFV: GLCM combined feature vector, LMFV3: Laws' mask feature vector computed using 1D filter of length 3, LMFV5: Laws' mask feature vector computed using 1D filter of length 5, LMFV7: Laws' mask feature vector computed using 1D filter of length 7, LMFV9: Laws' mask feature vector computed using 1D filter of length 9, GaFV: Gabor feature vector, SVM: Support vector machine, Exp: Experiment.

The brief description of the feature vectors for the design of SVM based CAC system for diagnosis of renal diseases is given in Table 4.1.

**Table 4.1** Brief description of feature vectors used for the design of SVM based CAC system for diagnosis of renal diseases.

| FV | Description | *l* |
|---|---|---|
| FFV | First order feature vector | 10 |
| GMFV | $GLCM_{mean}$ feature vector | 13 |
| GRFV | $GLCM_{range}$ feature vector | 13 |
| GRaFV | GLCM ratio feature vector | 13 |
| GAFV | GLCM additive feature vector | 13 |
| GCFV | GLCM combined feature vector | 26 |
| HFV | Higher order feature vector | 11 |
| LMFV3 | Laws' mask feature vector computed using 1D filter of length 3 | 30 |
| LMFV5 | Laws' mask feature vector computed using 1D filter of length 5 | 45 |
| LMFV7 | Laws' mask feature vector computed using 1D filter of length 7 | 30 |
| LMFV9 | Laws' mask feature vector computed using 1D filter of length 9 | 45 |
| GaFV | Gabor feature vector | 42 |

**Note**: FV: Feature vector, *l*: length of the feature vector, GLCM: Gray level co-occurrence matrix.

The brief description of the experiments carried out in the present work is given below:

*4.3.1 Experiment 1: Design of CAC system for renal diseases using statistical methods.*

As discussed earlier, the ROIs have been extracted from renal parenchyma region for normal and MRD classes, and from region inside the lesion for cyst class. In this experiment, feature extraction is performed using statistical methods. The classification of renal US images into normal, MRD and cyst classes is carried out using SVM classifier. The diagram for the experimental workflow for carrying out experiment 1 is given in Fig 4.4.

A brief description of the experiment is given below:

(*a*) *Feature Extraction Module*

Variety of methods (such as statistical, signal processing and transform domain methods) are available to extract the textural features. In this module, the potential of features obtained by using statistical methods (FOS, GLRL and GLCM) is evaluated for differential diagnosis between normal, MRD and cyst classes.

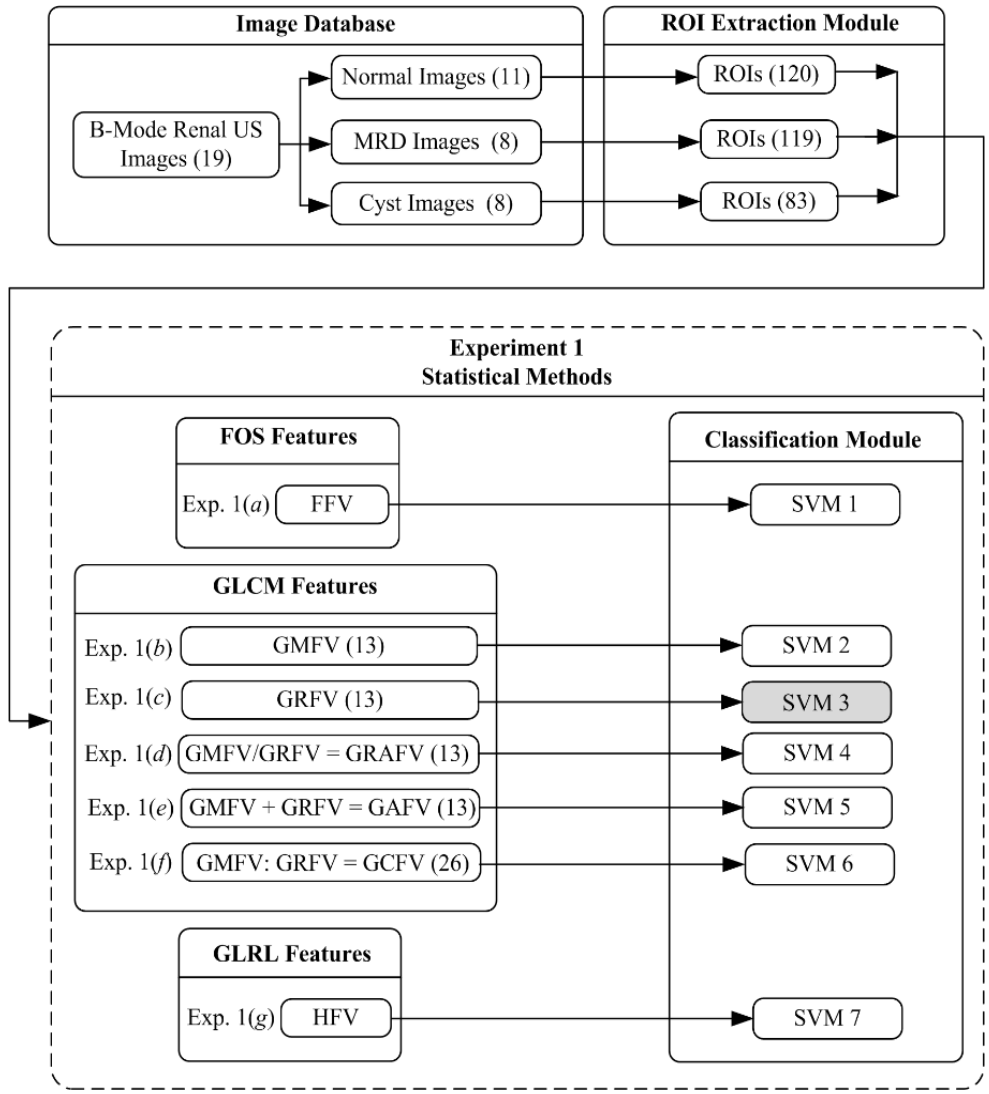


**Fig. 4.4** Workflow diagram of experiment 1: CAC system for diagnosis of renal diseases using statistical methods based feature vectors.
**Note**: MRD: Medical renal disease, FOS: First order statistics, GLCM: Gray level co-occurrence matrix, GLRL: Gray level run length matrix, FFV: First order feature vector, HFV: Higher order feature vector, GMFV: $GLCM_{mean}$ feature vector, GRFV: $GLCM_{range}$ feature vector, GRaFV: GLCM ratio feature vector, GAFV: GLCM additive feature vector, GCFV: GLCM combined feature vector, SVM: Support vector machine, Exp: Experiment.

*First Order Statistics (FOS)*: The FOS estimate the properties of an individual pixel value i.e., these statistics do not consider the spatial interaction between different image pixels. Ten FOS features namely, average grey level, standard deviation, smoothness, third moment, uniformity, entropy, variance, skewness, kurtosis and energy are extracted to form a first order feature vector (FFV) of length 10 [49,58-62].

*Second Order Statistics- GLCM Features*: The GLCM statistical features are derived by considering spatial relationship between two pixels. The occurrence of different combinations of pixel pairs of a specific gray level in an image is tabulated in GLCM.

The GLCM is formed for each ROI image for inter-pixel distance $d \in \{1, 2, 3 \ldots 10\}$ and direction $\theta° \in \{0°, 45°, 90°, 135°\}$. The four directional GLCM features (i.e. angular second moment (ASM), contrast (Cont), correlation (Corr), inverse difference moment (IDM), variance (Var), sum average (Sum Av), sum variance (Sum Var), difference variance (Diff Var), entropy (Ent), sum entropy (Sum Ent), difference entropy (Diff Ent), information measures of correlation-1 (InfMCorr1) and information measures of correlation-2 (InfMCorr2)) are computed for each inter-pixel distance $d \in \{1, 2, 3 \ldots, 10\}$.

From the computed four directional GLCM features, the $GLCM_{mean}$ feature vector (GMFV) and $GLCM_{range}$ feature vector (GRFV) are derived for different inter-pixel distances $d = i \in \{1, 2, 3 \ldots, 10\}$. For example the value of $ASM_{mean}$ and $ASM_{range}$ is computed by using equations (1 – 4) [56, 63-72].

$$ASM_{mean(d=i)} = \frac{ASM_{(0^o,d=i)} + ASM_{(45^o,d=i)} + ASM_{(90^o,d=i)} + ASM_{(135^o,d=i)}}{4} \quad (1)$$

$$ASM_{\max(d=i)} = \max(ASM_{(0^o,d=i)}, ASM_{(45^o,d=i)}, ASM_{(90^o,d=i)}, ASM_{(135^o,d=i)}) \quad (2)$$

$$ASM_{\min(d=i)} = \min(ASM_{(0^o,d=i)}, ASM_{(45^o,d=i)}, ASM_{(90^o,d=i)}, ASM_{(135^o,d=i)}) \quad (3)$$

$$ASM_{range\,(d=i)} = (ASM\_\max)_{(d=i)} - (ASM\_\min)_{(d=i)} \quad (4)$$

Here, $ASM_{0^o}$, $ASM_{45^o}$, $ASM_{90^o}$, $ASM_{135^o}$ are angular second moment values, calculated at 0º, 45º, 90º and 135º respectively. $ASM_{\max}$ and $ASM_{\min}$ denote the maximum and minimum values among all the four directions.

The GMFV and GRFV are combined in various ways to form three other feature vectors such as (*a*) division (GRaFV: GLCM ratio feature vector, computed by taking the ratio of GMFV and GRFV), (*b*) addition (GAFV: GLCM additive feature vector, computed by adding GMFV and GRFV) and (*c*) concatenation (GCFV: GLCM combined feature vector computed by concatenating the GMFV and GRFV).

*Higher Order Statistics- GLRL Features*: The gray level run length statistics consider interaction between two or more than two image pixels i.e. the sequence in which the same data value occurs in many consecutive data elements [73-75]. Higher order statistics (HOS) based GLRL features namely, short run emphasis, long run emphasis, gray level non-uniformity, run length non-uniformity, run percentage, low gray level run emphasis, high gray level run-emphasis, short run low gray level emphasis, short run high gray level emphasis, long run low gray level emphasis and long run high gray level emphasis are extracted to form a higher order feature vector (HFV) of length 11.

The extracted features are subjected to classification module for the classification task. The brief description of classification module is given below:

(*b*) *Classification Module*

The SVM classifier has been used for the classification task [40, 44, 60, 65, 70, 76-81]. For the detailed description SVM and its parameter optimization the readers are directed to the studies [76-81].

The results obtained after conducting experiment 1 are given below:

*4.3.1.1 Experiment 1(a): Evaluating the classification performance of FOS feature vector (FFV).*

In this experiment, classification performance of FFV is evaluated using SVM classifier. The results of the experiment are shown in Table 4.2.

**Table 4.2** Classification performance of FFV using SVM classifier for three class classification of renal US images.

| **FV (*l*)** | **CM** | | | | **OCA** | **ICA** |
|---|---|---|---|---|---|---|
| | | NOR | MRD | CYST | | |
| **FFV** (10) | NOR | 34 | 26 | 0 | 72.5 | 56.6 |
| | MRD | 12 | 47 | 0 | | 79.6 |
| | CYST | 1 | 0 | 22 | | 95.6 |

**Note:** FV: Feature vector, ***l***: length of the feature vector, CM: Confusion matrix, FFV: First order feature vector, NOR: Normal class, MRD: Medical renal disease class, OCA: Overall classification accuracy, ICA: Individual class accuracy. OCA and ICA values are expressed in percentage.

From Table 4.2, it is observed that maximum overall classification accuracy (OCA) of 72.5 % has been obtained with 10 different FOS features along with individual class accuracy (ICA) values of 56.6 %, 79.6 % and 95.6 % for normal, MRD and cyst classes respectively.

*4.3.1.2 Experiment 1(b): Evaluating the classification performance of $GLCM_{mean}$ feature vector (GMFV).*

In this experiment, classification performance of GMFV obtained by varying inter-pixel distance '*d'* from 1 to 10, is evaluated using SVM classifier. The results of the experiment are shown in Table 4.3.

**Table 4.3** Classification performance of GMFV for inter-pixel distance '*d'* varying from 1 to 10 using SVM classifier.

| FV (*l*) | *'d'* | OCA | $ICA_{NOR}$ | $ICA_{MRD}$ | $ICA_{Cyst}$ |
|---|---|---|---|---|---|
| **GMFV** (13) | 1 | 84.5 | 83.3 | 83.0 | 91.3 |
| | 2 | 83.1 | 81.6 | 79.6 | 95.6 |
| | 3 | 73.9 | 75 | 64.4 | 95.6 |
| | 4 | 78.1 | 75 | 74.5 | 95.6 |
| | 5 | 81.6 | 50.8 | 95.6 | 67.6 |
| | 6 | 66.9 | 70 | 52.5 | 95.6 |
| | 7 | 66.9 | 56.6 | 66.1 | 95.6 |
| | 8 | 76 | 73.3 | 71.1 | 95.6 |
| | 9 | 69.7 | 60 | 69.4 | 95.6 |
| | 10 | 70.4 | 61.6 | 69.4 | 95.6 |

**Note:** FV: Feature vector, *l*: length of the feature vector, *d*: Inter pixel distance, GMFV: $GLCM_{mean}$ feature vector, OCA: Overall classification accuracy, ICA: Individual class accuracy, NOR: Normal, MRD: Medical renal disease, $ICA_{NOR}$: ICA value for NOR class, $ICA_{MRD}$: ICA value for MRD class, $ICA_{Cyst}$ :ICA value for Cyst class, The OCA and ICA values are expressed in percentage.

From Table 4.3, it is observed that maximum OCA of 84.5 % has been obtained with 13 different $GLCM_{mean}$ features computed at inter-pixel distance '*d'* = 1 along with ICA value of 83.3 %, 83.0 % and 91.3 % for normal, MRD and cyst renal US image classes respectively.

*4.3.1.3 Experiment 1(c): Evaluating the classification performance of $GLCM_{range}$ feature vector (GRFV).*

In this experiment, classification performance of GRFV obtained by varying inter-pixel distance '*d'* from 1 to 10, is evaluated using SVM classifier. The results of the experiment are shown in Table 4.4.

**Table 4.4** Classification performance of GRFV for inter-pixel distance '*d'* varying from 1 to 10 using SVM classifier.

| FV (*l*) | *'d'* | OCA | $ICA_{NOR}$ | $ICA_{MRD}$ | $ICA_{Cyst}$ |
|---|---|---|---|---|---|
| **GRFV** (13) | 1 | 83.8 | 88.3 | 76.2 | 91.3 |
| | 2 | 78.1 | 80.0 | 72.8 | 86.9 |
| | 3 | 76.7 | 76.6 | 71.1 | 91.3 |
| | 4 | 66.2 | 63.3 | 61 | 86.9 |
| | 5 | 66.2 | 68.3 | 55.9 | 86.9 |
| | 6 | 69.0 | 76.6 | 54.2 | 86.9 |
| | 7 | 62.6 | 75.0 | 40.6 | 86.9 |
| | 8 | 64.0 | 73.3 | 47.4 | 82.6 |
| | 9 | 64.0 | 70.0 | 52.5 | 78.2 |
| | 10 | 67.1 | 83.3 | 45.7 | 82.6 |

**Note:** FV: Feature vector, *l*: length of the feature vector, *d*: Inter pixel distance, GRFV: $GLCM_{range}$ feature vector, OCA: Overall classification accuracy, ICA: Individual class accuracy, NOR: Normal class, MRD: Medical renal disease, $ICA_{NOR}$ : ICA value for NOR class, $ICA_{MRD}$ :ICA value for MRD class, $ICA_{Cyst}$ :ICA value for Cyst class, The OCA and ICA values are expressed in percentage.

From Table 4.4, it is observed that maximum OCA of 83.8 % has been obtained with 13 different $GLCM_{range}$ features computed at inter-pixel distance '*d'* = 1 along with ICA value of 88.3 %, 76.2 % and 91.3 % for normal, MRD and cyst renal US image classes respectively.

*4.3.1.4 Experiment 1(d): Evaluating the classification performance of GLCM ratio feature vector (GRaFV).*

In this experiment, classification performance of GRaFV obtained by varying inter-pixel distance '*d'* from 1 to 10, is evaluated using SVM classifier. The results of the experiment are shown in Table 4.5.

**Table 4.5** Classification performance of GRaFV for inter-pixel distance '*d'* varying from 1 to 10 using SVM classifier.

| FV (*l*) | *'d'* | OCA | $ICA_{NOR}$ | $ICA_{MRD}$ | $ICA_{Cyst}$ |
|---|---|---|---|---|---|
| **GRaFV** (13) | 1 | 78.8 | 73.3 | 81.3 | 86.9 |
| | 2 | 78.1 | 76.6 | 77.9 | 82.6 |
| | 3 | 72.5 | 61.6 | 77.9 | 86.9 |
| | 4 | 71.8 | 70 | 67.7 | 86.9 |
| | 5 | 66.2 | 56.6 | 69.4 | 82.6 |
| | 6 | 64.7 | 60 | 62.7 | 82.6 |
| | 7 | 58.4 | 60.0 | 49.1 | 78.2 |
| | 8 | 56.3 | 65 | 38.9 | 78.2 |
| | 9 | 54.2 | 45 | 52.2 | 78.2 |
| | 10 | 63.3 | 75 | 44 | 82.6 |

**Note:** FV: Feature vector, *l*: length of feature vector, *d*: Inter pixel distance, GRaFV: GLCM ratio feature vector, OCA: Overall classification accuracy, ICA: Individual class accuracy, NOR: Normal class, MRD: Medical renal disease, $ICA_{NOR}$: ICA value for NOR class, $ICA_{MRD}$: ICA value for MRD class, $ICA_{Cyst}$: ICA value for Cyst class, The OCA and ICA values are expressed in percentage.

From Table 4.5, it is observed that maximum OCA of 78.8 % has been obtained with 13 different GLCM ratio features computed at inter-pixel distance '*d'* = 1 along with ICA value of 73.3 %, 81.3 % and 86.9 % for normal, MRD and cyst renal US image classes respectively.

*4.3.1.5 Experiment 1(e): Evaluating the classification performance of GLCM additive feature vector (GAFV).*

In this experiment, classification performance of GAFV obtained by varying inter-pixel distance '*d'* from 1 to 10, is evaluated using SVM classifier. The results of the experiment are shown in Table 4.6.

**Table 4.6** Classification performance of GAFV for inter-pixel distance '*d'* varying from 1 to 10 using SVM classifier.

| FV (*l*) | *'d'* | OCA | $ICA_{NOR}$ | $ICA_{MRD}$ | $ICA_{Cyst}$ |
|---|---|---|---|---|---|
| **GAFV** (13) | 1 | 80.2 | 81.6 | 74.5 | 91.3 |
| | 2 | 80.2 | 78.3 | 76.2 | 95.6 |
| | 3 | 74.6 | 65 | 77.9 | 91.3 |
| | 4 | 71.8 | 70 | 64.4 | 95.6 |
| | 5 | 71.8 | 66.7 | 67.7 | 95.6 |
| | 6 | 68.3 | 63.3 | 64.4 | 91.3 |
| | 7 | 72.5 | 61.6 | 74.5 | 95.6 |
| | 8 | 69.7 | 56.6 | 74.5 | 91.3 |
| | 9 | 64.7 | 53.3 | 64.4 | 95.6 |
| | 10 | 61.2 | 50 | 61 | 91.3 |

**Note:** FV: Feature vector, *l*: length of feature vector, GAFV: GLCM additive feature vector, *d*: Inter pixel distance, OCA: Overall classification accuracy, ICA: Individual class accuracy, NOR: Normal class, MRD: Medical renal disease, $ICA_{NOR}$: ICA value for NOR class, $ICA_{MRD}$: ICA value for MRD class, $ICA_{Cyst}$: ICA value for Cyst class, The OCA and ICA values are expressed in percentage.

From Table 4.6, it is observed that maximum OCA of 80.2 % has been obtained with 13 different GLCM ratio features computed at inter-pixel distance '*d'* = 1 along with ICA values of 81.6 %, 74.5 % and 91.3 % for normal, MRD and cyst renal US image class.

*4.3.1.6 Experiment 1(f): Evaluating the classification performance of GLCM combined feature vector (GCFV).*

In this experiment, classification performance of GCFV obtained by varying inter-pixel distance '*d'* from 1 to 10, is evaluated using SVM classifier. The results of the experiment are shown in Table 4.7.

**Table 4.7** Classification performance of GCFV for inter-pixel distance *'d'* varying from 1 to 10 using SVM classifier.

| FV (*l*) | *'d'* | OCA | $ICA_{NOR}$ | $ICA_{MRD}$ | $ICA_{Cyst}$ |
|---|---|---|---|---|---|
| **GCFV** (26) | 1 | 85.9 | 86.6 | 83.0 | 91.3 |
| | 2 | 81.6 | 83.3 | 89.7 | 95.6 |
| | 3 | 79.5 | 78.3 | 74.5 | 95.6 |
| | 4 | 70.4 | 70.0 | 61.0 | 95.6 |
| | 5 | 73.2 | 65 | 72.8 | 95.6 |
| | 6 | 69.7 | 63.3 | 67.7 | 91.3 |
| | 7 | 65.4 | 68.3 | 52.5 | 91.3 |
| | 8 | 69.7 | 63.3 | 67.7 | 91.3 |
| | 9 | 68.3 | 58.3 | 69.4 | 91.3 |
| | 10 | 59.8 | 43.3 | 66.1 | 86.9 |

**Note:** FV: Feature vector, *l*: length of the feature vector, *d*: Inter pixel distance, GCFV: GLCM combined feature vector, OCA: Overall classification accuracy, ICA: Individual class accuracy, NOR: Normal class, MRD: Medical renal disease, $ICA_{NOR}$**:** ICA value for NOR class, $ICA_{MRD}$: ICA value for MRD class, $ICA_{Cyst}$ : ICA value for Cyst class, The OCA and ICA values are expressed in percentage.

From Table 4.7, it is observed that maximum OCA of 85.9 % has been obtained with 26 combined $GLCM_{mean}$ and $GLCM_{range}$ features computed at inter-pixel distance '*d'* = 1 along with ICA value of 86.6 %, 83.0 % and 91.3 % for normal, MRD and cyst renal US image classes respectively.

*4.3.1.7 Experiment 1(g): Evaluating the classification performance of higher order feature vector (HFV).*

In this experiment, classification performance of HFV is evaluated using SVM classifier. The results of the experiment are shown in Table 4.8.

**Table 4.8** Classification performance of HFV using SVM classifier for three classes of renal US Images.

| FV (*l*) | CM | | | | OCA | ICA |
|---|---|---|---|---|---|---|
| | | NOR | MRD | CYST | | |
| **HFV** (11) | NOR | 38 | 22 | 0 | 71.8 | 63.3 |
| | MRD | 17 | 42 | 0 | | 71.1 |
| | CYST | 1 | 0 | 22 | | 95.6 |

**Note:** FV: Feature vector, *l*: length of feature vector, HFV: Higher order feature vector, CM: Confusion matrix, MRD: Medical renal disease class, NOR: Normal class, OCA: Overall classification accuracy, ICA: Individual class accuracy, The OCA and ICA values are expressed in percentage.

From Table 4.8, it is observed that OCA of 71.8 % has been obtained with 11 GLRL features along with ICA value of 63.3 %, 71.1 % and 95.6 % for normal, MRD and cyst renal US image classes respectively.

*From experiment 1, it is observed that for features extracted using statistical methods, maximum OCA of 85.9 % has been obtained with combined $GLCM_{mean}$ and $GLCM_{range}$ feature vector (GCFV) computed at inter-pixel distance 'd' = 1 along with ICA values of 86.6 %, 83.0 % and 91.3 % for normal, MRD and cyst image classes respectively. The detailed result obtained from concatenation of $GLCM_{mean}$ and $GLCM_{range}$ is given in Table 4.9.*

**Table 4.9** Classification performance of GCFV using SVM classifier for three classification of renal US Images at inter-pixel distance '*d*'=1.

| **FV (*l*)** | **CM** | | | | **OCA** | **ICA** |
|---|---|---|---|---|---|---|
| | | NOR | MRD | CYST | | |
| **GCFV** (26) | NOR | 52 | 7 | 1 | 85.9 | 86.6 |
| | MRD | 10 | 49 | 0 | | 83.0 |
| | CYST | 2 | 0 | 21 | | 91.3 |

**Note:** FV: Feature vector, *l*: length of the feature vector, GCFV: GLCM combined feature vector, CM: Confusion matrix, NOR: Normal class, MRD: Medical renal disease class, OCA: Overall classification accuracy, ICA: Individual class accuracy, The OCA and ICA values are expressed in percentage.

### *4.3.2 Experiment 2: Design of CAC system for classification of renal diseases using features computed from signal processing based methods.*

As discussed earlier, the ROIs have been extracted from renal parenchyma region for normal and MRD classes, and from region inside the lesion for renal cyst renal US image class. In this experiment, feature extraction is performed using features obtained from signal processing methods. The classification of US images into normal, MRD and cyst classes is carried out using SVM classifier.

The diagram for the experimental workflow for experiment 2 is given in Fig 4.5. Brief description of the experiment is given below:

(*a*) *Feature Extraction Module*

In this module, the potential of signal processing based, Laws' mask texture features computed using 1D filters of length 3, 5, 7 and 9 is evaluated for differential diagnosis between normal, MRD and cyst renal disease.

*Laws' mask texture features*: Laws' masks features computed using 1D filter of length 3, 5, 7 and 9 are used to compute five statistical parameters i.e. mean, standard deviation, skewness, kurtosis and entropy from each ROI [82-88].

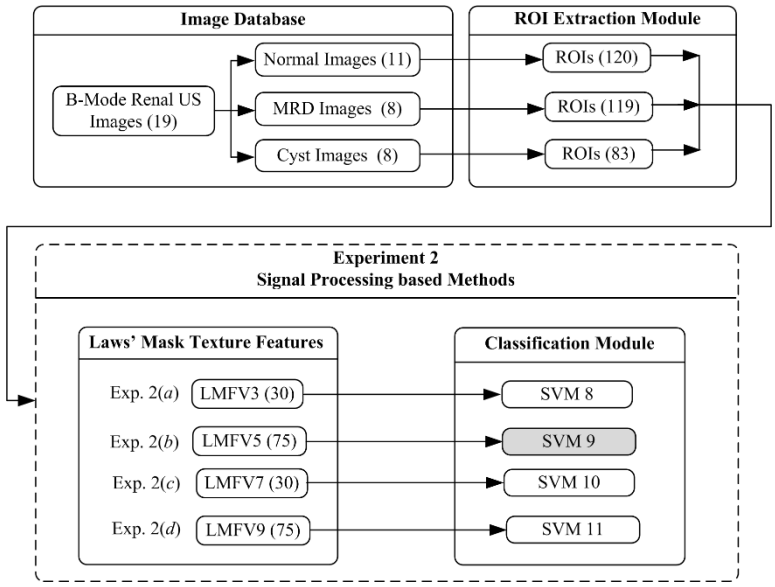


**Fig. 4.5** Workflow diagram of experiment 2: CAC system for diagnosis of renal diseases using Laws' mask feature vectors (LMFVs).
**Note**: MRD: Medical renal disease, LMFV3: Laws' mask feature vector computed using 1D filter of length 3, LMFV5: Laws' mask feature vector computed using 1D filter of length 5, LMFV7: Laws' mask feature vector computed using 1D filter of length 7, LMFV9: Laws' mask feature vector computed using 1D filter of length 9, SVM: Support vector machine, Exp: Experiment.

Description of Laws' masks features computed using 1D filter of different lengths is given in Table 4.10.

**Table 4.10** Description of Laws' mask of different lengths

| Length of 1-D filter | 1-D filter coefficients | No. of 2D Laws' mask | No. of TR images |
|---|---|---|---|
| 3 | L3= [1, 2, 1]<br>E3= [-1, 0, 1]<br>S3= [-1, 2, -1] | 9 | 6 |
| 5 | L5= [1, 4, 6, 4, 1]<br>E5= [−1, −2, 0, 2, 1]<br>S5= [−1, 0, 2, 0, −1]<br>W5= [−1, 2, 0, −2 1]<br>R5= [1, −4, 6, −4, 1] | 25 | 15 |
| 7 | L7= [1, 6, 15, 20, 15, 6, 1]<br>E7= [−1 −4, −5, 0, 5, 4, 1]<br>S7= [−1, −2, 1, 4, 1, −2, −1] | 9 | 6 |
| 9 | L9= [1, 8, 28, 56, 70, 56, 28, 8, 1]<br>E9= [1, 4, 4, −4, −10, −4, 4, 4, 1]<br>S9= [1, 0, −4, 0, 6, 0, −4, 0, 1]<br>W9= [1, −4, 4, −4, −10, 4, 4, −4, 1]<br>R9= [1, −8, 28, −56, 70, −56, 28, −8, 1] | 25 | 15 |

**Note**: TR: Rotation invariant texture images.

An algorithm to carry out Laws' mask analysis using special 1D filters of length 5 is shown in Fig. 4.6.

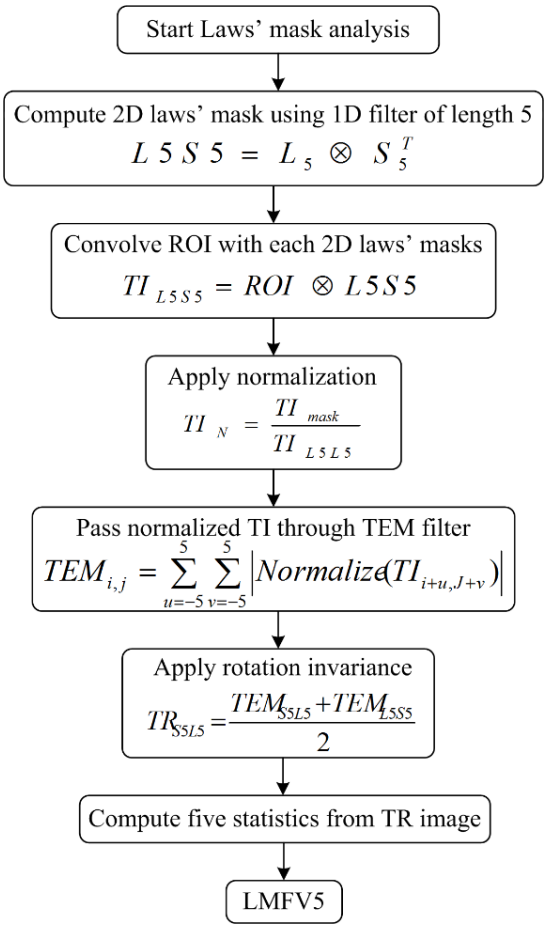


**Fig. 4.6** Laws' mask analysis algorithm using special 1D filters of length 5

Laws' masks analysis using 1D filters of length 3, 5, 7 and 9 are used to compute different feature vectors as (*a*) LMFV3 (Laws' mask feature vector computed using 1D filter of length 3), (*b*) LMFV5 (Laws' mask feature vector computed using 1D filter of length 5), (*c*) LMFV7 (Laws' mask feature vector computed using 1D filter of length 7) and (*d*) LMFV9 (Laws' mask feature vector computed using 1D filter of length 9).

(*b*) *Classification module*

The brief description of classification module is given in section 4.3.1 (*b*). The results obtained after conducting experiment 2 are given below:

*4.3.2.1 Experiment 2(a): Evaluating the classification performance of Laws' mask feature vector computed using 1D filter of length 3 (LMFV3)*

In this experiment, classification performance of LMFV3 is evaluated using SVM classifier. The results of the experiment are shown in Table 4.11.

**Table 4.11** Classification performance of texture features obtained by LMFV3 using SVM classifier.

| FV (*l*) | CM | | | | OCA | ICA |
|---|---|---|---|---|---|---|
| | | NOR | MRD | CYST | | |
| **LMFV3** (30) | NOR | 43 | 17 | 0 | 76.6 | 71.6 |
| | MRD | 15 | 44 | 0 | | 74.5 |
| | CYST | 2 | 0 | 21 | | 91.3 |

**Note:** FV: Feature vector, *l*: length of the feature vector, LMFV3: Laws' mask feature vector computed using 1D filter of length 3, CM: Confusion matrix, NOR: Normal class, MRD: Medical renal disease class, OCA: Overall classification accuracy, ICA: Individual class accuracy, The OCA and ICA values are expressed in percentage.

From Table 4.11, it is observed that an OCA of 76.6 % has been obtained with 30 Laws' mask features obtained using 1D filter of length 3, along with ICA values of 71.6 %, 74.5 % and 91.3 % for normal, MRD and cyst renal US image classes respectively.

*4.3.2.2 Experiment 2(b): Evaluating the classification performance of Laws' mask feature vector computed using 1D filter of length 5 (LMFV5)*

In this experiment, classification performance of LMFV5 is evaluated using SVM classifier. The results of the experiment are shown in Table 4.12.

**Table 4.12** Classification performance of texture features obtained by LMFV5 using SVM classifier.

| FV (*l*) | CM | | | | OCA | ICA |
|---|---|---|---|---|---|---|
| | | NOR | MRD | CYST | | |
| **LMFV5** (75) | NOR | 48 | 11 | 1 | 79.5 | 80.0 |
| | MRD | 15 | 44 | 0 | | 74.5 |
| | CYST | 2 | 0 | 21 | | 91.3 |

**Note:** FV: Feature vector, *l*: length of the feature vector, LMFV5: Laws' mask feature vector computed using 1D ilter of length 5, CM: Confusion matrix, MRD: Medical renal disease class, NOR: Normal class, OCA: Overall lassification accuracy, ICA: Individual class accuracy, The OCA and ICA values are expressed in percentage.

From Table 4.12, it is observed that an OCA of 79.5 % has been obtained with 75 Laws' mask features computed using 1D filter of length 5, along with ICA values of 80.0 %, 74.5 % and 91.3 % for normal, MRD and cyst renal US image classes respectively.

*4.3.2.3 Experiment 2(c): Evaluating the classification performance of Laws' mask feature vector computed using 1D filter of length 7 (LMFV7)*

In this experiment, classification performance of LMFV7 is evaluated using SVM classifier. The results of the experiment are shown in Table 4.13.

**Table 4.13** Classification performance of texture features obtained by LMFV7 using SVM classifier.

| FV (*l*) | CM | | | | OCA | ICA |
|---|---|---|---|---|---|---|
| | | NOR | MRD | CYST | | |
| **LMFV7** (30) | NOR | 36 | 24 | 0 | 71.8 | 60.0 |
| | MRD | 14 | 45 | 0 | | 76.2 |
| | CYST | 2 | 0 | 21 | | 91.3 |

**Note:** FV: Feature vector, ***l***: length of the feature vector, LMFV7: Laws' mask feature vector computed using 1D filter of length 7, CM: Confusion matrix, MRD: Medical renal disease class, NOR: Normal class, OCA: Overall classification accuracy, ICA: Individual class accuracy, The OCA and ICA values are expressed in percentage.

From Table 4.13, it is observed that OCA of 71.8 % has been obtained with 30 Laws' mask features computed using 1D filter of length 7, along with ICA values of 60.0 %, 76.2 % and 91.3 % for normal, MRD and cyst renal US image classes respectively.

*4.3.2.4 Experiment 2 (d): Evaluating the classification performance of Laws' mask feature vector computed using 1D filter of length 9 (LMFV9)*

In this experiment, classification performance of LMFV9 is evaluated using SVM classifier. The results of the experiment are shown in Table 4.14.

**Table 4.14** Classification performance of texture features obtained by LMFV9 using SVM classifier.

| FV (*l*) | CM | | | | OCA | ICA |
|---|---|---|---|---|---|---|
| | | NOR | MRD | CYST | | |
| **LMFV9** (75) | NOR | 51 | 6 | 3 | 71.8 | 85.0 |
| | MRD | 28 | 31 | 0 | | 52.5 |
| | CYST | 3 | 0 | 20 | | 86.9 |

**Note:** FV: Feature vector, *l*: length of the feature vector, LMFV9: Laws' mask feature vector computed using 1D filter of length 9, CM: Confusion matrix, MRD: Medical renal disease class, NOR: Normal class, OCA: Overall classification accuracy, ICA: Individual class accuracy, The OCA and ICA values are expressed in percentage.

From Table 4.14, it is observed that an OCA of 71.8 % has been obtained with 75 Laws' mask feature vector computed using 1D filter of length 9, along with ICA values of 85.0 %, 52.5 % and 86.9 % for normal, MRD and cyst renal US image classes respectively.

*From experiment 2, it is observed that, using signal processing based methods for feature extraction, maximum OCA of 79.5 % has been obtained from Laws' mask feature vector computed using 1D filter of length 5 (LMFV5) along with ICA values of 80 %, 74.5 % and 91.3 % for normal, MRD and cyst image classes respectively.*

*4.3.3 Experiment 3: Design of CAC system for classification renal diseases using transform domain methods using Gabor feature vector (GaFV).*

As discussed earlier, the ROIs have been extracted from renal parenchyma region for normal and MRD classes, and from regions inside the lesion for renal cyst renal US image class. In this experiment, feature extraction is performed using features obtained from transform domain methods. The classification of renal US images into normal, MRD and cyst classes is carried out using SVM classifier. The diagram for the experimental workflow for experiment 3 is given in Fig. 4.7. Brief description of the experiment is given below:

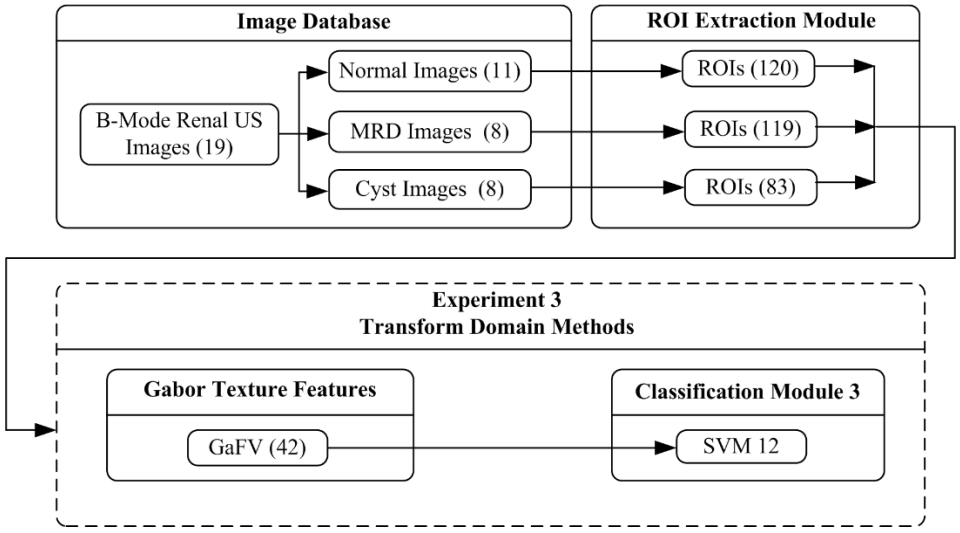


**Fig. 4.7** Workflow diagram of experiment 3: CAC system for diagnosis of renal diseases using Gabor texture feature vector (GaFV).
**Note**: MRD: Medical renal disease, GaFV: Gabor feature vector, SVM: Support vector machine, Exp: Experiment.

(*a*) *Feature Extraction Module*

*Two Dimensional Gabor Wavelet Transform*: A set of frequency and orientation selective filters (i.e. capturing energy at specific frequency and orientation) are applied to an image that results in 2-D Gabor wavelet transform. For instance, if three scales (0, 1 and 2) and seven angles (22.5°, 45°, 67.5°, 90°, 112.5°, 135° and 157.5°) are considered than it results in formation of 21 (7 × 3) wavelets. Hence, 21 feature images are obtained when these 21 wavelets are convolved with an ROI image. Each of these image represents image information at specific scale and orientation [51, 76, 89-97].

From these 21 feature images, mean and standard deviation are computed as texture descriptors forming a feature vector of length 42 (21 × 2). The real part of 21 wavelets resulting from a 13 × 13 convolution mask with three scales and seven orientations are shown in Fig. 4.8.

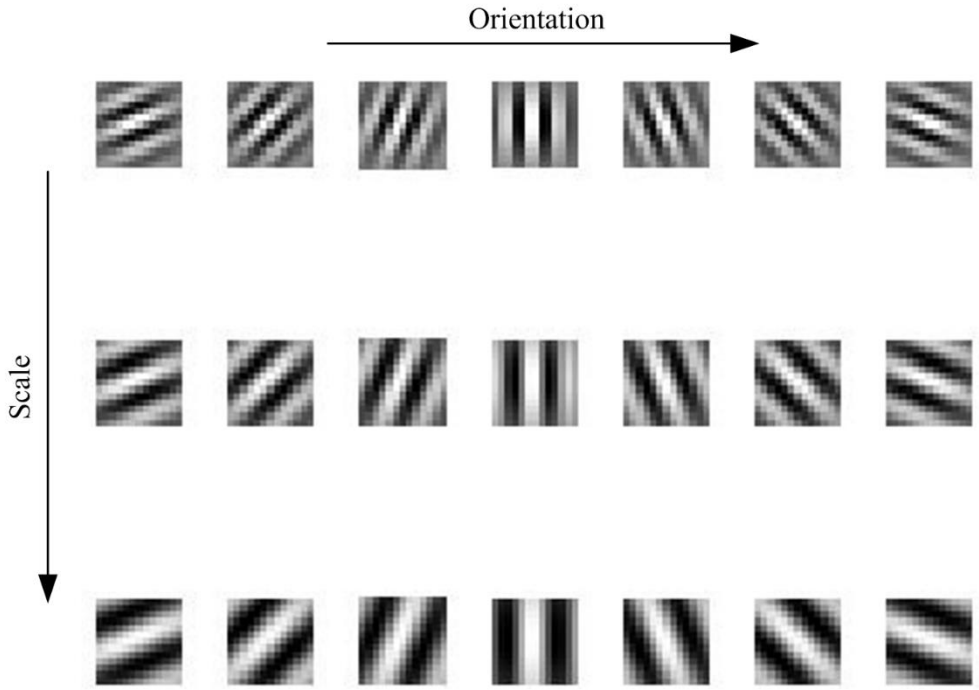


**Fig. 4.8** Real part of Gabor filter family of 21 wavelets evaluated at 3 scales and 7 orientations.
**Note**: Orientation: 22.5°, 45°, 67.5°, 90°, 112.5°, 135° and 157.5° from left to right.
Scale: 0, 1 and 2 from top to bottom.

(*b*) *Classification module*

The brief description of classification module is given in section 4.3.1 (*b*).

In this experiment, classification performance of GaFV evaluated at 3 scales and 7 orientations, is tested by using SVM classifier. The results of the experiment are shown in Table 4.15.

**Table 4.15** Classification performance of GaFV using SVM classifier.

| **FV(*l*)** | **CM** | | | | **OCA** | **ICA** |
|---|---|---|---|---|---|---|
| | | NOR | MRD | CYST | | |
| **GaFV** (42) | NOR | 40 | 20 | 0 | 80.2 | 66.6 |
| | MRD | 7 | 52 | 0 | | 88.1 |
| | CYST | 1 | 0 | 22 | | 95.6 |

**Note:** FV: Feature vector, *l*: length of the feature vector, GaFV: Gabor feature vector, CM: Confusion matrix, MRD: Medical renal disease class, NOR: Normal class, OCA: Overall classification accuracy, ICA: Individual class accuracy, The OCA and ICA values are expressed in percentage.

From Table 4.15, it is observed that an OCA of 80.2 % has been obtained with 42 different 2D Gabor features, along with ICA values of 66.6 %, 88.1 % and 95.6 % for normal, MRD and cyst renal US image classes respectively.

## 4.4 Comparative analysis of the experiments conducted for Design of SVM based CAC System for Diagnosis of Renal Diseases

On conducting exhaustive experiments by using statistical methods, signal processing based methods and transform domain methods for feature extraction, a comparison can be drawn between the highest OCAs achieved by the texture features by respective methods. A brief description of the comparative analysis is given in Table 4.16.

**Table 4.16** Comparative analysis of statistical, signal processing and transform domain methods.

| Methods | FV (*l*) | OCA | $ICA_{NOR}$ | $ICA_{MRD}$ | $ICA_{Cyst}$ |
|---|---|---|---|---|---|
| Exp. 1: Statistical Methods | GCFV (26) | 85.9 | 86.6 | 83.0 | 91.3 |
| Exp. 2: Signal Processing Methods | LMFV5 (75) | 79.5 | 80.0 | 74.5 | 91.3 |
| Exp. 3: Transform Domain Methods | GaFV (42) | 80.2 | 66.6 | 88.1 | 95.6 |

**Note:** FV: Feature vector, *l*: length of the feature vector, GCFV: GLCM combined feature vector, LMFV5: Laws' mask feature vector computed using 1D filter of length 5, GaFV: Gabor feature vector evaluated at 3 scales and 7 orientations, FV: Feature vector, OCA: Overall classification accuracy, ICA: Individual class accuracy, NOR: Normal class, MRD: Medical renal disease, $ICA_{NOR}$: ICA value for NOR class, $ICA_{MRD}$: ICA value for MRD class, $ICA_{Cyst}$ : ICA value for Cyst class, Exp.: Experiment, The OCA and ICA values are expressed in percentage.

From Table 4.16, it is observed that the GLCM combined feature vector (GCFV) consisting of combination of $GLCM_{mean}$ and $GLCM_{range}$ features is most efficient for classification of renal US images into normal, MRD and cyst classes. This GCFV is further subjected to wrapper based Genetic algorithm SVM (GA-SVM) method for selection of optimal features. Considering the above result, one more experiment is conducted.

### *4.4.1 Experiment 4: Evaluating the classification performance of GLCM combined feature vector (GCFV) using GA-SVM.*

The classification performance of the prominent features selected from GLCM combined feature vector (GCFV) is evaluated in this experiment. The diagram for the experimental workflow for experiment 4 is given in Fig. 4.9. GCFV is subjected to wrapper based GA-SVM technique for feature selection. Classification is performed using SVM classifier.

*GA-SVM*: GA-SVM is a hybrid algorithm that utilizes genetic-algorithm simultaneously in order to optimize the parameters of SVM and select relevant features with classification. The difference between the GA-SVM method and normal GA lies in the ways to design the chromosome.

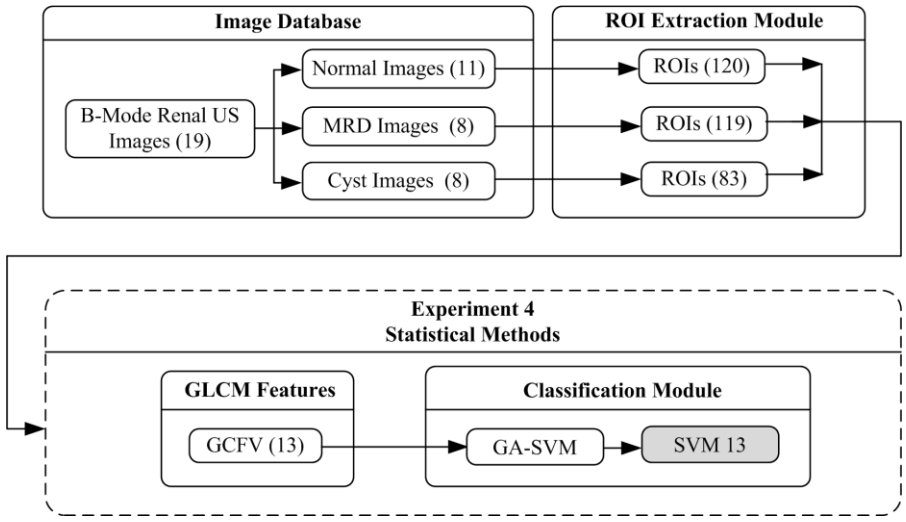


**Fig. 4.9** Workflow diagram of experiment 4: CAC system for diagnosis of renal diseases using GA- SVM.
**Note**: MRD: Medical renal disease, ROIs: Regions of interest, GRFV: $GLCM_{range}$ feature vector, GA-SVM: Genetic algorithm support vector machine, SVM: Support vector machine.

For application of genetic algorithm, two steps are required, (*a*) adequate representation, (*b*) appropriate fitness function.

For the purpose of feature selection, binary representation is used to extract the appropriate features. SVM classifier gives the training accuracy which is applied as fitness function [65, 98-101].

It involves seven main steps:

(*i*) Random creation of the initial population of possible candidate solution.

(*ii*) A 48-bit binary mask represents each chromosome where each bit corresponds to a single feature. 0 at any location indicates that the corresponding feature is irrelevant.

(*iii*) The performance of each individual is measured by the appropriate fitness function.

(*iv*) Selection of individuals (Roulette wheel selection) which are believed to be fit and have high probability to enter into the mating pool.

(*v*) Recombination of the selected individuals in the mating pool using cross-over operator for the generation of next-generation offspring.

(*vi*) Application of mutation operator to the offspring with low probability to ensure variations in the pool of solutions.

(*vii*) Evaluation of offspring using fitness function and those with the higher fitness value are considered to form a new population.

In this experiment, classification performance of the 16 prominent features from statistical method based GLCM combined feature vector (GCFV) of length 26 is evaluated. The brief description of the results obtained using GA-SVM is given in Table 4.17.

**Table 4.17** Classification performance of GCFV using SVM classifier.

| **FV (*l*)** | **CM** | | | | **OCA** | **ICA** |
|---|---|---|---|---|---|---|
| **GCFV** (16) | | NOR | MRD | CYST | | |
| | NOR | 52 | 7 | 1 | 83.8 | 86.6 |
| | MRD | 13 | 46 | 0 | | 77.9 |
| | CYST | 2 | 0 | 21 | | 91.3 |

**Note:** FV: Feature vector, *l*: length of the feature vector, GCFV: GLCM combined feature vector, CM: Confusion matrix, NOR: Normal class, MRD: Medical renal disease class, OCA: Overall classification accuracy, ICA: Individual classification accuracy, The OCA and ICA values are expressed in percentage.

From Table 4.17, it is observed that on subjecting GCFV to wrapper based GA-SVM technique for selection of optimal features, 16 optimal texture features consisting of 7 $GLCM_{mean}$ features ($ASM_{mean}$, $Cont_{mean}$, $Var_{mean}$, $SumAv_{mean}$, $SumVar_{mean}$, $DiffVar_{mean}$, $InfMCorr1_{mean}$) and 9 $GLCM_{range}$ features ($ASM_{range}$, $Corr_{range}$, $Var_{range}$, $IDM_{range}$, $SumAv_{range}$, $SumVar_{range}$, $Ent_{range}$, $DiffVar_{range}$, $InfMCorr1_{range}$) yielded an OCA of 83.8 % with ICA values of 86.6 %, 77.9 % and 91.3 % for normal, MRD and cyst classes respectively.

## 4.5 Proposed SVM based CAC System Design for diagnosis of Renal Disease

The result of the study indicates that GLCM combined feature vector (GCFV) yields the highest OCA of 85.9 % at inter-pixel distance '*d*' = 1 with ICA values of 86.6 %, 83.0 % and 91.3 % for normal, MRD and cyst classes respectively. Hence, it is observed that the GCFV is most efficient for classification of renal ultrasound images into normal, MRD and cyst classes. It can be concluded that out of 26 $GLCM_{mean}$ and $GLCM_{range}$ features, 16 texture features consisting of 7 $GLCM_{mean}$ features ($ASM_{mean}$, $Cont_{mean}$, $Var_{mean}$, $SumAv_{mean}$, $SumVar_{mean}$, $DiffVar_{mean}$, $InfMCorr1_{mean}$) and 9 $GLCM_{range}$ features ($ASM_{range}$, $Corr_{range}$, $Var_{range}$, $IDM_{range}$, $SumAv_{range}$, $SumVar_{range}$, $Ent_{range}$, $DiffVar_{range}$, $InfMCorr1_{range}$) yielded an OCA of 83.8 % with individual classification accuracy values of 86.6 %, 77.9 % and 91.3 % for normal, MRD and cyst classes respectively.

Hence, they are prominent for classification of normal, MRD and cyst renal US images.

The promising results obtained from the study indicate that the proposed CAC system design using selected $GLCM_{mean}$ and $GLCM_{range}$ features can be routinely used in clinical environment for classification of renal diseases. The diagram of the proposed GA-SVM based CAC system is for diagnosis of renal disease is shown in Fig. 4.10.

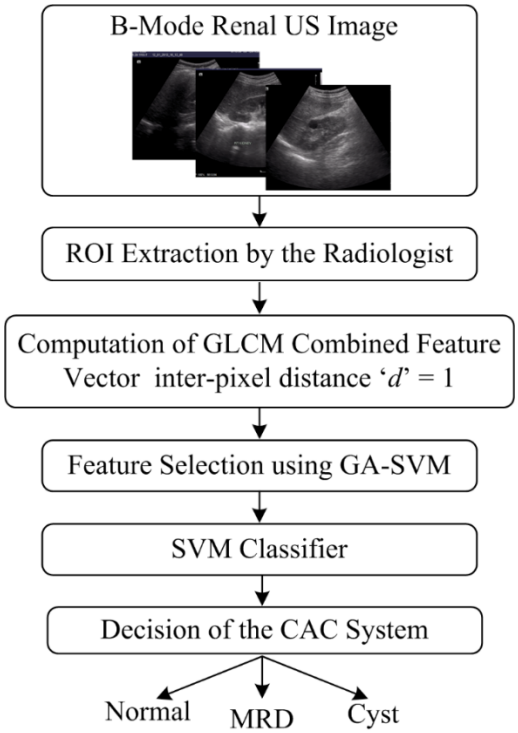


**Fig. 4.10** Proposed GA-SVM based CAC system for diagnosis of renal diseases.
**Note**: GMFV: $GLCM_{mean}$ feature vector, GRFV: $GLCM_{range}$ feature vector, GCFV: GLCM combined feature vector, GA-SVM: Genetic algorithm support vector machine.

## 4.6 Concluding Remarks

In present study, an attempt has been made to classify renal US images into normal, MRD and cyst classes using SVM classifier. The texture features are extracted from ROIs from parenchymal region in case of normal and MRD class and from lesion in case of cyst class. Various experiments are conducted using statistical, signal processing and transform domain methods. The features obtained are subjected to SVM classifier for the classification task.

It is observed that GLCM combined feature vector (GCFV) yields the highest OCA of 85.9 % at inter-pixel distance '*d*' = 1 with ICA values of 86.6 %, 83.0 % and 91.3 % for normal, MRD and cyst classes respectively. Hence, GLCM combined feature vector obtained from statistical methods is most efficient for classification of renal ultrasound images into normal, MRD and cyst classes.

It can also be concluded that out of 26 $GLCM_{mean}$ and $GLCM_{range}$ features, 16 texture features consisting of 7 $GLCM_{mean}$ features ($ASM_{mean}$, $Cont_{mean}$, $Var_{mean}$, $SumAv_{mean}$, $SumVar_{mean}$, $DiffVar_{mean}$, $InfMCorr1_{mean}$) and 9 $GLCM_{range}$ features ($ASM_{range}$, $Corr_{range}$, $Var_{range}$, $IDM_{range}$, $SumAv_{range}$, $SumVar_{range}$, $Ent_{range}$, $DiffVar_{range}$, $InfMCorr1_{range}$) are prominent for classification of normal, MRD and cyst renal US images.

In next chapter the significance of textural changes in renal parenchyma region is evaluated which is also looked upon by radiologist for diagnosis of MRD. Hence, individual contribution of parenchyma region is utilized by extracting absolute texture features from parenchyma region. The ANFC is used for the classification task.

# Chapter 5

# ANFC based CAC System for Diagnosis of Medical Renal Disease using Absolute Texture Features

## 5.1 Introduction

Renal diseases hamper the working of kidney which performs important function of chemical regulation. Early diagnosis of MRD is important as it hampers the parenchymal region of kidney which is forms the most essential and functional unit of the organ. Hence timely investigation of MRD is important, failing which may lead to further complication, often severe as renal cancer.

The radiologists make the differential diagnosis between normal and MRD renal US image classes by looking at the textural changes in renal parenchyma region. Renal parenchyma in normal kidney appears hypoechoic with respect to renal sinus with visible cortico-medullary differentiation. But in MRD, the echogenicity of renal parenchyma increases and it becomes iso-echoic with respect to renal sinus. Also, the cortico-medullary differentiation is lost. In present work, an attempt has been made to design an ANFC based CAC system for diagnosis of MRD by utilizing the characteristics from parenchymal region of the kidney. The design of this module considers absolute features obtained from ROIs extracted from renal parenchyma region (PROIs). These PROIs are extracted from parenchyma region of normal and MRD renal US image class, considering the change in nature of echogenicity of parenchyma region, for normal and MRD classification. The PROIs extraction from normal and MRD renal US images is shown in Fig. 5.1. Accordingly, this chapter incorporates an ANFC based CAC system for diagnosis of MRD using absolute texture features.

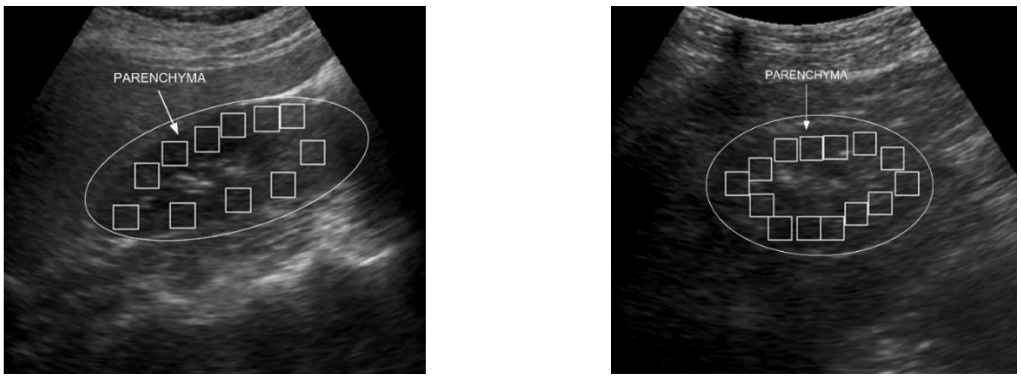


**Fig. 5.1** Sample US images of (*a*) normal, (*b*) MRD renal US image with ROIs marked.
**Note**: PROI are extracted from renal parenchyma region.

## 5.2 Dataset Description and its Bifurcation for Design of ANFC based CAC System for Diagnosis of Medical Renal Disease using Absolute Texture Features

The work has been carried out on 19 B-mode renal US images consisting of 11 normal and 8 MRD images. The image assessment and data collection protocols are defined in chapter 3, section 3.3 and 3.4.1 respectively.

The ROIs of size 25 × 25 pixels have been extracted from the renal parenchyma region (PROIs). The classification is made on basis of the absolute features extracted from renal parenchyma PROIs. The brief description of the ROI extraction protocols is given in section 3.4.2.1 (*iii*) of chapter 3.

A total of 120 and 119 PROIs are extracted from 11 normal images and 8 MRD images respectively. These PROIs are bifurcated to form training and testing sets for classification purpose. Brief description of data bifurcation protocol is given in chapter 3, section 3.4.3 (*ii*). Image database and its bifurcation into training and testing sets for classification is shown in Fig. 5.2.

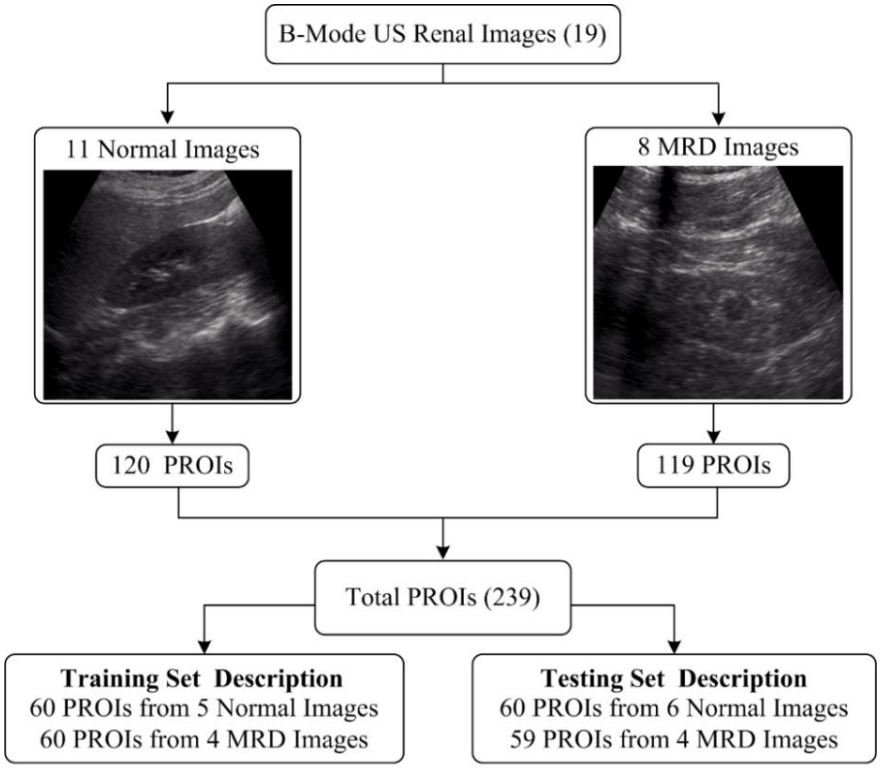


**Fig. 5.2** Dataset description and its bifurcation into training and testing sets.
**Note:** PROIs: Parenchymal regions of interest, SROIs: Sinus regions of interest.

## 5.3 Experimental Workflow for the Design of ANFC based CAC System for Diagnosis of Medical Renal Disease using Absolute Texture Features

The block diagram of the experimental workflow for design of ANFC based CAC system for diagnosis of MRD using absolute texture features is shown in Fig. 5.3. For evaluating the performance of the proposed CAC system, rigorous experimentation has been carried out for the diagnosis of MRD. The ROI extraction (as discussed above) is followed by feature extraction and classification. Feature extraction has been conducted using statistical methods, signal processing methods and transform domain methods. Classification is performed using ANFC.

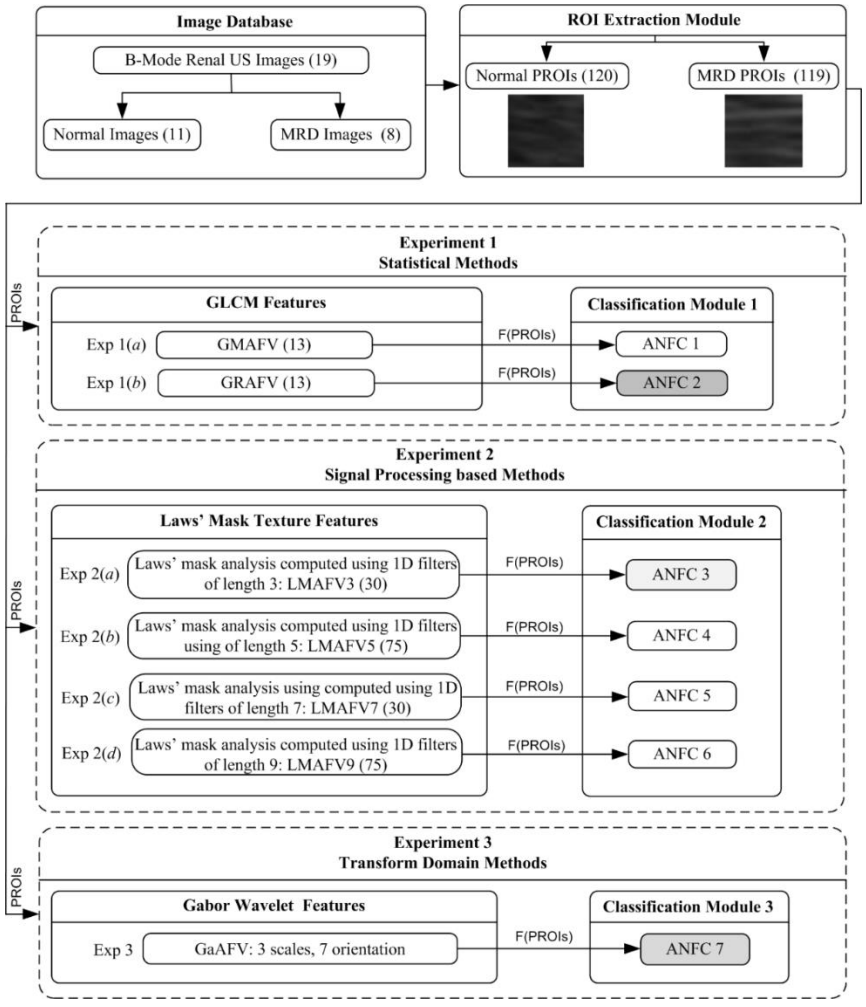


**Fig. 5.3** Experimental workflow for design of ANFC based CAC system for diagnosis of MRD using absolute texture features.

**Note**: MRD: Medical renal disease, GLCM: Gray level co-occurrence matrix, GMAFV: $GLCM_{mean}$ absolute feature vector, GRAFV: $GLCM_{range}$ absolute feature vector, LMAFV 3: Laws' mask absolute feature vector computed using 1D filter of length 3, LMAFV 5: Laws' mask absolute feature vector computed using 1D filter of length 5, LMAFV 7: Laws' mask absolute feature vector computed using 1D filter of length 7, LMAFV 9: Laws' mask absolute feature vector computed using 1D filter of length 9, GaAFV: Gabor absolute feature vector, ANFC: Adaptive neuro-fuzzy classifier.

The brief description of the feature vectors for the design of SVM based CAC system for diagnosis of renal diseases is given in Table 5.1.

**Table 5.1** Brief description of feature vectors used for design of ANFC based CAC system for diagnosis of medical renal diseases using absolute features.

| FV | Description | *l* |
|---|---|---|
| GMAFV | $GLCM_{mean}$ absolute feature vector | 13 |
| GRAFV | $GLCM_{range}$ absolute feature vector | 13 |
| LMAFV3 | Laws' mask absolute feature vector computed using 1D filter of length 3 | 30 |
| LMAFV5 | Laws' mask absolute feature vector computed using 1D filter of length 5 | 45 |
| LMAFV7 | Laws' mask absolute feature vector computed using 1D filter of length 7 | 30 |
| LMAFV9 | Laws' mask absolute feature vector computed using 1D filter of length 9 | 45 |
| GaAFV | Gabor absolute feature vector | 42 |

**Note**: FV: Feature vector, *l*: length of the feature vector, GLCM: Gray level co-occurrence matrix.

The brief description of the experiments carried out is given below:

*5.3.1 Experiment 1: Design of CAC system for diagnosis of MRD using statistical methods.*

The classification of normal and MRD renal US images is carried out in this experiment using statistical methods based GLCM features. The $GLCM_{mean}$ absolute feature vector (GMAFV) and $GLCM_{range}$ absolute feature vector (GRAFV) are computed at inter-pixel distance '*d*' = 1. The brief description of feature extraction module using statistical methods is given in chapter 4, section 4.3.1 (*a*). The workflow diagram of experiment 1 is shown in Fig. 5.4. These GMAFV and GRAFV are subjected to classification module using ANFC for classification as explained below:

*Adaptive neuro-fuzzy classifier:* Classification success is affected negatively in some fuzzy sets due to overlapping. This overlapping of classes degrades the performance of the classifier. Adaptive neuro-fuzzy classifier forms the solution to this overlapping problem by using the concept of linguistic hedges.

The implementation of linguistic hedges also improves the meaning of classical fuzzy rules. To indicate the effect of linguistic hedges, an additional layer is added to the existing neuro-fuzzy classifier. In order to describe the feature space with fuzzy regions, and to control each region with fuzzy rules, fuzzy membership parameters and fuzzy cluster weights should be optimized with an optimization-method. In ANFC, scale conjugate gradient optimization method is used to adapt the network parameters namely, center of the Gaussian function (*c*), width of the Gaussian function (σ) and linguistic hedge value of the Gaussian function (*P*).

The learning capability of IF-THEN rules that are constructed as a network of the inference system, is used to approximate non-linear functions. These rules are adapted with neural network. As a result, fuzzy classification system and neural-network are combined with their superior properties. The implementation of linguistic hedges on fuzzy rules helps to give them a better definition by modifying the effect of fuzzy sets on fuzzy rules. The linguistic hedge value (*P*) effects the selection degree of a class. Also, linguistic hedges are forced to binary values such as $P = 0$ or $P = 1$, which is used for feature selection [102-113].

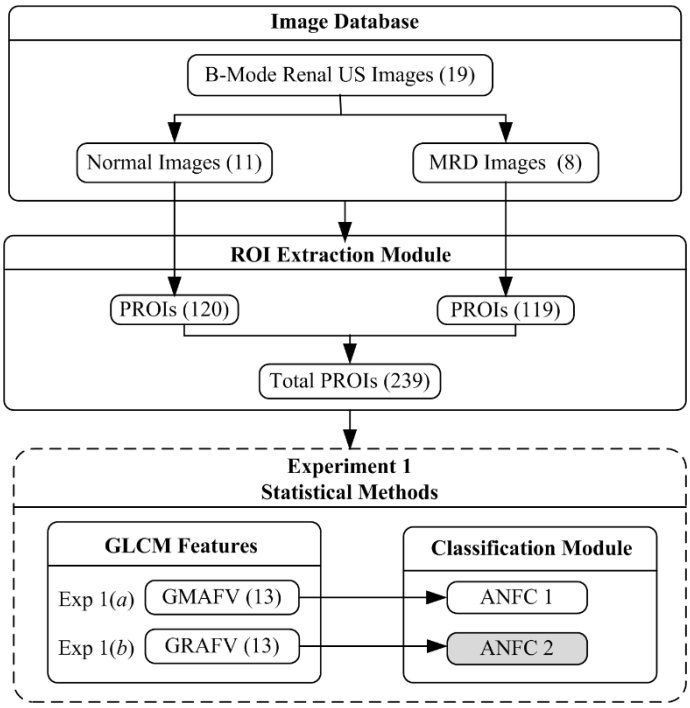


**Fig. 5.4** Workflow diagram of experiment 1: CAC system for diagnosis of MRD using GLCM absolute feature vectors.
**Note**: MRD: Medical renal disease, GLCM: Gray level co-occurrence matrix, GMAFV: $GLCM_{mean}$ absolute feature vector, GRAFV: $GLCM_{range}$ absolute feature vector, ANFC: Adaptive neuro-fuzzy classifier, Exp: Experiment.

The results obtained after conducting experiment 1 are given below:

*5.3.1.1 Experiment 1(a): Evaluating the classification performance of $GLCM_{mean}$ absolute feature vector (GMAFV).*

In this experiment, classification performance of GMAFV is evaluated at inter-pixel distance '*d*' = 1 using ANFC. The results of the experiment are shown in Table 5.2.

**Table 5.2** Classification performance of GMAFV using ANFC at inter-pixel distance '*d'* = 1.

| **FV (*l*)** | **CM** | | | **OCA** | **ICA** |
|---|---|---|---|---|---|
| **GMAFV** (13) | | NOR | MRD | | |
| | NOR | 46 | 14 | 78.1 | 76.6 |
| | MRD | 12 | 47 | | 79.6 |

**Note:** FV: Feature vector, *l*: length of the feature vector, GMAFV: $GLCM_{mean}$ absolute feature vector, CM: Confusion matrix, NOR: Normal class, MRD: Medical renal disease class, OCA: Overall classification accuracy, ICA: Individual class accuracy, The OCA and ICA values are expressed in percentage.

From Table 5.2, it is observed that an overall classification accuracy (OCA) of 78.1 % has been obtained with 13 different $GLCM_{mean}$ features computed at inter-pixel distance '*d'* = 1, along with individual class accuracy (ICA) values of 76.6 % and 79.6 % for normal and MRD classes respectively.

*5.3.1.2 Experiment 1(b): Evaluating the classification performance of $GLCM_{range}$ absolute feature vector (GRAFV).*

In this experiment, classification performance of GRAFV is evaluated at inter-pixel distance '*d'* = 1 using ANFC. The results of the experiment are shown in Table 5.3.

**Table 5.3** Classification performance of GRAFV using ANFC at inter-pixel distance '*d'* = 1.

| **FV (*l*)** | **CM** | | | **OCA** | **ICA** |
|---|---|---|---|---|---|
| **GRAFV** (13) | | NOR | MRD | | |
| | NOR | 56 | 4 | 84.8 | 93.3 |
| | MRD | 15 | 44 | | 74.5 |

**Note:** FV: Feature vector, *l*: length of the feature vector, GRAFV: $GLCM_{range}$ absolute feature vector, CM: Confusion matrix, NOR: Normal class, MRD: Medical renal disease class, OCA: Overall classification accuracy, ICA: Individual class accuracy, The OCA and ICA values are expressed in percentage.

From Table 5.3, it is observed that maximum OCA of 84.8 % has been obtained with 13 different $GLCM_{range}$ features computed at inter-pixel distance '*d'* = 1, along with ICA values of 93.3 % and 74.5 % for normal and MRD classes respectively.

*Hence, among statistical methods based $GLCM_{mean}$ and $GLCM_{range}$ absolute features, GRAFV outperforms GMAFV by yielding an OCA of 84.8 % along with ICA values of 93.3 % and 74.5 % for normal and MRD classes respectively.*

*5.3.2 Experiment 2: Design of CAC system for diagnosis of MRD using features obtained from signal processing methods.*

The classification of normal and MRD renal US images is carried out in this experiment using signal processing methods based Laws' texture features.

The brief description of feature extraction module is given in chapter 4, section 4.3.2 (*a*). Feature vectors are computed using Laws' texture feature vector computed using 1D filter of length 3, 5, 7 and 9. These LMAFV3, LMAFV5, LMAFV7 and LMAFV9 are subjected for the classification task using ANFC. The brief description of classification using ANFC is explained in section 5.3.1. The workflow diagram of experiment 2 is shown in Fig. 5.5.

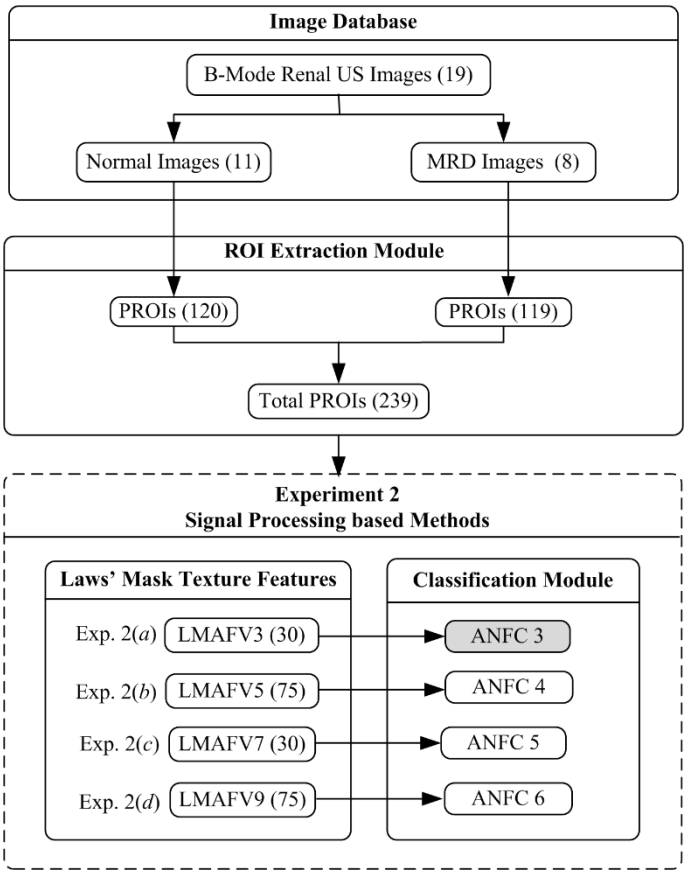


**Fig. 5.5** Workflow diagram of experiment 2: CAC system for diagnosis of MRD using Laws' mask absolute feature vectors (LMAFVs).
**Note**: MRD: Medical renal disease, LMAFV 3: Laws' mask absolute feature vector computed using 1D filter of length 3, LMAFV 5: Laws' mask absolute feature vector computed using 1D filter of length 5, LMAFV 7: Laws' mask absolute feature vector computed using 1D filter of length 7, LMAFV 9: Laws' mask absolute feature vector computed using 1D filter of length 9, ANFC: Adaptive neuro-fuzzy classifier, Exp: Experiment.

The results obtained after conducting experiment 2 are given below:

*5.3.2.1 Experiment 2(a): Evaluating the classification performance of Laws' mask absolute feature vector computed using 1D filter of length 3 (LMAFV3).*

In this experiment, classification performance of LMAFV3 is evaluated using ANFC.

The results of the experiment are shown in Table 5.4.

**Table 5.4** Classification performance of LMAFV3 using ANFC.

| FV (*l*) | CM | | | OCA | ICA |
|---|---|---|---|---|---|
| **LMAFV3** (30) | | NOR | MRD | | |
| | NOR | 45 | 15 | 73.1 | 75.0 |
| | MRD | 17 | 42 | | 71.1 |

**Note:** FV: Feature vector, *l*: length of the feature vector, LMAFV 3: Laws' mask absolute feature vector computed using 1D filter of length 3, CM: Confusion matrix, NOR: Normal class, MRD: Medical renal disease class, OCA: Overall classification accuracy, ICA: Individual class accuracy, The OCA and ICA values are expressed in percentage.

From Table 5.4, it is observed that maximum OCA of 73.1 % has been obtained with 30 different laws' mask features computed using filters of length 3, along with ICA values of 75.0 % and 71.1 % for normal and MRD classes respectively.

*5.3.2.2 Experiment 2(b): Evaluating the classification performance of Laws' mask absolute feature vector computed using 1D filter of length 5(LMAFV5).*

In this experiment, classification performance of LMAFV5 is evaluated using ANFC. The results of the experiment are shown in Table 5.5.

**Table 5.5** Classification performance of LMAFV5 using ANFC.

| FV (*l*) | CM | | | OCA | ICA |
|---|---|---|---|---|---|
| **LMAFV5** (75) | | NOR | MRD | | |
| | NOR | 42 | 18 | 71.4 | 70.0 |
| | MRD | 16 | 43 | | 72.8 |

**Note:** FV: Feature vector, *l*: length of the feature vector, LMAFV5: Laws' mask absolute feature vector computed using 1D filter of length 5, CM: Confusion matrix, NOR: Normal class, MRD: Medical renal disease class, OCA: Overall classification accuracy, ICA: Individual class accuracy, The OCA and ICA values are expressed in percentage.

From Table 5.5, it is observed that maximum OCA of 71.4 % has been obtained with 75 different Laws' mask absolute features computed using 1D filter of length 5, along with ICA values of 70.0 % and 72.8 % for normal and MRD classes respectively.

*5.3.2.3 Experiment 2(c): Evaluating the classification performance of Laws' mask absolute feature vector computed using 1D filter of length 7 (LMAFV7).*

In this experiment, classification performance of LMAFV7 is evaluated using ANFC.

The results of the experiment are shown in Table 5.6.

**Table 5.6** Classification performance of LMAFV7 using ANFC.

| FV (*l*) | CM | | | OCA | ICA |
|---|---|---|---|---|---|
| | | NOR | MRD | | |
| **LMAFV7** (30) | NOR | 38 | 22 | 71.4 | 63.3 |
| | MRD | 12 | 47 | | 79.6 |

**Note:** FV: Feature vector, *l*: length of the feature vector, LMAFV 7: Laws' mask absolute feature vector computed using 1D filter of length 7, CM: Confusion matrix, NOR: Normal class, MRD: Medical renal disease class, OCA: Overall classification accuracy, ICA: Individual class accuracy, The OCA and ICA values are expressed in percentage.

From Table 5.6, it is observed that maximum OCA of 71.4 % has been obtained with 30 different Laws' mask absolute features computed using 1D filter of length 7, along with ICA values of 63.3 % and 79.6 % for normal and MRD classes respectively.

*5.3.2.4 Experiment 2(d): Evaluating the classification performance of Laws' mask absolute feature vector computed using 1D filter of length 9 (LMAFV9).*

In this experiment, classification performance of LMAFV9 is evaluated using ANFC. The results of the experiment are shown in Table 5.7.

**Table 5.7** Classification performance of LMAFV9 using ANFC.

| FV (*l*) | CM | | | OCA | ICA |
|---|---|---|---|---|---|
| | | NOR | MRD | | |
| **LMAFV9** (75) | NOR | 47 | 16 | 69.7 | 78.3 |
| | MRD | 24 | 36 | | 61.0 |

**Note:** FV: Feature vector, *l*: length of the feature vector, LMAFV 9: Laws' mask absolute feature vector computed using 1D filter of length 9, CM: Confusion matrix, NOR: Normal class, MRD: Medical renal disease class, OCA: Overall classification accuracy, ICA: Individual class accuracy, The OCA and ICA values are expressed in percentage.

From Table 5.7, it is observed that maximum OCA of 69.7 % has been obtained with 75 different Laws' mask absolute features computed using 1D filter of length 9, along with ICA values of 78.3 % and 61.0 % for normal and MRD classes respectively.

*Hence, from the above experiment conducted using signal processing based methods, it can be concluded that Laws' mask texture features, LMAFV3 (Laws' mask absolute feature vector computed using 1D filter of length 3) performs best by yielding an OCA of 73.1 % along with ICA values of 75.0 % and 71.1 % for normal and MRD classes respectively.*

*5.3.3 Experiment 3: Design of CAC system for diagnosis of MRD using Gabor texture absolute features.*

The classification of normal and MRD renal US images is carried out in this experiment using transform domain Gabor 2D wavelet texture features.

The brief description of transform domain feature extraction is given in chapter 4, section 4.3.3 (*a*). Feature vector is computed using Gabor absolute texture feature at 3 scales and 7 orientation. This GaAFV is subjected for the classification task using ANFC. The brief description of classification using ANFC is explained in section 5.3.1. The workflow diagram of experiment 3 is shown in Fig. 5.6.

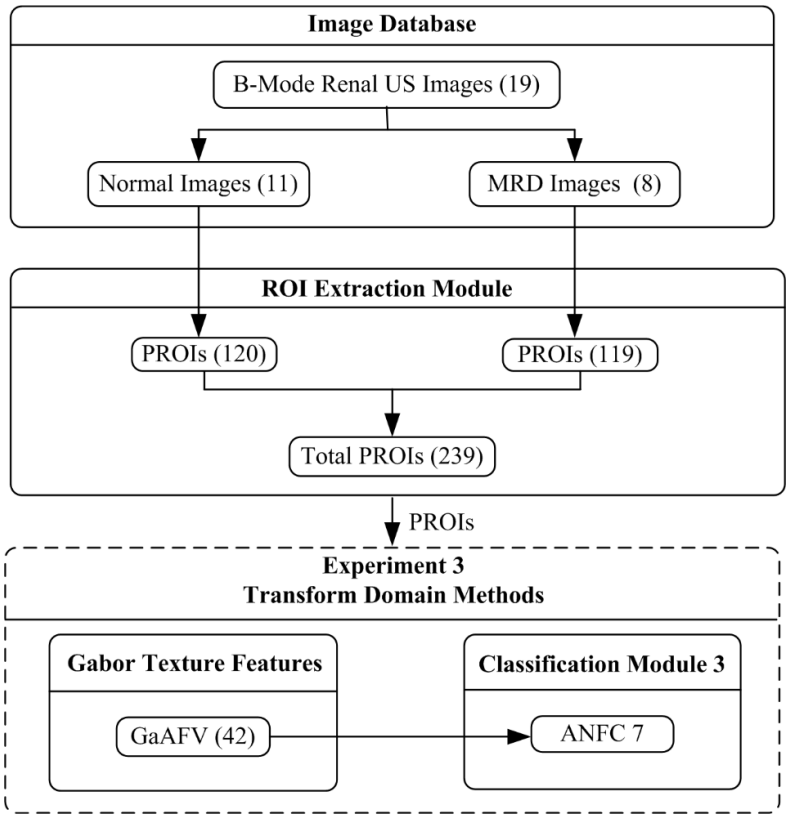


**Fig. 5.6** Workflow diagram of experiment 3: CAC system for diagnosis of MRD using Gabor absolute texture feature vector (GaAFV).
**Note**: MRD: Medical renal disease, GaAFV: Gabor absolute feature vector, ANFC: Adaptive neuro-fuzzy classifier, Exp: Experiment.

In this experiment, classification performance of GaAFV is evaluated using ANFC. The results of the experiment are shown in Table 5.8.

**Table 5.8** Classification performance of GaAFV3 using ANFC.

| FV (*l*) | CM | | | OCA | ICA |
|---|---|---|---|---|---|
| **GaAFV** (42) | | NOR | MRD | 67.2 | |
| | NOR | 49 | 11 | | 81.6 |
| | MRD | 28 | 31 | | 52.5 |

**Note:** FV: Feature vector, *l*: length of the feature vector, GaAFV: Gabor absolute feature vector, CM: Confusion matrix, MRD: Medical renal disease class, NOR: Normal class, OCA: Overall classification accuracy, ICA: Individual class accuracy, The OCA and ICA values are expressed in percentage.

From Table 5.8, it is observed that an OCA of 67.2 % has been obtained with 42 different Gabor texture features at 3 scales and 7 orientation, along with ICA values of 81.6 % and 52.5 % for normal and MRD classes respectively.

## 5.4 Comparative Analysis of the Experiments Conducted for Design of ANFC based CAC System for Diagnosis of MRD using Absolute Texture Features

On conducting exhaustive experiments on statistical methods, signal processing methods and transform domain methods, a comparison can be drawn between the highest OCAs achieved by the absolute texture features. A brief description of the comparative analysis is given in Table 5.9.

**Table 5.9** Comparative analysis of statistical, signal processing and transform domain methods.

| Methods | FV (*l*) | OCA | $ICA_{NOR}$ | $ICA_{MRD}$ |
|---|---|---|---|---|
| Exp. 1: Statistical Methods | GRAFV (13) | 84.8 | 93.3 | 74.5 |
| Exp. 2: Signal Processing based Methods | LMAFV3 (30) | 73.1 | 75.0 | 71.1 |
| Exp. 3: Transform Domain Methods | GaAFV (42) | 67.2 | 81.6 | 52.5 |

**Note:** FV: Feature vector, *l*: length of the feature vector, GRAFV: $GLCM_{range}$ absolute feature vector, LMAFV3: Laws' mask absolute feature vector computed using 1D filter of length 3, GaAFV: Gabor absolute feature vector evaluated at 3 scales and 7 orientations, OCA: Overall classification accuracy, ICA: Individual class accuracy, NOR: Normal class, MRD: Medical renal disease, $ICA_{NOR}$: ICA value for NOR class, $ICA_{MRD}$: ICA value for MRD class, The OCA and ICA values are expressed in percentage.

From Table 5.9, it is observed that the maximum OCA of 84.8 % is achieved by $GLCM_{range}$ feature vector computed using absolute features extracted from renal parenchyma PROIs. The ICA values for normal and MRD are 93.3 % and 74.5 % respectively.

## 5.5 Proposed ANFC based CAC System Design for Diagnosis of MRD using Absolute Texture Features

Based on the experiments conducted above, it is observed that statistical methods based $GLCM_{range}$ feature vector, computed at inter-pixel distance '*d*' = 1 yields the highest OCA of 84.8 % with the ICA values of 93.3 % and 74.5 % for normal and MRD classes respectively.

Hence, it is observed that the GRAFV is the most efficient for classification of renal US images into normal and MRD classes. The diagram of proposed CAC system for diagnosis of MRD using absolute texture features is given in Fig. 5.7.

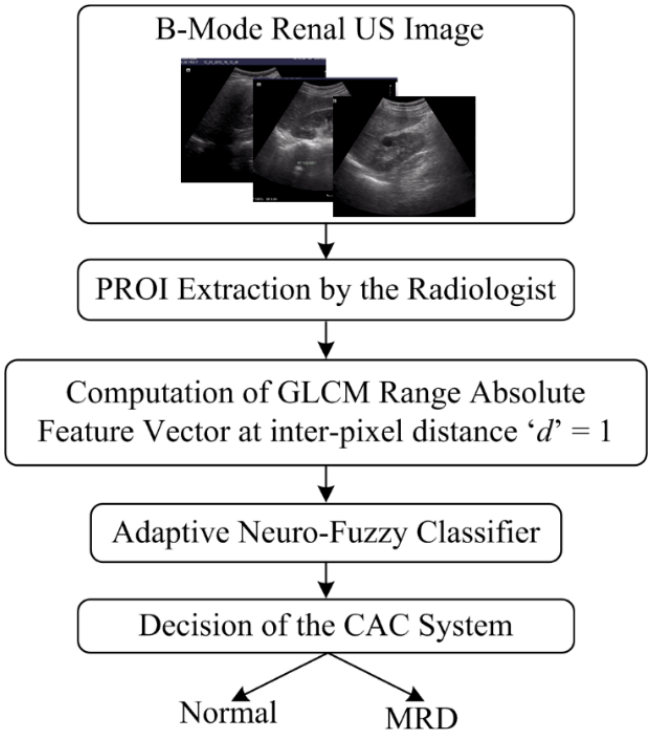


**Fig. 5.7** Proposed CAC system for diagnosis of MRD using absolute texture features.

## 5.6 Concluding Remarks

In the present study, an attempt has been made to evaluate the significance of textural changes in renal parenchyma for diagnosis of MRD. The PROIs are extracted from renal parenchymal region from both, normal and MRD renal US image classes. Various experiments are conducted using statistical, signal processing and transform domain methods.

The absolute features obtained from these methods are subjected for classification using ANFC classifier. It is observed that statistical methods based $GLCM_{range}$ feature vector, computed at inter-pixel distance '*d*' = 1 yields the highest OCA of 84.8 % with the ICA values of 93.3 % and 74.5 % for normal and MRD classes respectively.

The result of the study indicates that $GLCM_{range}$ absolute feature vector is the most efficient for classification of renal US images into normal and MRD classes. Therefore selected $GLCM_{range}$ absolute features can be routinely used in clinical environment for diagnosis of MRD.

The radiologists also consider the textural changes in renal parenchymal region with respect to renal sinus, which exhibits same hyperechoic appearance in both the cases i.e. normal and MRD renal US images. In next chapter, the ratio features obtained from renal parenchyma and renal sinus region are utilized for classification into normal and MRD renal US image using ANFC.

# Chapter 6

# ANFC based CAC System for Diagnosis of Medical Renal Disease using Texture Ratio Features

## 6.1 Introduction

In earlier study, an ANFC based CAC system proposed for diagnosis of renal disease based on the changes in texture of renal parenchymal region as looked upon by the radiologists in renal US images was discussed. Hence, absolute texture features were extracted from PROIs only.

In present classification problem, a further observational step of considering renal sinus region along with renal parenchymal region is taken up, as looked upon by the radiologists. Renal sinus region exhibits hyperechoic nature in case of normal as well as MRD renal US image class.

In normal renal US image, renal parenchyma appears slightly hypoechoic with respect to renal sinus and cortico-medullary differentiation can also be made. But in MRD, the echogenicity of renal parenchyma increases and it becomes iso-echoic with respect to renal sinus [11, 19, 114-117]. Hence, the difference in echogenicity of renal parenchyma for normal and MRD renal US image classes can be observed with respect to echogenicity of renal sinus which exhibits same hyperechoic nature in both the cases.

Accordingly, in this chapter, an attempt has been made to design an ANFC based CAC system for diagnosis of MRD by utilizing textural ratio characteristics of renal parenchymal as well as renal sinus region. The classification is made on basis of the texture ratio features obtained from renal parenchyma PROIs and renal sinus SROIs from both normal and MRD renal US image.

The sample images with PROIs and SROIs marked from normal and MRD renal US images is given in Fig 6.1. The feature vector computed using PROI is divided by feature vector computed using SROI resulting in ratio feature vector.

The brief representation of computation of ratio feature vector from features extracted from PROIs and SROIs is given in Fig. 6.2. Hence, this chapter incorporates an ANFC based CAC system for diagnosis of MRD using texture ratio features.

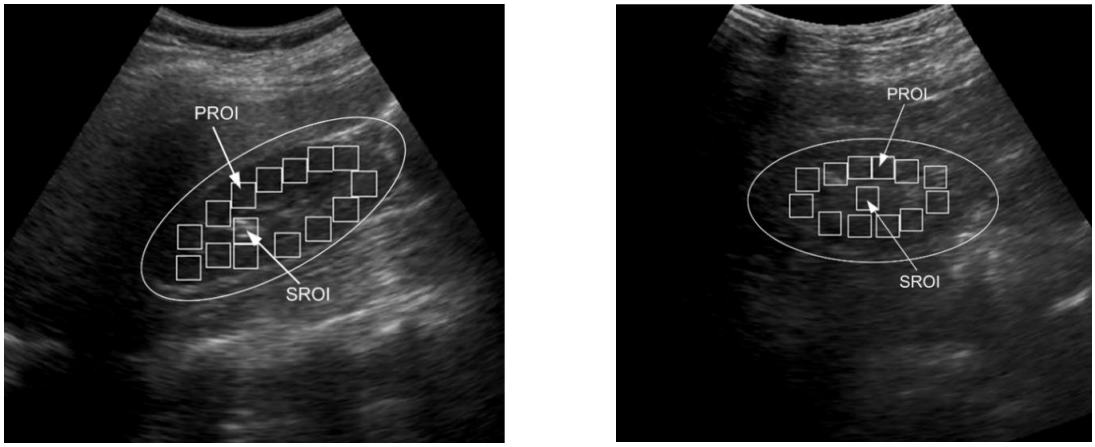


**Fig. 6.1** (*a*) A sample US image of (*a*) normal and (*b*) MRD with PROIs and SROIs marked.
**Note**: PROI are extracted from renal parenchyma region, SROI are extracted from renal sinus region.

This classification is also compared with the classification performance of ANFC based CAC system for diagnosis of MRD using absolute texture features (*chapter 5*) computed from PROIs.

$$RFV = \frac{FV[\blacksquare]_{PROI}}{FV[\blacksquare]_{SROI}}$$

**Fig. 6.2** Computation of RFV from features extracted from PROI and SROI.
**Note**: RFV: Ratio feature vector, FV: Feature vector.

## 6.2 Dataset Description and its Bifurcation for Design of ANFC based CAC System for Diagnosis of MRD using Texture Ratio Features

The work has been carried out on 19 B-mode renal US images consisting of 11 normal and 8 MRD images. The image assessment and data collection protocols are defined in chapter 3, section 3.3 and 3.4.1 respectively.

The ROIs of size 25 × 25 pixels have been extracted from the renal parenchyma region (SROIs) as well as renal sinus region (PROIs). The classification is made on basis of the ratio of features extracted from renal parenchyma PROIs and renal sinus SROIs. The brief description of the ROI extraction protocols is given in section 3.4.2.1 (*iv*) of chapter 3.

Total of 120 PROIs are extracted from 11 normal images along with one centrally located SROI from each image. Similarly, 119 PROIs are extracted from 8 MRD images along with one centrally located SROI from each image. These PROIs and SROIs are bifurcated to form training and testing sets for classification purpose. Brief description of data bifurcation protocol

is given in chapter 3, section 3.4.3 (*iii*). The image database and its bifurcation into training and testing sets for classification is given in Fig. 6.3.

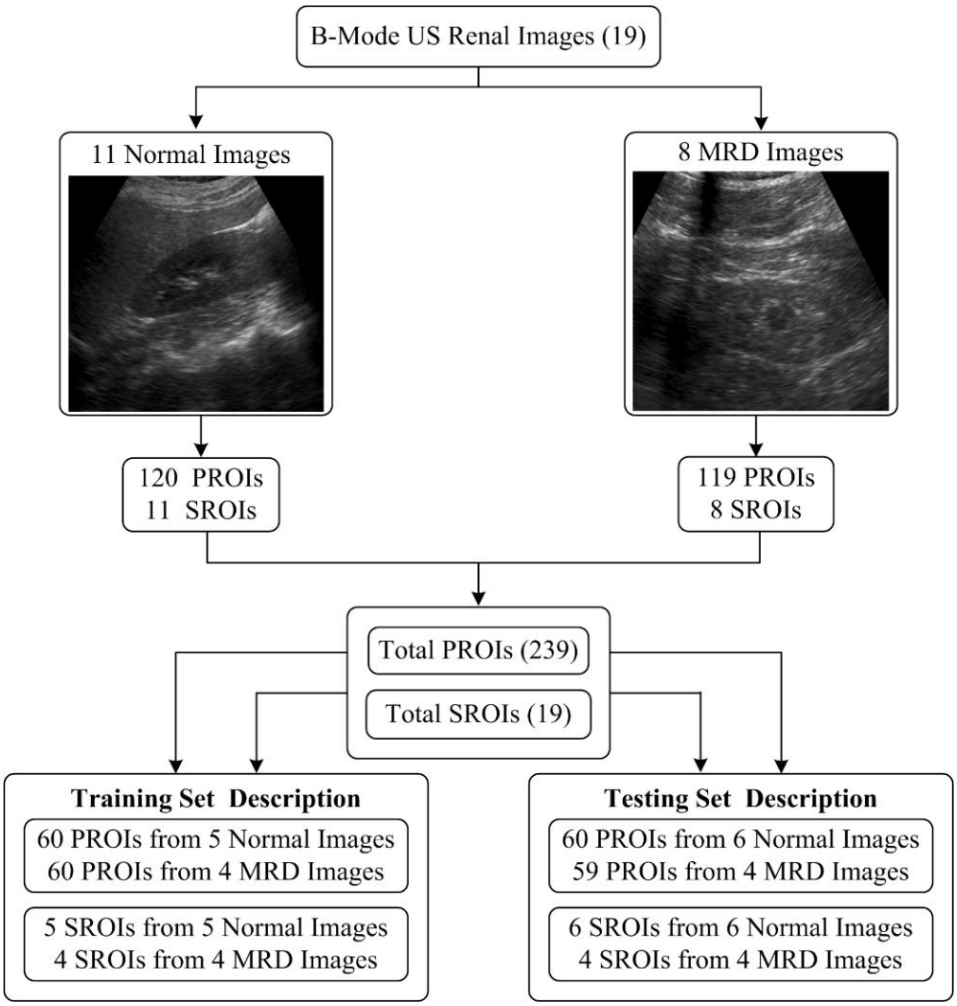


**Fig. 6.3** Dataset description and its bifurcation into training and testing sets.

## 6.3 Experimental Workflow for the Design of ANFC based CAC System for Diagnosis of Medical Renal Disease using Texture Ratio Features

The block diagram of the experimental workflow for design of ANFC based CAC system for diagnosis of MRD using texture ratio features is shown in Fig. 6.4. For evaluating the performance of the proposed CAC system, rigorous experimentation has been carried out for the diagnosis of MRD.

The ROI extraction (as discussed above) is followed by feature extraction and classification. Feature extraction has been conducted using statistical methods, signal processing methods and transform domain methods. Classification is performed using ANFC.

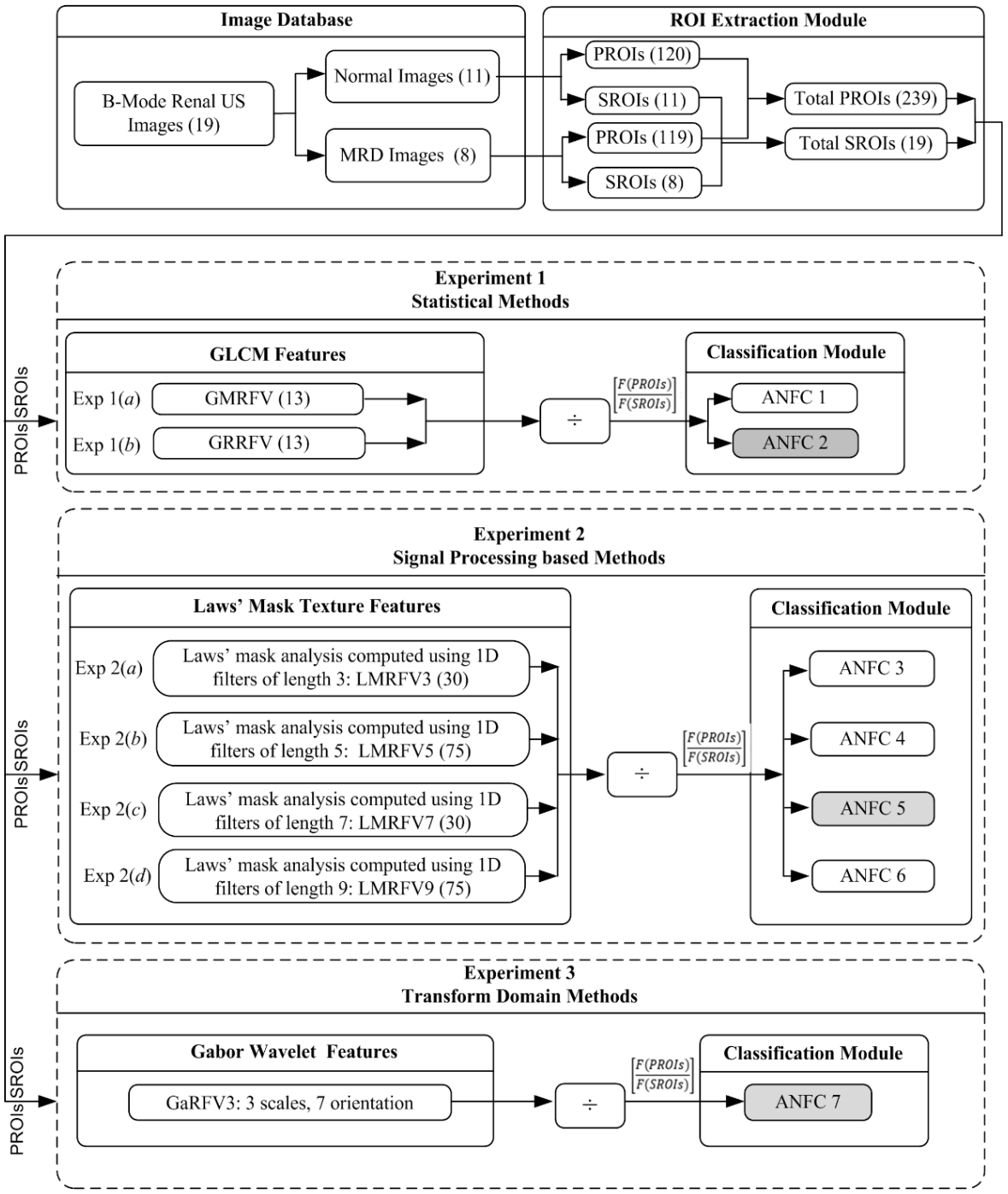


**Fig. 6.4** Experimental workflow for design of ANFC based CAC system for diagnosis of MRD using texture ratio features.

**Note**: MRD: Medical renal disease, GLCM: Gray level co-occurrence matrix, GMRFV: $GLCM_{mean}$ feature ratio vector, GRRFV: $GLCM_{range}$ feature ratio vector, LMRFV 3: Laws' mask ratio feature vector computed using 1D filter of length 3, LMRFV 5: Laws' mask ratio feature vector computed using 1D filter of length 5, LMRFV 7: Laws' mask ratio feature vector computed using 1D filter of length 7, LMRFV 9: Laws' mask ratio feature vector computed using 1D filter of length 9, GaRFV: Gabor ratio feature vector, ANFC: Adaptive Neuro-fuzzy classifier.

The brief description of feature vectors used for the design of ANFC based CAC system for diagnosis of medical renal diseases using texture ratio features is given in Table 6.1.

**Table 6.1** Brief description of feature vectors used for the design of ANFC based CAC system for diagnosis of medical renal diseases using texture ratio features.

| FV | Description | *l* |
|---|---|---|
| GMRFV | $GLCM_{mean}$ ratio feature vector | 13 |
| GRRFV | $GLCM_{range}$ ratio feature vector | 13 |
| LMRFV3 | Laws' mask ratio feature vector computed using 1D filter of length 3 | 30 |
| LMRFV5 | Laws' mask ratio feature vector computed using 1D filter of length 5 | 45 |
| LMRFV7 | Laws' mask ratio feature vector computed using 1D filter of length 7 | 30 |
| LMRFV9 | Laws' mask ratio feature vector computed using 1D filter of length 9 | 45 |
| GaRFV | Gabor ratio feature vector | 42 |

**Note**: FV: Feature vector, *l*: length of the feature vector, GLCM: Gray level co-occurrence matrix.

The brief description of the experiments carried out is given below:

*6.3.1 Experiment 1: Design of CAC system for diagnosis of MRD using statistical methods.*

The classification of normal and MRD renal US images is carried out in this experiment using statistical methods based GLCM features. The $GLCM_{mean}$ ratio feature vector (GMRFV) and $GLCM_{range}$ ratio feature vector (GRRFV) are computed at inter-pixel distance '*d*' = 1.

The brief description of feature extraction module using statistical methods is given in chapter 4, section 4.3.1 (*a*). These GMRFV and GRRFV are subjected to the classification module. The brief description of ANFC is given in chapter 5, section 5.3.1. The workflow diagram of experiment 1 is shown in Fig. 6.5.

The results obtained after conducting experiment 1 are given below:

*6.3.1.1 Experiment 1(a): Evaluating the classification performance of $GLCM_{mean}$ ratio feature vector (GMRFV).*

In this experiment, classification performance of GMRFV is evaluated at inter-pixel distance '*d'* = 1 using ANFC. The results of the experiment are shown in Table 6.2.

**Table 6.2** Classification performance of GMRFV using ANFC at *d* = 1.

| FV (*l*) | CM | | | OCA | ICA |
|---|---|---|---|---|---|
| **GMRFV** (13) | | NOR | MRD | | |
| | NOR | 50 | 10 | 87.3 | 83.3 |
| | MRD | 5 | 54 | | 91.5 |

**Note:** FV: Feature vector, *l*: length of the feature vector, GMRFV: $GLCM_{mean}$ ratio feature vector, CM: Confusion matrix, NOR: Normal class, MRD: Medical renal disease class, OCA: Overall classification accuracy, ICA: Individual classification accuracy, The OCA and ICA values are expressed in percentage.

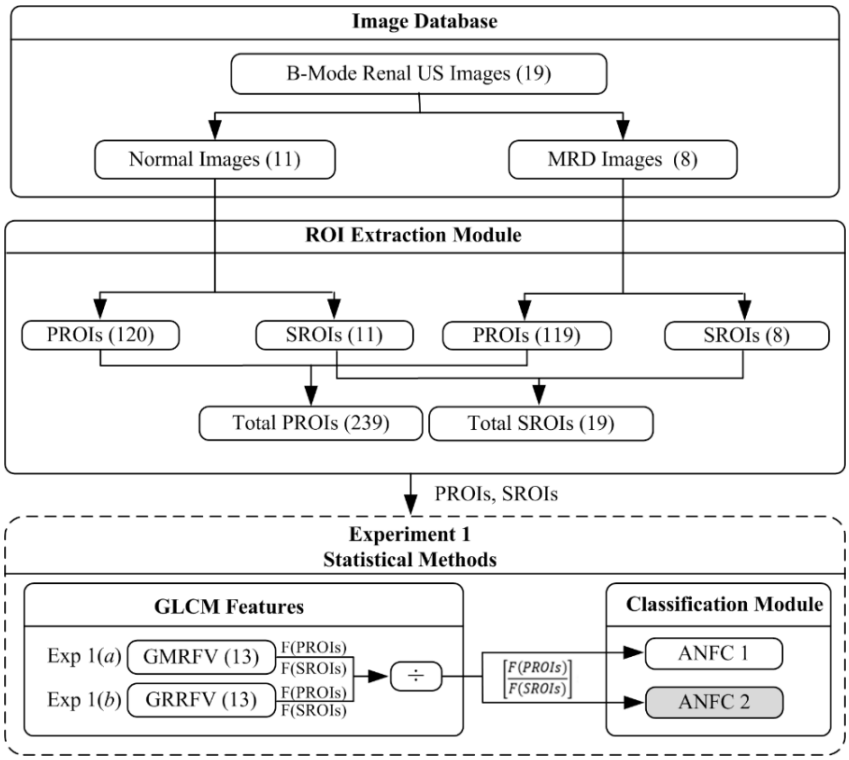


**Fig. 6.5** Workflow diagram of experiment 1: CAC system for diagnosis of MRD using GLCM ratio feature vectors.
**Note**: MRD: Medical renal disease, GLCM: Gray level co-occurrence matrix, GMRFV: $GLCM_{mean}$ feature ratio vector, GRRFV: $GLCM_{range}$ ratio feature vector, ANFC: Adaptive neuro-fuzzy classifier, Exp: Experiment

From Table 6.2, it is observed that an OCA of 87.3 % has been obtained with 13 different $GLCM_{mean}$ features computed at inter-pixel distance '*d'* = 1, along with ICA values of 83.3 % and 91.5 % for normal and MRD classes respectively.

*6.3.1.2 Experiment 1(b): Evaluating the classification performance of $GLCM_{range}$ ratio feature vector (GRRFV).*

In this experiment, classification performance of GRRFV at inter-pixel distance '*d'* = 1 is evaluated using ANFC. The results of the experiment are shown in Table 6.3.

**Table 6.3** Classification performance of GRRFV using ANFC at inter-pixel distance '*d'* = 1.

| **FV (*l*)** | **CM** | | | **OCA** | **ICA** |
|---|---|---|---|---|---|
| | | NOR | MRD | | |
| **GRRFV** (13) | NOR | 51 | 9 | 89.9 | 85 |
| | MRD | 3 | 56 | | 94.9 |

**Note:** FV: Feature vector, *l*: length of the feature vector, GRRFV: $GLCM_{range}$ ratio feature vector, CM: Confusion matrix, NOR: Normal class, MRD: Medical renal disease class, OCA: Overall classification accuracy, ICA: Individual classification accuracy, The OCA and ICA values are expressed in percentage.

From Table 6.3, it is observed that maximum OCA of 89.9 % has been obtained with 13 different $GLCM_{range}$ features computed at inter-pixel distance '*d'* = 1, along with ICA values of 85 % and 94.9 % for normal and MRD classes respectively.

*Hence, among statistical methods, $GLCM_{mean}$ and $GLCM_{range}$ features, GRRFV outperforms GMRFV by yielding an OCA of 89.9 % along with ICA values of 85.0 % and 94.9 % for normal and MRD classes respectively.*

*6.3.2 Experiment 2: Design of CAC system for diagnosis of MRD using features obtained from signal processing methods.*

The classification of normal and MRD renal US images is carried out in this experiment using signal processing based Laws' mask texture features. The brief description of signal processing based feature extraction is given in chapter 4, section 4.3.2 (*a*). Feature vectors are computed using Laws' mask ratio feature vector computed using 1D filter of length 3, 5, 7 and 9. These LMRFV3, LMRFV5, LMRFV7 and LMRFV9 are subjected to the classification module. The brief description of ANFC is explained in chapter 5, section 5.3.1. The workflow diagram of experiment 2 is shown in Fig. 6.6.

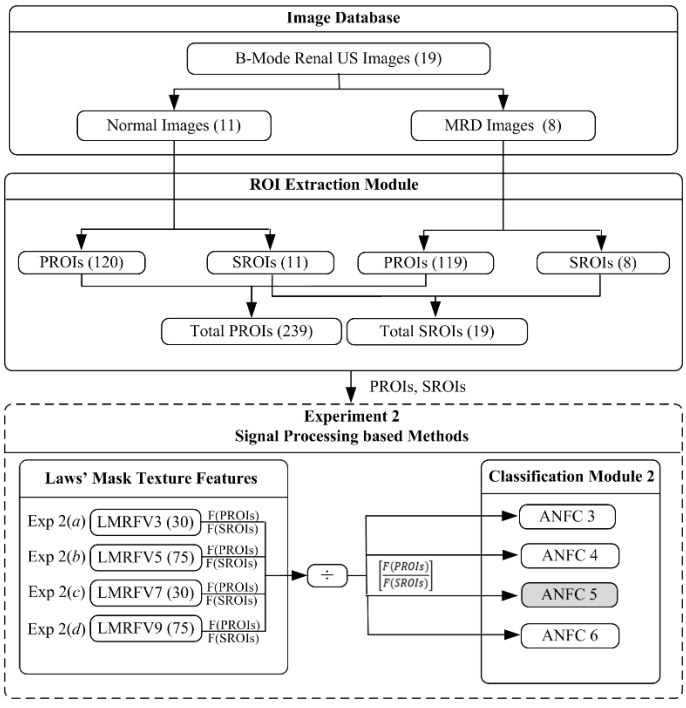


**Fig. 6.6** Workflow diagram of experiment 2: CAC system for renal diagnosis of MRD using Laws' mask ratio feature vectors (LMRFVs).
**Note:** LMRFV 3: Laws' mask ratio feature vector computed using 1D filter of length 3, LMRFV 5: Laws' mask ratio feature vector computed using 1D filter of length 5, LMRFV 7: Laws' mask ratio feature vector computed using 1D filter of length 7, LMRFV 9: Laws' mask ratio feature vector computed using 1D filter of length 9.

The results obtained after conducting experiment 2 are given below:

*6.3.2.1 Experiment 2(a): Evaluating the classification performance of Laws' mask ratio feature vector computed using 1D filter of length 3 (LMRFV3).*

In this experiment, classification performance of LMRFV3 is evaluated using ANFC. The results of the experiment are shown in Table 6.4.

**Table 6.4** Classification performance of LMRFV3 using ANFC.

| **FV (*l*)** | **CM** | | | **OCA** | **ICA** |
|---|---|---|---|---|---|
| **LMRFV3** (30) | | NOR | MRD | | |
| | NOR | 40 | 20 | 78.1 | 66.6 |
| | MRD | 6 | 53 | | 89.8 |

**Note:** FV: Feature vector, *l*: length of the feature vector, LMRFV 3: Laws' mask ratio feature vector computed using 1D filter of length 3, CM: Confusion matrix, MRD: Medical renal disease class, NOR: Normal class, OCA: Overall classification accuracy, ICA: Individual classification accuracy, The OCA and ICA values are expressed in percentage.

From Table 6.4, it is observed that maximum OCA of 78.1 % has been obtained with 30 different Laws' mask ratio features computed using 1D filter of length 3, along with ICA values of 66.6 % and 89.8 % for normal and MRD classes respectively.

*6.3.2.2 Experiment 2(b): Evaluating the classification performance of Laws' mask ratio feature vector computed using 1D filter of length 5 (LMRFV5).*

In this experiment, classification performance of LMRFV5 is evaluated using ANFC. The results of the experiment are shown in Table 6.5.

**Table 6.5** Classification performance of LMRFV5 using ANFC.

| **FV (*l*)** | **CM** | | | **OCA** | **ICA** |
|---|---|---|---|---|---|
| **LMRFV5** (75) | | NOR | MRD | | |
| | NOR | 44 | 16 | 83.1 | 73.3 |
| | MRD | 4 | 55 | | 93.2 |

**Note:** FV: Feature vector, *l*: length of the feature vector, LMRFV 5: Laws' mask ratio feature vector computed using 1D filter of length 5, CM: Confusion matrix, MRD: Medical renal disease class, NOR: Normal class, OCA: Overall classification accuracy, ICA: Individual classification accuracy, The OCA and ICA values are expressed in percentage.

From Table 6.5, it is observed that maximum OCA of 83.1 % has been obtained with 75 different Laws' mask ratio feature vector computed using 1D filter of length 5, along with ICA values of 73.3 % and 93.2 % for normal and MRD classes respectively.

*6.3.2.3 Experiment 2(c): Evaluating the classification performance of Laws' mask ratio feature vector computed using 1D filter of length 7 (LMRFV7).*

In this experiment, classification performance of LMRFV7 is evaluated using ANFC. The results of the experiment are shown in Table 6.6.

**Table 6.6** Classification performance of LMRFV7 using ANFC.

| **FV (*l*)** | **CM** | | | **OCA** | **ICA** |
|---|---|---|---|---|---|
| **LMRFV7** (30) | | NOR | MRD | | |
| | NOR | 47 | 13 | 88.2 | 78.3 |
| | MRD | 1 | 58 | | 98.3 |

**Note:** FV: Feature vector, *l*: length of the feature vector, LMRFV7: Laws' mask ratio feature vector computed using 1D filter of length 7, CM: Confusion matrix, NOR: Normal class, MRD: Medical renal disease class, OCA: Overall classification accuracy, ICA: Individual classification accuracy, The OCA and ICA values are expressed in percentage.

From Table 6.6, it is observed that maximum OCA of 88.2 % has been obtained with 30 different Laws' mask ratio feature vector computed using 1D filter of length 7, along with ICA values of 78.3 % and 98.3 % for normal and MRD classes respectively.

*6.3.2.4 Experiment 2(d): Evaluating the classification performance of Laws' mask ratio feature vector computed using 1D filter of length 9 (LMRFV9).*

In this experiment, classification performance of LMRFV9 is evaluated using ANFC. The results of the experiment are shown in Table 6.7.

**Table 6.7** Classification performance of LMFV9 using ANFC.

| **FV (*l*)** | **CM** | | | **OCA** | **ICA** |
|---|---|---|---|---|---|
| **LMRFV9** (75) | | NOR | MRD | | |
| | NOR | 52 | 8 | 78.1 | 86.6 |
| | MRD | 18 | 41 | | 69.4 |

**Note:** FV: Feature vector, *l*: length of the feature vector, LMRFV 9: Laws' mask ratio feature vector computed using 1D filter of length 9, CM: Confusion matrix, NOR: Normal class, MRD: Medical renal disease class, OCA: Overall classification accuracy, ICA: Individual classification accuracy, The OCA and ICA values are expressed in percentage.

From Table 6.7, it is observed that maximum OCA of 78.1 % has been obtained with 30 different Laws' mask ratio feature vector computed using 1D filter of length 9, along with ICA values of 86.6 % and 69.4 % for normal and MRD classes respectively.

*Hence, among signal processing based Laws' mask texture features, LMRFV7 performs best by yielding an OCA of 88.2 % along with ICA values of 78.3 % and 98.3 % for normal and MRD classes respectively.*

*6.3.3 Experiment 3: Design of CAC system for diagnosis of MRD using Gabor texture ratio features (GaRFV).*

The classification of normal and MRD renal US images is carried out in this experiment using transform domain Gabor 2D wavelet texture ratio features. The brief description of transform domain feature extraction is given in chapter 4, section 4.3.3 (*a*).

The Gabor features are computed using Gabor wavelets obtained by using 7 different orientations (22.5˚, 45˚, 67.5˚, 90˚, 112.5˚, 135˚, 157.5˚) and 3 scale values (0, 1, 2). This GaRFV is subjected to the classification module. The brief description of ANFC is given in chapter 5, section 5.3.1. The workflow diagram of experiment 3 is shown in Fig. 6.7.

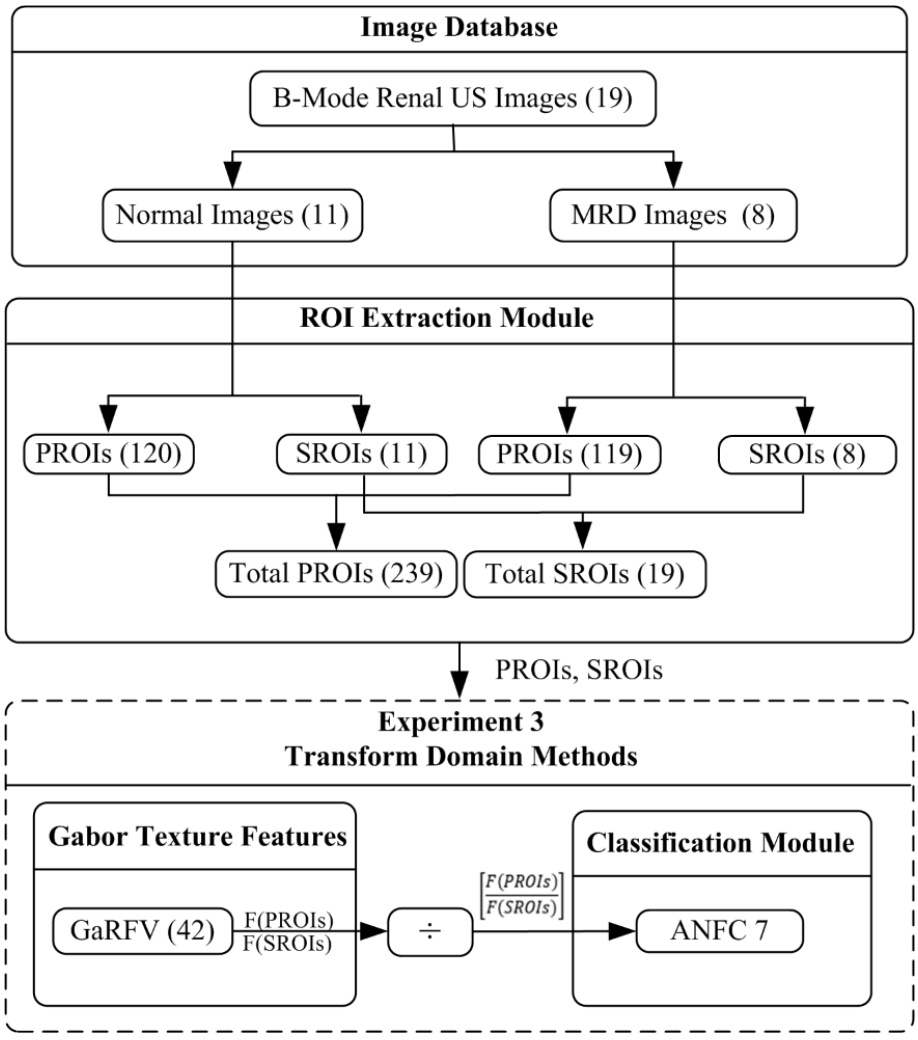


**Fig. 6.7** Workflow diagram of experiment 3: CAC system for diagnosis of MRD using Gabor texture ratio feature vector (GaRFV).
**Note:** GaRFV: Gabor ratio feature vector.

In this experiment, classification performance of GaRFV is evaluated using ANFC. The results of the experiment are shown in Table 6.8.

**Table 6.8** Classification performance of GaRFV using ANFC.

| FV (*l*) | CM | | | OCA | ICA |
|---|---|---|---|---|---|
| **GaRFV** (42) | | NOR | MRD | | |
| | NOR | 43 | 17 | 79.8 | 71.6 |
| | MRD | 7 | 52 | | 88.1 |

**Note:** FV: Feature vector, *l*: length of the feature vector, GaRFV: Gabor ratio feature vector, CM: Confusion matrix, NOR: Normal class, MRD: Medical renal disease class, OCA: Overall classification accuracy, ICA: Individual classification accuracy, The OCA and ICA values are expressed in percentage.

From Table 6.8, it is observed that an OCA of 79.8 % has been obtained with 42 different Gabor texture features at 3 scales and 7 orientation, along with ICA values of 71.6 % and 88.1 % for normal and MRD classes respectively.

## 6.4 Comparative analysis of the Experiments Conducted for Design of ANFC based CAC System for Diagnosis of MRD using Ratio Texture Features

On conducting exhaustive experiments on statistical methods, signal processing based methods and transform domain methods, a comparison can be drawn between the highest overall classification accuracies achieved by the texture ratio features in their respective domains. A brief description of the comparative analysis is given in Table 6.9.

**Table 6.9** Comparative analysis of statistical methods, signal processing methods and transform domain methods.

| Methods | FV (*l*) | OCA | $ICA_{NOR}$ | $ICA_{MRD}$ |
|---|---|---|---|---|
| Exp.1: Statistical Methods | GRRFV (13) | 89.9 | 85 | 94.9 |
| Exp.2: Signal Processing based Methods | LMRFV7 (30) | 88.2 | 78.3 | 98.3 |
| Exp.3: Transform Domain Methods | GaRFV (42) | 79.8 | 71.6 | 88.1 |

**Note:** FV: Feature vector, *l*: Length of the feature vector, GRRFV: $GLCM_{range}$ ratio feature vector, LMRFV7: Laws' mask ratio feature vector computed using 1D filter of length 7, GaRFV: Gabor ratio feature vector evaluated at 3 scales and 7 orientations, OCA: Overall classification accuracy, NOR: Normal class, MRD: Medical renal disease, $ICA_{NOR}$: ICA value for NOR class, $ICA_{MRD}$: ICA value for MRD class, Exp.: Experiment, The OCA and ICA values are expressed in percentage.

Hence, it is observed that the maximum OCA of 89.9 % is achieved by $GLCM_{range}$ feature vector at inter-pixel distance '*d*' = 1, computed using ratio of features extracted from renal parenchyma and renal sinus region. The ICA values for normal and MRD are 85.0 % and 94.9 % respectively.

## 6.5 Comparison of ANFC based CAC System for Diagnosis of Medical Renal Disease using Texture Ratio Features with Other Proposed CAC Systems

The present approach that utilizes the texture ratio features obtained by taking the ratio of features from renal parenchyma PROIs and renal sinus SROIs, is compared with the approach that utilized absolute features from renal parenchymal PROIs only (chapter 5). A comparative analysis is made on the two different proposed approaches on basis of the classification results, shown in Table 6.10.

**Table 6.10** Comparative analysis of results obtained from absolute and ratio feature vectors.

| **Methods** | **OCA$_{PROI}$ (FV)** *(Absolute features)* | **OCA$_{PROI/SROI}$ (FV)** *(Ratio features)* |
|---|---|---|
| Statistical Methods | 78.1 (GMAFV) | 87.3 (GMRFV) |
| | 84.8 (GRAFV) | 89.9 (GRRFV) |
| Signal Processing based Methods | 73.1 (LMAFV3) | 78.1 (LMRFV3) |
| | 71.4 (LMAFV5) | 83.1 (LMRFV5) |
| | 71.4 (LMAFV7) | 88.2 (LMRFV7) |
| | 69.7 (LMAFV9) | 78.1 (LMRFV9) |
| Transform Domain Methods | 67.2 (GaAFV) | 79.8 (GaRFV) |

**Note:** GMAFV: GLCM$_{mean}$ absolute feature vector, GRAFV: GLCM$_{range}$ absolute feature vector, LMAFV 3: Laws' mask absolute feature vector computed using 1D filter of length 3, LMAFV 5: Laws' mask absolute feature vector computed using 1D filter of length 5, LMAFV 7: Laws' mask absolute feature vector computed using 1D filter of length 7, LMAFV 9: Laws' mask absolute feature vector computed using 1D filter of length 9, GaAFV: Gabor absolute feature vector, GMRFV: GLCM$_{mean}$ ratio feature vector, GRRFV: GLCM$_{range}$ ratio feature vector, LMRFV 3: Laws' mask ratio feature vector computed using 1D filter of length 3, LMRFV 5: Laws' mask ratio feature vector computed using 1D filter of length 5, LMRFV 7: Laws' mask ratio feature vector computed using 1D filter of length 7, LMRFV 9: Laws' mask ratio feature vector computed using 1D filter of length 9, GaRFV: Gabor ratio feature vector.

It can be observed that the approach used in present study that utilizes the texture ratio features obtained by taking the ratio of features extracted from PROIs and SROIs yield better results by all of the three methods, namely, statistical, signal processing and transform domain methods, as compared to the approach that utilized absolute features from PROIs only. Among statistical methods, GRRFV yields the maximum OCA of 89.9 %, among signal processing based methods, LMFV7 yield best results with an OCA of 88.2 % and from transform domain methods, GaRFV yields the maximum OCA of 79.8 %. All of the maximum OCA values are obtained from the texture ratio features and it is clearly observed that results are better with the design of the proposed CAC system that utilizes texture ratio features. Out of all the features extracted, it is observed that statistical methods based GLCM$_{range}$ texture ratio features yield the best results (OCA = 89.9 %).

## 6.6 Proposed ANFC based CAC System Design for Diagnosis of MRD using Texture Ratio Features

The result of the study indicates that statistical methods based $GLCM_{range}$ feature vector, computed at inter-pixel distance '*d*' = 1 yields the highest overall classification accuracy of 89.9 % with the individual classification accuracy values of 85.0 % and 94.9 % for normal and MRD classes respectively. Also, the results show significant increase in the accuracies by using the approach presented in this chapter (considering the ratio of texture features extracted from renal parenchyma and renal sinus) as compared to the approach used in chapter 5 (considering the features extracted from renal parenchyma only). Hence, it is observed that the GRRFV is most efficient for classification of renal ultrasound images into normal and MRD classes using texture ratio features. The promising results obtained from the study indicate that the proposed CAC system design using $GLCM_{range}$ features can be routinely used in clinical environment for diagnosis of MRD. The diagram of proposed CAC system for diagnosis of MRD using texture ratio features is given in Fig. 6.8.

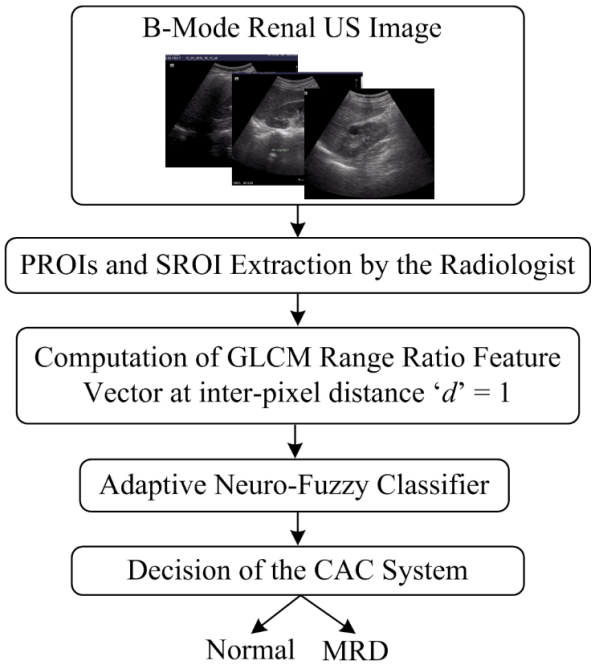


**Fig. 6.8** Proposed CAC system for diagnosis of MRD using texture ratio features.

## 6.7 Concluding Remarks

In the present study, an attempt has been made to evaluate the significance of textural changes in renal parenchyma with respect to renal sinus region for diagnosis of MRD.

For the proposed CAC system design, the PROIs are extracted from renal parenchymal region and SROIs are extracted from renal sinus region from both, normal and MRD renal US image classes. Texture ratio features are computed by taking the ratio of features extracted from PROIs and SROIs. Various experiments are conducted using statistical, signal processing and transform domain methods. The texture ratio features obtained from these methods are subjected for classification using ANFC classifier. It is observed that statistical methods based $GLCM_{range}$ feature vector, computed at inter-pixel distance '*d'* = 1 yields the highest OCA of 89.9 % with ICA values of 85.0 % and 94.9 % for normal and MRD classes respectively. Also, the results of the study indicate that the proposed design of ANFC based CAC system using texture ratio features is more efficient than the design that utilized absolute features only. The $GLCM_{range}$ ratio feature vector proves to be the most efficient for classification of renal US images into normal and MRD classes. Therefore selected $GLCM_{range}$ texture ratio features can be routinely used in clinical environment for diagnosis of MRD.

In next chapter, the textural changes in renal parenchymal region with respect to renal sinus region (which exhibits same hyperechoic appearance in both the cases i.e. normal and MRD renal US images) along with textural changes in renal parenchymal alone are considered. Therefore, the combined features obtained from PROIs and ratio of PROIs and SROIs are utilized for the diagnosis of MRD. Also, from Table 6.10, it is clear that GRRFV, LMRFV7 and GaRFV computed from texture ratio features yield the highest OCA among the statistical, signal processing and transform domain methods respectively. Therefore, the efficacy of $GLCM_{range}$, Laws' mask features computed using 1D filter of length 7 and Gabor texture features evaluated at 3 scales and 7 orientations is evaluated using combined texture features in the next chapter.

# Chapter 7

# ANFC based CAC System for Diagnosis of Medical Renal Disease using Combined Texture Features

## 7.1 Introduction

In previous chapters, various attempts have been made to design CAC systems for diagnosis of MRD. An ANFC based CAC system proposed in *chapter 5* utilized the absolute texture features computed from PROIs only. Another ANFC based CAC system proposed in *chapter 6* utilized the texture ratio features for diagnosis of MRD.

The performance of these CAC systems is compared and it is observed that the CAC system design using texture ratio feature yield higher accuracy in comparison to CAC system design using absolute features. Hence, it can be concluded that the CAC system design using texture ratio features performs better than the CAC system using absolute features.

This chapter incorporates a CAC system design utilizing the combination of the absolute features computed from PROIs and texture ratio features computed from PROIs and SROIs. The sample images of normal and MRD renal US images with PROIs and SROIs marked is shown in chapter 6, Fig. 6.1. The features that performed best among statistical, signal processing and transform domain methods are used for the present work. It is observed that among statistical methods, $GLCM_{range}$ ratio features yield the best OCA of 87.3 %, among signal processing based methods, Laws' mask ratio feature vector computed using 1D filter of length 7 yield the best OCA of 88.2 %, and in transform domain methods, 2D Gabor wavelet ratio features obtained by using 3 scales and 7 orientations yield an OCA of 79.8 %.

Accordingly, the features that performed best among statistical, signal processing and transform domain methods are only considered for design of ANFC based CAC system using combined feature vector.

The combined feature vector (CFV) is computed by combining the absolute feature vector (computed from PROIs only) and ratio feature vector (computed by taking the ratio of feature vectors computed using PROIs and corresponding SROI). An example to demonstrate the computation of CFV is shown in Fig. 7.1.

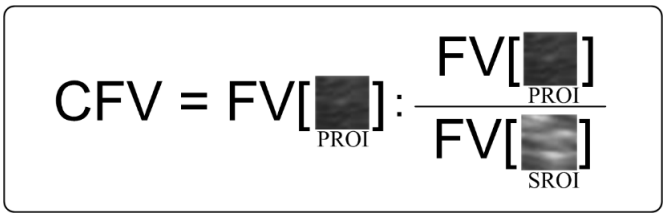


**Fig. 7.1** Computation of CFV from features extracted from PROIs alone and ratio of PROIs and SROI.
**Note**: CFV: Combined feature vector, FV: Feature vector, PROI: Parenchyma region of interest, SROI: Sinus region of interest.

Therefore, in the present work an ANFC based CAC system is proposed using combined texture features for diagnosis of MRD.

## 7.2 Dataset Description and its Bifurcation for Design of ANFC based CAC System for Diagnosis of MRD using Combined Texture Features

The work has been carried out on 19 B-mode renal US images consisting of 11 normal and 8 MRD images. The image assessment and data collection protocols are defined in chapter 3, section 3.3 and 3.4.1 respectively.

The ROIs of size 25 × 25 have been extracted from the renal parenchyma region (SROIs) as well as renal sinus region (PROIs). The classification is made on basis of the absolute features extracted from renal parenchyma PROIs and the ratio of features extracted from PROIs and renal sinus SROIs. The brief description of the ROI extraction protocols is given in chapter 3, section 3.4.2.1 (*v*).

Total of 120 PROIs are extracted from 11 normal images along with one centrally located SROI from each image. Similarly, 119 PROIs are extracted from 8 MRD images along with one centrally located SROI from each image. These PROIs and SROIs are bifurcated to form training and testing sets for classification purpose. Brief description of data bifurcation protocol is given in chapter 3, section 3.4.3 (*iv*). The image database and its bifurcation into training and testing sets for classification is given in chapter 6, Fig. 6.2.

## 7.3 Experimental Workflow for the Design of ANFC based CAC System for Diagnosis of Medical Renal Disease using Combined Texture Features

The block diagram of the experimental workflow for design of ANFC based CAC system for diagnosis of MRD using combined texture features is shown in Fig. 7.2. For evaluating the performance of the proposed CAC system, rigorous experimentation has been carried out for the diagnosis of MRD using statistical, signal processing and transform domain methods. The ROI extraction (as discussed above) is followed by feature extraction and classification. Classification is performed using ANFC.

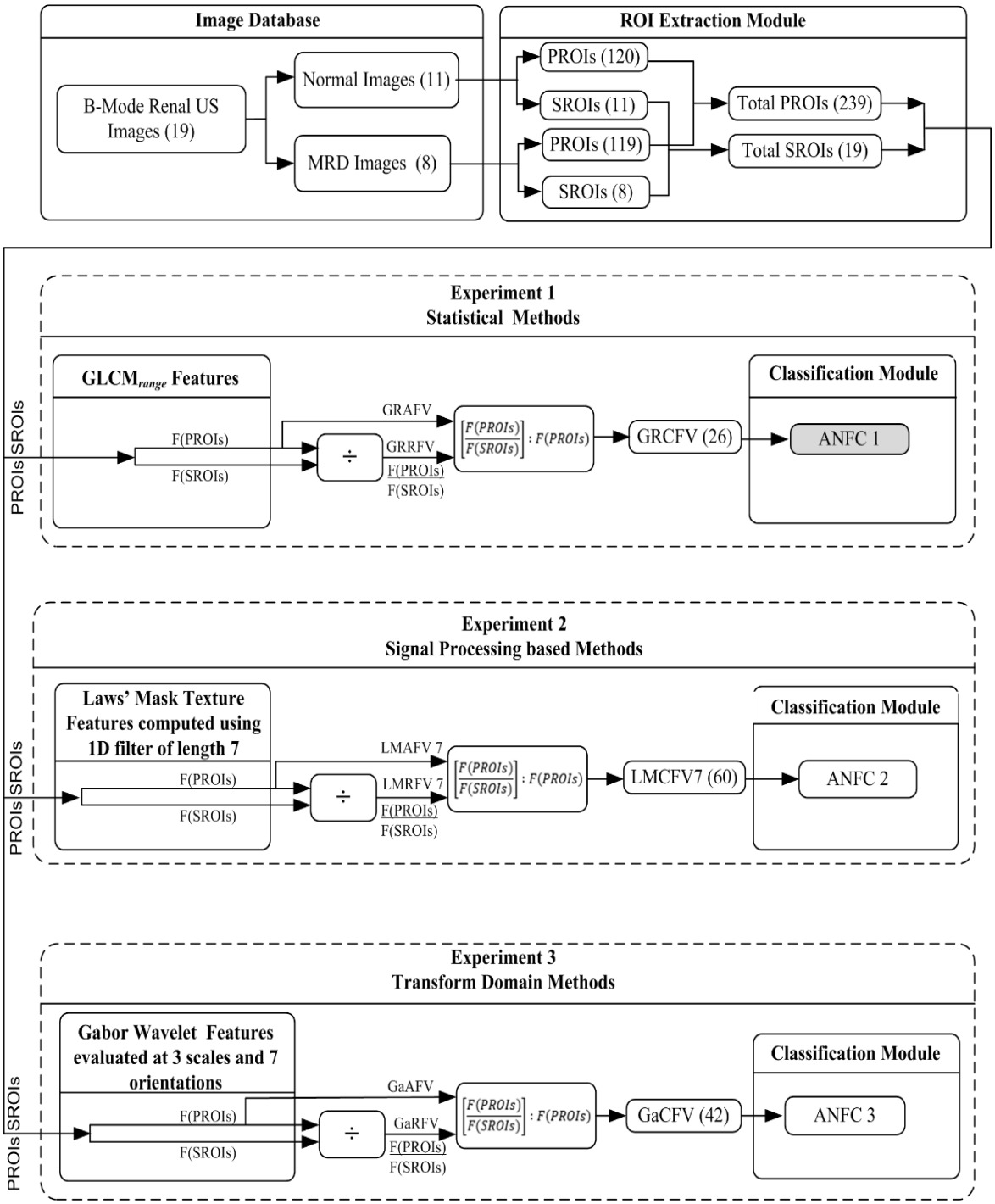


**Fig. 7.2** Experimental workflow for design of ANFC based CAC system for diagnosis of MRD using combined texture features.

**Note**: MRD: Medical renal disease, GLCM: Gray level co-occurrence matrix, GRCFV: GLCM$_{range}$ combined feature vector, LMAFV 7: Laws' mask absolute feature vector computed using 1D filter of length 7, LMRFV 7: Laws' mask ratio feature vector computed using 1D filter of length 7, LMCFV 7: Laws' mask combined feature vector computed using 1D filter of length 7, GaAFV: Gabor absolute feature vector, GaRFV: Gabor ratio feature vector, GaCFV: Gabor combined feature vector, ANFC: Adaptive Neuro-fuzzy classifier.

The brief description of feature vectors used for design of ANFC based CAC system for diagnosis of medical renal diseases using combined texture features is given in Table 7.1.

**Table 7.1** Brief description of feature vectors used for the design of ANFC based CAC system for diagnosis of medical renal diseases using texture ratio features.

| FV | Description | *l* |
|---|---|---|
| GRCFV | $GLCM_{range}$ combined feature vector | 13 |
| LMCFV3 | Laws' mask combined feature vector computed using 1D filter of length 3 | 30 |
| LMCFV5 | Laws' mask combined feature vector computed using 1D filter of length 5 | 45 |
| LMCFV7 | Laws' mask combined feature vector computed using 1D filter of length 7 | 30 |
| LMCFV9 | Laws' mask combined feature vector computed using 1D filter of length 9 | 45 |
| GaCFV | Gabor combined feature vector | 42 |

**Note**: FV: Feature vector, *l*: length of the feature vector, GLCM: Gray level co-occurrence matrix.

The brief description of the experiments carried out is given below:

*7.3.1 Experiment 1: Design of CAC system for diagnosis of MRD using $GLCM_{range}$ combined feature vector (GRCFV).*

The classification of normal and MRD renal US images is carried out in this experiment using statistical methods based GLCM features. The $GLCM_{range}$ combined feature vector (GRCFV) is computed at inter-pixel distance '*d*' = 1. The brief description of feature extraction module using statistical methods is given in chapter 4, section 4.3.1 (a). This GRCFV is subjected to the classification module. The brief description of ANFC is given in chapter 5, section 5.3.1. The workflow diagram of *experiment 1* is shown in Fig. 7.3.

The results obtained after conducting *experiment 1* are given below:

In this experiment, classification performance of GRCFV at inter-pixel distance '*d*'= 1 is evaluated using ANFC. The results of the experiment are shown in Table 7.2.

**Table 7.2** Classification performance of GRCFV using ANFC at inter-pixel distance '*d'* = 1.

| FV (*l*) | CM | | | OCA | ICA |
|---|---|---|---|---|---|
| GRAFV: GRRFV = **GRCFV** (26) | | NOR | MRD | | |
| | NOR | 54 | 6 | 94.9 | 90 |
| | MRD | 0 | 59 | | 100 |

**Note:** FV: Feature vector, *l*: Length of the feature vector, GACFV: $GLCM_{range}$ absolute feature vector, GRCFV: $GLCM_{range}$ ratio feature vector, GRCFV: $GLCM_{range}$ combined feature vector, CM: Confusion matrix, NOR: Normal class, MRD: Medical renal disease class, OCA: Overall classification accuracy, ICA: Individual classification accuracy, The OCA and ICA values are expressed in percentage.

From Table 7.2, It is observed that an OCA of 94.9 % is obtained from 26 different $GLCM_{range}$ combined features computed at inter-pixel distance '*d'* = 1, along with ICA values of 90 % and 100 % for normal and MRD classes respectively.

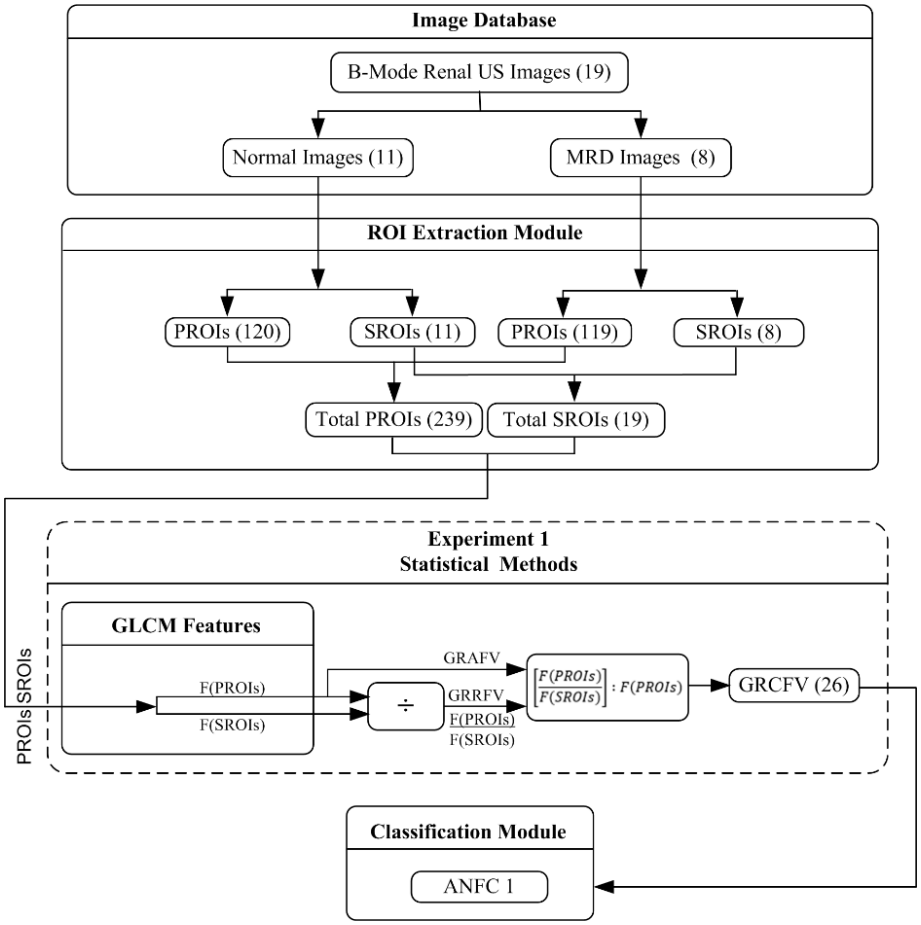


**Fig. 7.3** Workflow diagram of *experiment* 1: CAC system for diagnosis of MRD using $GLCM_{range}$ combined texture feature vector (GRCFV).
**Note:** GRAFV: $GLCM_{range}$ absolute feature vector, GRRFV: $GLCM_{range}$ ratio feature vector, GRCFV: $GLCM_{range}$ combined feature vector.

### *7.3.2 Experiment 2: Design of CAC system for diagnosis of MRD using Laws' mask combined feature vector computed by using 1D filter of length 7 (LMCFV 7).*

The classification of normal and MRD renal US images is carried out in this experiment using signal processing based Laws' texture features. The brief description of signal processing based feature extraction is given in chapter 4, section 4.3.2 (*a*).

Feature vectors are computed using Laws' mask combined features computed using 1D filter of length 7. This LMFV7 is subjected for the classification task using ANFC. The brief description of ANFC is given in chapter 5, section 5.3.1. The workflow diagram of *experiment* 2 is shown in Fig. 7.4.

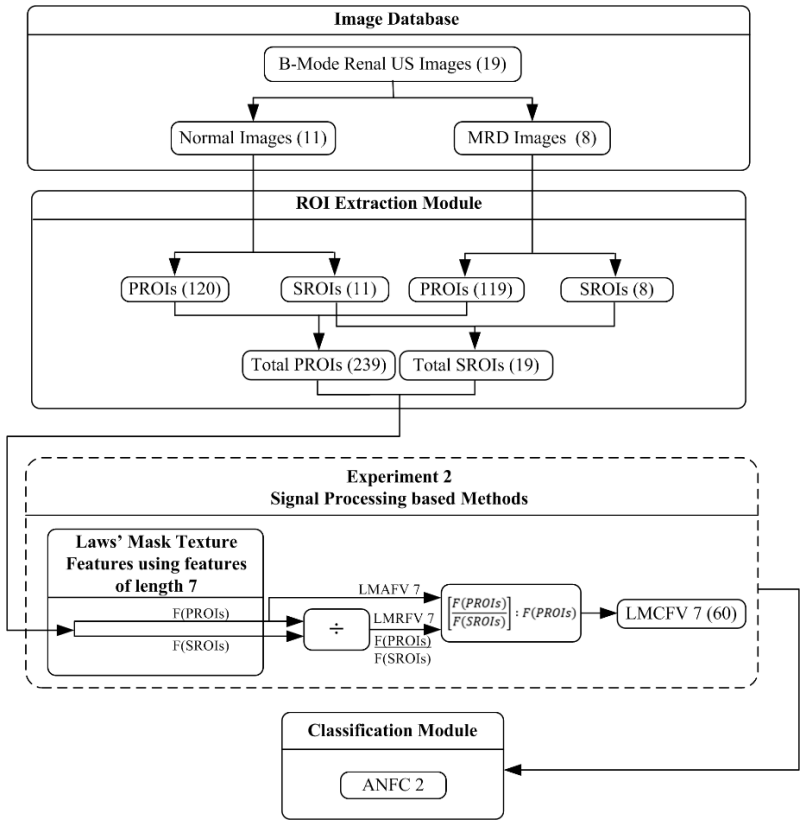


**Fig. 7.4** Workflow diagram of experiment 2: CAC system for diagnosis of MRD using Laws' mask combined texture feature vectors (LMCFVs).
**Note:** LMAFV 7: Laws' mask absolute feature vector computed using 1D filter of length 7, LMRFV 7: Laws' mask ratio feature vector computed using 1D filter of length 3, LMCFV 3: Laws' mask combined feature vector computed using 1D filter of length 7.

In this experiment, classification performance of LMCFV7 is evaluated using ANFC. The results of the experiment are shown in Table 7.3.

**Table 7.3** Classification performance of LMCFV7 using ANFC.

| **FV (*l*)** | **CM** | | | **OCA** | **ICA** |
|---|---|---|---|---|---|
| LMAFV7: LMRFV7 = **LMCFV7** (60) | | NOR | MRD | | |
| | NOR | 54 | 6 | 89.9 | 90.0 |
| | MRD | 6 | 53 | | 89.9 |

**Note:** FV: Feature vector, *l*: Length of the feature vector, LMAFV 7: Laws' mask absolute feature vector computed using 1D filter of length 7, LMRFV 7: Laws' mask ratio feature vector computed using 1D filter of length 7, LMCFV 7: Laws' mask combined feature vector computed using 1D filter of length 7, CM: Confusion matrix, NOR: Normal class, MRD: Medical renal disease class, OCA: Overall classification accuracy, ICA: Individual classification accuracy, The OCA and ICA values are expressed in percentage.

From Table 7.3, it is observed that OCA of 89.9 % has been obtained with 30 different Laws' mask combined features computed using 1D filter of length 7, along with ICA values of 90.0 % and 89.9 % for normal and MRD classes respectively.

*7.3.3 Experiment 3: Design of CAC system for diagnosis of MRD using Gabor combined feature vector (GaCFV).*

The classification of normal and MRD renal US images is carried out in this experiment using transform domain Gabor 2D wavelet texture features. The brief description of transform domain feature extraction methods using Gabor wavelet is given in chapter 4, section 4.3.3 (*a*). Feature vector is computed using 2D Gabor features, using Gabor wavelets obtained by using 7 different orientations (22.5˚, 45˚, 67.5˚, 90˚, 112.5˚, 135˚, 157.5˚) and 3 scale values (0, 1, 2). This GaCFV is subjected for the classification task using ANFC. The brief description of ANFC is given in chapter 5, section 5.3.1. The workflow diagram of experiment *3* is shown in Fig. 7.5.

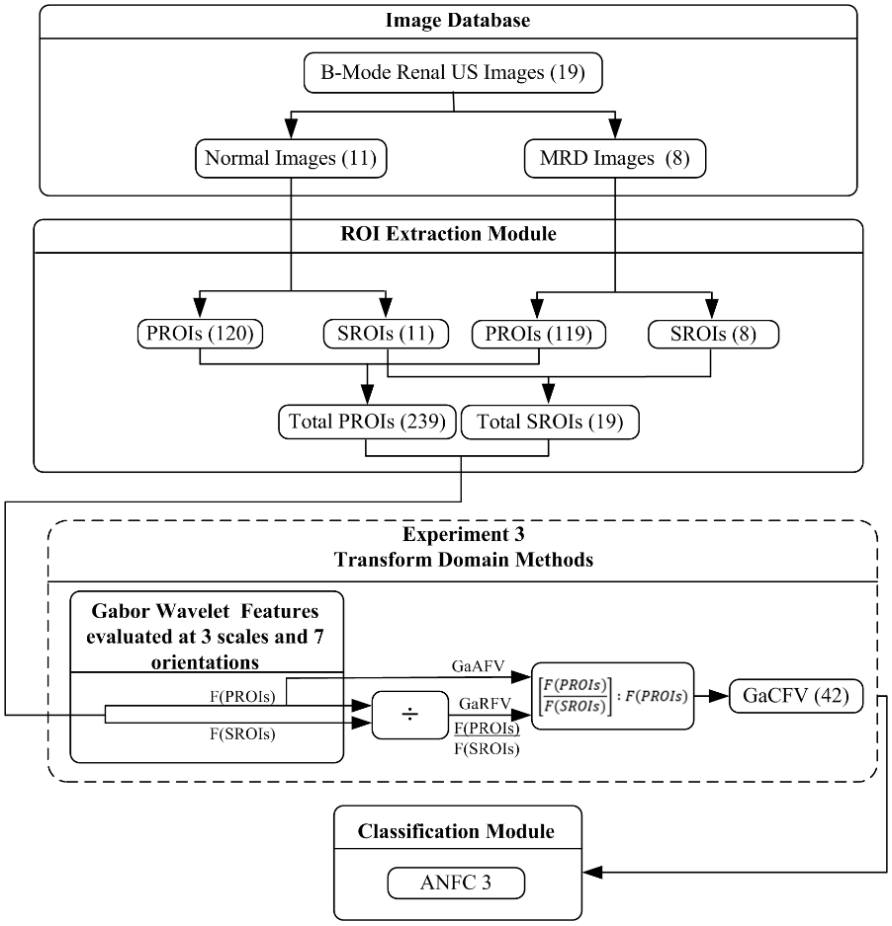


**Fig. 7.5** Workflow diagram of experiment 3: CAC system for diagnosis of MRD using Gabor combined texture feature vector (GaCFV).
**Note:** GaAFV: Gabor absolute feature vector, GaRFV: Gabor ratio feature vector, GaCFV: Gabor combined feature vector.

In this experiment, classification performance of GaCFV is evaluated using ANFC. The results of the experiment are shown in Table 7.4.

**Table 7.4** Classification performance of GaCFV using ANFC.

| **FV (*l*)** | **CM** | | | **OCA** | **ICA** |
|---|---|---|---|---|---|
| GaAFV: GaRFV = **GaCFV** (84) | | NOR | MRD | | |
| | NOR | 45 | 15 | 80.6 | 75.0 |
| | MRD | 8 | 51 | | 86.4 |

**Note:** FV: Feature vector, *l*: Length of the feature vector, GaAFV: Gabor absolute feature vector, GaRFV: Gabor ratio feature vector, GaCFV: Gabor combined feature vector, CM: Confusion matrix, MRD: Medical renal disease class, NOR: Normal class, OCA: Overall classification accuracy, ICA: Individual classification accuracy, The OCA and ICA values are expressed in percentage.

From Table 7.4, it is observed that maximum OCA of 80.6 % has been obtained with 84 Gabor texture features evaluated by using 3 scales and 7 orientation, along with ICA values of 75.0 % and 86.4 % for normal and MRD classes respectively.

## 7.4 Comparative Analysis of the Experiments Conducted for Design of ANFC based CAC System for Diagnosis of MRD using Combined Texture Features

On conducting exhaustive experiments on statistical, signal processing and transform domain methods, a comparison can be drawn between the highest OCAs achieved by the combined texture features. A brief description of the comparative analysis is given in Table 7.5.

**Table 7.5** Comparative analysis of statistical, signal processing and transform domain methods.

| **Methods** | **FV (*l*)** | **OCA** | **$ICA_{NOR}$** | **$ICA_{MRD}$** |
|---|---|---|---|---|
| Statistical Methods | GRCFV (26) | 94.9 | 90.0 | 100 |
| Signal Processing Methods | LMCFV7 (60) | 89.9 | 90.0 | 89.9 |
| Transform Domain Methods | GaCFV (84) | 80.6 | 75.0 | 86.4 |

**Note:** FV: Feature vector, *l*: Length of the feature vector, GRCFV: $GLCM_{range}$ combined feature vector, LMCFV7: Laws' mask combined feature vector computed using 1D filter of length 7, GaCFV: Gabor combined feature vector evaluated at 3 scales and 7 orientations, OCA: Overall classification accuracy, NOR: Normal class, MRD: Medical renal disease, $ICA_{NOR}$: ICA value for NOR class, $ICA_{MRD}$: ICA value for MRD class, The OCA and ICA values are expressed in percentage.

From Table 7.5, it is observed that the maximum OCA of 94.9 % is achieved by $GLCM_{range}$ combined feature vector computed using combination of absolute and ratio features extracted from renal parenchyma and renal sinus region. The ICA values for normal and MRD are 90.0 % and 100 % respectively.

## 7.5 Comparison of ANFC based CAC System for Diagnosis of Medical Renal Disease using Combined Texture Features with Other Proposed CAC System

The present approach that utilizes the combination of absolute features extracted from PROIs and texture ratio features extracted from PROIs and SROIs for classification between normal and MRD renal US images.

The results from this approach are compared with the other proposed approaches that utilized absolute features extracted from PROIs only (*chapter 5*), and texture ratio features extracted from PROIs and SROIs.

A comparative analysis is made on the three different proposed approaches on basis of the classification results, shown in Table 7.6.

**Table 7.6** Comparative analysis of results obtained from absolute, ratio and combined feature vectors.

| **Methods** | **OCA $_{PROI}$ (FV)** *(Absolute features)* | **OCA$_{PROI/SROI}$ (FV)** *(Ratio features)* | **OCA $_{[PROI/SROI]:\ PROI}$ (FV)** *(Combined features)* |
|---|---|---|---|
| Statistical Methods | 84.8 (GRAFV) | 89.9 (GRRFV) | 94.9 (GRCFV) |
| Signal Processing based Methods | 71.4 (LMAFV3) | 88.2 (LMRFV7) | 89.9 (LMCFV7) |
| Transform Domain Methods | 67.2 (GaAFV) | 79.8 (GaRFV) | 80.6 (GaCFV) |

**Note:** OCA$_{PROI}$ : Overall classification accuracy obtained by using absolute features, OCA$_{PROI\ /\ SROI}$ : Overall classification accuracy obtained by using ratio features, OCA $_{[PROI/SROI]:\ PROI}$: Overall classification accuracy obtained by using combined features, GRAFV: GLCM$_{range}$ absolute feature vector, GRRFV: GLCM$_{range}$ ratio feature vector, GRCFV: GLCM$_{range}$ combined feature vector, LMAFV7: Laws' mask absolute feature vector computed using 1D filter of length 7, LMRFV7: Laws' mask ratio feature vector computed using 1D filter of length 7, LMCFV7: Laws' mask combined feature vector computed using 1D filter of length 7, GaAFV: Gabor absolute feature vector, GaRFV: Gabor ratio feature vector, GaRFV: Gabor combined feature vector.

From Table 7.6, it can be observed that the approach used in present study that utilizes the combination of absolute and texture ratio features yields best results by all of the three methods, namely, statistical, signal processing and transform domain, as compared to the approach that utilized absolute features (from PROIs only), and texture ratio features (from ratio of features extracted from PROIs and SROIs).

Also, out of all the features extracted, it is observed that statistical method based GLCM$_{range}$ combined features yielded the best results.

Based on the above results, one more experiment is conducted.

*7.5.1 Experiment 4: Design of CAC system for diagnosis of MRD using prominent features from GLCM$_{range}$ combined feature vector (GRCFV) using ANFC with feature selection.*

The GRCFV is further subjected to ANFC for selection of optimal features using linguistic hedge values. The combined features with linguistic hedge value greater than 0.4288 are selected for classification as shown in Fig 7.6.

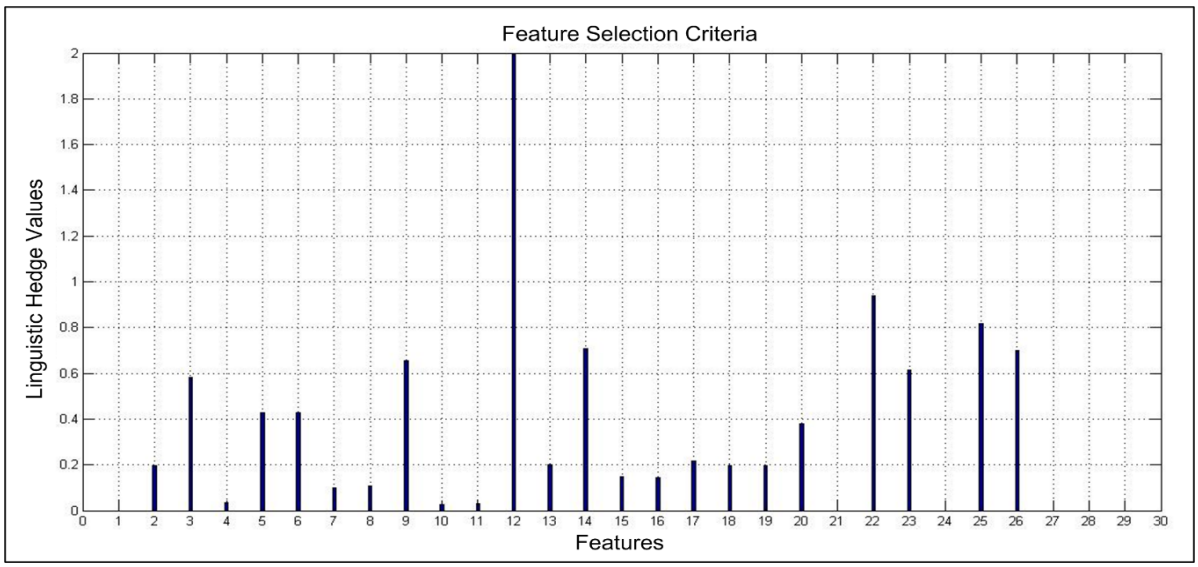


**Fig. 7.6** Graphical representation of linguistic hedge values used for feature selection of combined texture GLCM features.

The results of *experiment* 4 are given as follows:

(*a*) It is observed that 9 optimal texture features consisting of 4 absolute GLCM$_{range}$ features (Corr$_{range}$, IDM$_{range}$, Ent$_{range}$ and InfMCorr1$_{range}$) and 5 texture ratio GLCM$_{range}$ features (Ent$_{range}$, ASM$_{range}$, DiffVar$_{range}$, InfMCorr1$_{range}$ and InfMCorr2$_{range}$) were selected for classification.

(*b*) It is observed that 9 optimal GLCM$_{range}$ combined texture features yielded the OCA of 95.7 % along with ICA values of 91.6 % and 100 % for normal and MRD classes respectively as shown in Table 7.7.

**Table 7.7** Classification performance of GRCFV using feature selection from ANFC.

| **FV (*l*)** | **CM** | | | **OCA** | **ICA** |
|---|---|---|---|---|---|
| GRAFV: FRRFV = **GRCFV** (60) | | NOR | MRD | | |
| | NOR | 55 | 5 | 95.7 | 91.6 |
| | MRD | 0 | 59 | | 100 |

**Note:** FV: Feature vector, *l*: Length of the feature vector, GRCFV: GLCM$_{range}$ combined feature vector, CM: Confusion matrix, NOR: Normal class, MRD: Medical renal disease class, OCA: Overall classification accuracy, ICA: Individual classification accuracy, The OCA and ICA values are expressed in percentage.

From Table 7.7, it can be concluded that out of 26 combined $GLCM_{range}$ features, 9 (5 absolute and 4 ratio) features are prominent for classification of normal and MRD renal US images and can provide a significant aid to the radiologists for diagnosis of MRD.

## 7.6 Proposed ANFC based CAC System Design for Diagnosis of MRD using Combined Texture Features

The result of the study indicates that statistical method based $GLCM_{range}$ feature vector, computed at inter-pixel distance '*d*' = 1 yields the highest OCA of 95.7 % with the ICA values of 91.6 % and 100 % for normal and MRD classes respectively using 9 prominent combined texture features consisting of 4 absolute $GLCM_{range}$ features (Corr, IDM, Ent and InfMCorr1) and 5 texture ratio $GLCM_{range}$ features (Ent, ASM, DiffVar, InfMCorr1 and InfMCorr2) combined $GLCM_{range}$ features . The combination of absolute and texture ratio features contribute to 100 % classification accuracy for diagnosis of MRD disease. Hence, it is observed that the GRCFV is most efficient for classification of renal ultrasound images into normal and MRD classes. The promising results obtained from the study indicate that the proposed CAC system design using 9 prominent combined $GLCM_{range}$ features can be routinely used in clinical environment for diagnosis of MRD. The diagram of proposed ANFC based CAC system for diagnosis of renal diseases is given in Fig. 7.7.

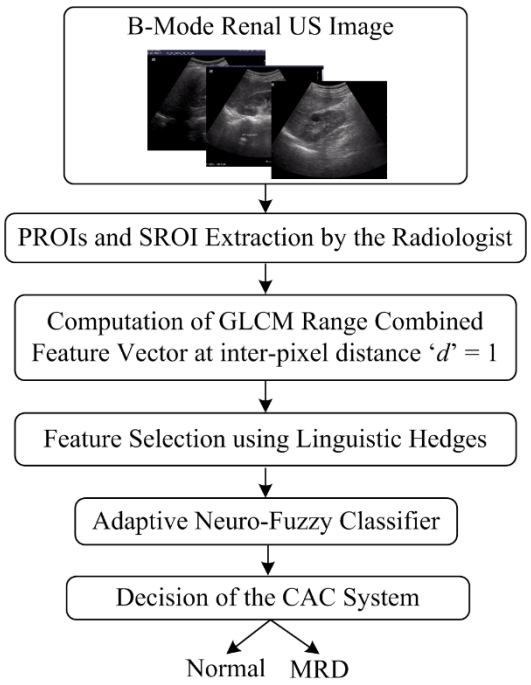


**Fig. 7.7** Proposed ANFC based CAC System for diagnosis of MRD using combined texture features.

## 7.7 Concluding Remarks

In the present study, an attempt has been made to evaluate the combined significance of textural changes in renal parenchyma alone as well as with respect to renal sinus region for diagnosis of MRD. Combined texture features are computed by combining the absolute texture features extracted from PROIs and texture ratio features extracted from PROIs and SROIs. Various experiments are conducted using statistical, signal processing and transform domain methods. The combined texture features obtained from these methods are subjected to classification using ANFC classifier. It is observed that statistical methods based $GLCM_{range}$ combined feature vector (GRCFV), computed at inter-pixel distance '*d*' = 1 yields the highest OCA of 94.9 % with ICA values of 90.0 % and 100 % for normal and MRD classes respectively. The prominent texture features from the GRCFV having linguistic hedge values greater than 0.4288 are selected for classification using ANFC that resulted in OCA of 95.7 % along with ICA values of 91.6 % and 100 % for normal and MRD classes respectively. The results of the study indicate that the proposed design of ANFC based CAC system using combined texture features is most efficient than the other proposed CAC designs for diagnosis of MRD. Therefore selected $GLCM_{range}$ combined texture features can be routinely used in clinical environment for diagnosis of MRD.

In next chapter a brief conclusion of the different designs of proposed CAC systems is presented along with their efficiency contribution. The limitations and future scope of the work is also discussed.

# Chapter 8

## Conclusion and Future Scope

The present chapter gives the brief conclusion of all the proposed CAC system designs utilizing key areas in renal ultrasound images in order to achieve best classification accuracies for classification of renal diseases. These CAC systems are designed to provide possible objective aid to the radiologists to assist them in decision-making.

A generalized workflow of an interactive system for diagnosis of renal diseases is given in Fig 8.1. The brief summary of the proposed CAC systems is given as follows.

### 8.1 Module 1- SVM based CAC System for Diagnosis of Renal Disease (*Chapter 4*)

An efficient design of CAC system has been proposed to classify renal US images into normal, MRD and cyst classes using SVM classifier. The texture features are extracted from ROIs from parenchymal region in case of normal and MRD class and from lesion in case of cyst class. Various experiments are conducted using statistical, signal processing and transform domain methods. The features obtained are subjected to SVM classifier for the classification task. The GLCM combined feature vector (GCFV) yields the highest OCA of 85.9 % at inter-pixel distance '*d*' = 1 with ICA values of 86.6 %, 83.0 % and 91.3 % for normal, MRD and cyst classes respectively.

Hence, GLCM combined feature vector obtained from statistical methods is found to be the most efficient for classification of renal ultrasound images into normal, MRD and cyst classes. It can also be concluded that out of 26 $GLCM_{mean}$ and $GLCM_{range}$ features, 16 texture features consisting of 7 $GLCM_{mean}$ features ($ASM_{mean}$, $Cont_{mean}$, $Var_{mean}$, $SumAv_{mean}$, $SumVar_{mean}$, $DiffVar_{mean}$, $InfMCorr1_{mean}$) and 9 $GLCM_{range}$ features ($ASM_{range}$, $Corr_{range}$, $Var_{range}$, $IDM_{range}$, $SumAv_{range}$, $SumVar_{range}$, $Ent_{range}$, $DiffVar_{range}$, $InfMCorr1_{range}$) are prominent for classification of normal, MRD and cyst renal US images.

The promising results obtained from proposed SVM based CAC system for classification of renal diseases indicate that the CAC system design using selected $GLCM_{mean}$ and $GLCM_{range}$ features can be routinely used in clinical environment for classification of renal diseases.

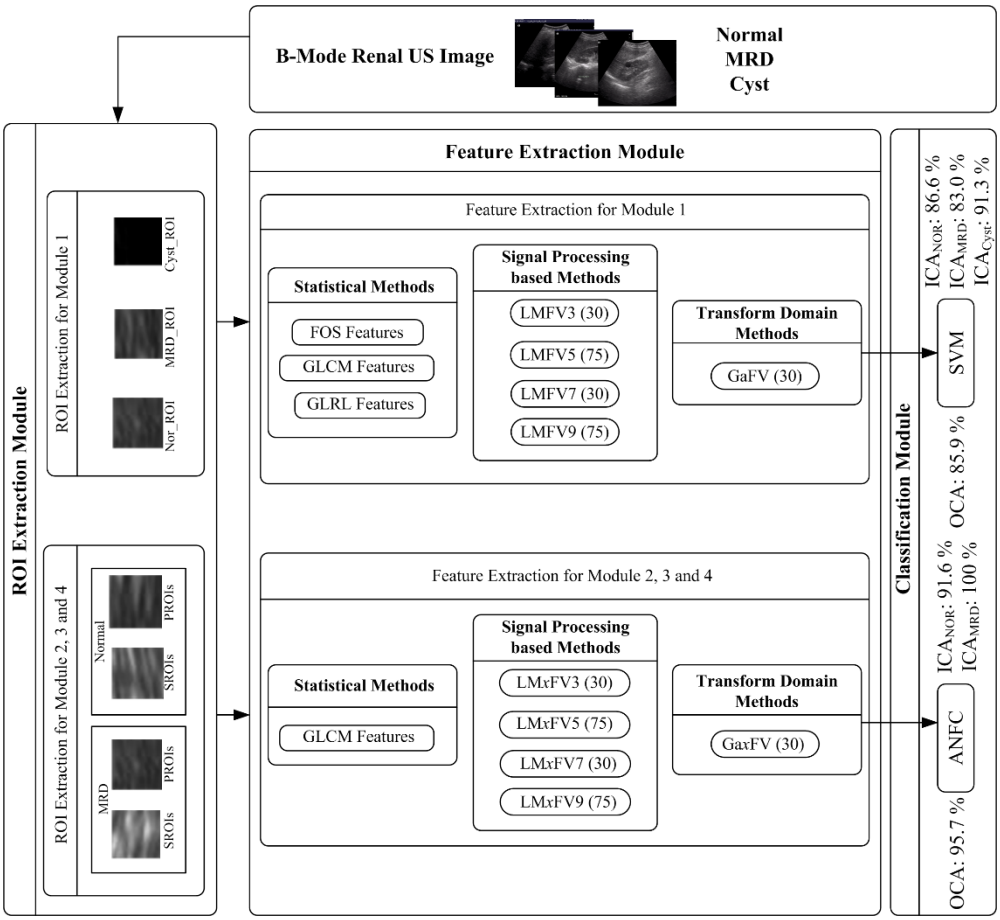


**Fig. 8.1** A generalized workflow of interactive system for diagnosis of renal diseases.

**Note**: FOS: First order statistics, GLCM: Gray level co-occurrence matrix, GLRL: Gray level run-length matrix, MRD: Medical renal disease, ROI: Region of interest, PROI: Parenchymal region of interest, SROI: Sinus region of interest, LMFV3: Laws' mask feature vector computed using 1D filter of length 3, LMFV5: Laws' mask feature vector computed using 1D filter of length 5, LMFV7: Laws' mask feature vector computed using 1D filter of length 7, LMFV9: Laws' mask feature vector computed using 1D filter of length 9, GaFV: Gabor feature vector, SVM: Support vector machine, ANFC: Absolute neuro-fuzzy classifier, OCA: Overall classification accuracy, NOR: Normal, MRD: Medical renal disease, $ICA_{NOR}$: ICA value for NOR class, $ICA_{MRD}$: ICA value for MRD class, $ICA_{Cyst}$ :ICA value for Cyst class, *x*: absolute (A), ratio (R) and combined (C) for module 2, 3 and 4 respectively. For module 4, only LMCFV7 has been evaluated as Laws' mask filter of length 7 is yielding highest OCA among all Laws' mask feature vectors computed in module 2 and 3.

## 8.2 Module 2 - ANFC based CAC System for Diagnosis of Renal Disease using Absolute Texture Features (*Chapter 5*)

An efficient design of CAC system has been proposed that evaluates the significance of textural changes in renal parenchyma for diagnosis of MRD. For the proposed CAC system design, the PROIs are extracted from renal parenchyma region from both, normal and MRD renal US image classes.

Various experiments are conducted using statistical, signal processing and transform domain methods. The absolute features obtained from these methods are subjected for classification using ANFC classifier.

The statistical methods based $GLCM_{range}$ feature vector, computed at inter-pixel distance '*d'* = 1 yields the highest OCA of 84.8 % with the ICA values of 93.3 % and 74.5 % for normal and MRD classes respectively. The $GLCM_{range}$ absolute feature vector is the most efficient for classification of renal US images into normal and MRD classes. Therefore the proposed CAC system design using $GLCM_{range}$ absolute features can be routinely used in clinical environment for diagnosis of MRD.

## 8.3 Module 3- ANFC based CAC System for Diagnosis of Renal Disease using Texture Ratio Features (*Chapter 6*)

An efficient design of CAC system been proposed that evaluates the significance of textural changes in renal parenchyma with respect to renal sinus region for diagnosis of MRD. For the proposed CAC system design, the PROIs are extracted from renal parenchymal region and SROIs are extracted from renal sinus region from both, normal and MRD renal US image classes.

Texture ratio features are computed by taking the ratio of features extracted from PROIs and SROIs. The texture ratio features obtained statistical methods based $GLCM_{range}$ feature vector, computed at inter-pixel distance '*d'* = 1 yields the highest OCA of 89.9 % with ICA values of 85.0 % and 94.9 % for normal and MRD classes respectively. Also, the proposed design of ANFC based CAC system using texture ratio features is more efficient than the design that utilized absolute features only. The $GLCM_{range}$ ratio feature vector proves to be the most efficient for classification of renal US images into normal and MRD classes. Therefore the proposed CAC system using $GLCM_{range}$ texture ratio features can be routinely used in clinical environment for diagnosis of MRD.

## 8.4 Module 4- ANFC based CAC System for Diagnosis of Renal Disease Using Combined Texture Features (*Chapter 7*)

An efficient design of CAC system is proposed that utilized the ratio of features from renal parenchyma and renal sinus region in combination with absolute features from parenchyma region only, for diagnosis of MRD.

The statistical method based combined $GLCM_{range}$ feature vector, computed at inter-pixel distance '*d*' = 1 yields the highest OCA of 95.7 % with ICA values of 91.6 % and 100 % for normal and MRD classes respectively using 9 prominent $GLCM_{range}$ features consisting of 4 absolute $GLCM_{range}$ features (Corr, IDM, Ent and InfMCorr1) and 5 ratio $GLCM_{range}$ features (Ent, ASM, DiffVar, InfMCorr1 and InfMCorr2). The combined texture features contribute to 100 % classification accuracy for diagnosis of MRD disease.

A significant increase in the OCAs is observed using proposed CAC system design using combined texture features as compared to the previously discussed CAC system designs. Hence, GRCFV is the most efficient for classification of renal ultrasound images into normal and MRD classes.

Therefore the proposed ANFC based CAC system design using 9 prominent combined $GLCM_{range}$ features can be routinely used in clinical environment for diagnosis of MRD.

## 8.5 Conclusion

Four different modules proposed the designs of four different CAC systems in *chapter 4, 5, 6 and 7* which laid the foundation of classification of renal disease.

A brief comparison of classification performance obtained by different CAC system designs implemented for the proposed interactive system for diagnosis of renal diseases using B-Mode US images is depicted in Table 8.1.

**Table 8.1** Classification performance of different proposed CAC systems.

| *CAC System Designs* | *Image Class* | *OCA* | *ICA* |
|---|---|---|---|
| *Module 1*: SVM based CAC system for diagnosis of renal disease. | Normal<br>MRD<br>Cyst | 85.9 | 86.6<br>83.0<br>91.3 |
| *Module 2*: ANFC based CAC system for diagnosis of MRD using absolute texture features. | Normal<br>MRD | 84.8 | 93.3<br>74.5 |
| *Module 3*: ANFC based CAC system for diagnosis of MRD using ratio texture features. | Normal<br>MRD | 89.9 | 85.0<br>94.9 |
| *Module 4*: ANFC based CAC system for diagnosis of MRD using combined texture features. | Normal<br>MRD | 95.7 | 91.6<br>100 |

**Note:** MRD: Medical renal disease, SVM: Support vector machine, OCA: Overall classification accuracy, The OCA and ICA values are expressed in percentage.

From Table 8.1, it can be observed that

(*a*) *Module 1* yields the maximum OCA of 85.9 % by using combined GLCM features for three class classification of renal diseases into **normal, MRD and cyst**. Therefore, the SVM based CAC system using combined GLCM combined features should be used for diagnosis of renal diseases using B-Mode US images as shown in Fig. 8.2 (*a*).

(*b*) *Module 4* yields the best performance (OCA = 95.7 %) for characterization of **normal and MRD** B-Mode renal US images. Therefore, the ANFC based CAC system using prominent combined $GLCM_{range}$ features should be used for diagnosis of MRD using B-Mode US images as shown in Fig 8.2 (*b*).

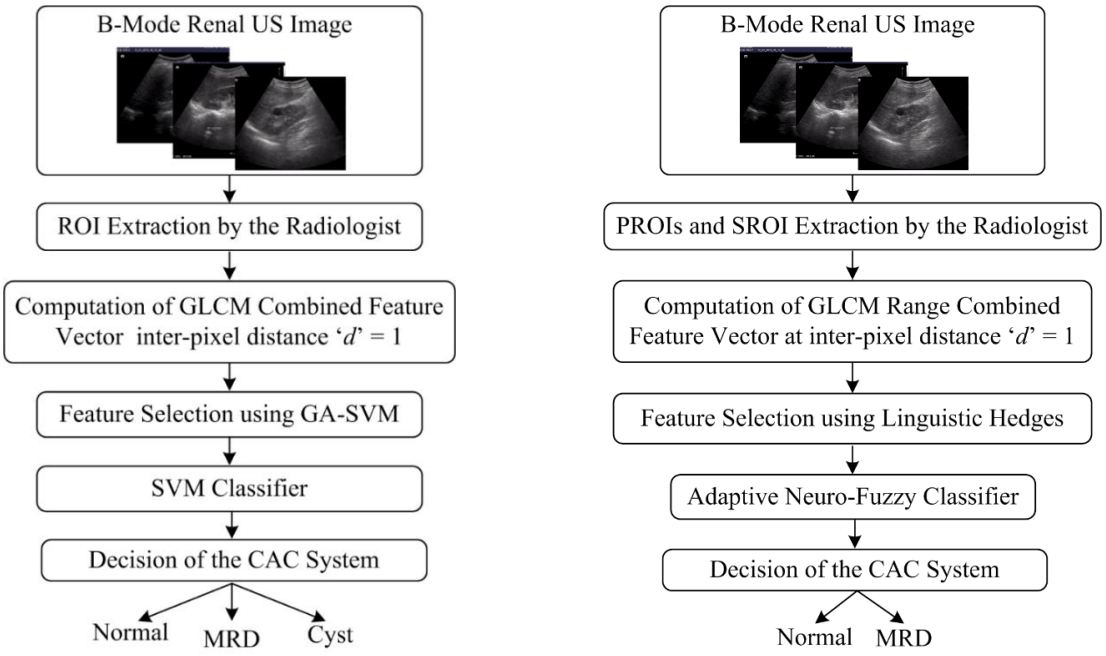


(*a*) (*b*)

**Fig. 8.3** (*a*) Proposed SVM based CAC system for diagnosis of renal diseases, (*b*) Proposed ANFC based CAC System for diagnosis of MRD using combined texture features.

## 8.6 Limitations and Future Scope

Limitation of the present work is that it has been carried out on a limited dataset. Following are the recommendations for future work:

(*i*) In the present work, 35 digital B-mode renal US images recorded by Siemens ACUSON X300 ultrasound machine have been used. The efficacy of the proposed CAC system designs should also be tested on the images recorded by different US machines.

(*ii*) There is no benchmark database of graded MRD images which has been made publically available for research purposes. Such database is extremely required for developing CAC systems for differential diagnosis between mild, moderate and severe grades of MRD. An attempt should be made to develop such a database by collaborating with different hospitals.

(*iii*) The grading of MRD depends on the degree of severity of the disease. If MRD of grade 3 is found, it has higher chances of progression to chronic kidney disease. Also, the differential diagnosis between normal and mild MRD is a daunting challenge for experienced radiologists. Therefore CAC system design for classification between normal, mild, moderate and severe MRD cases is extremely required.

(*iv*) For differential diagnosis between different grades of MRD, the radiologists look at the textural changes of the renal parenchyma with respect to liver. Therefore, for collection of images of different grades of MRD, care should be taken to image liver along with kidney.

(*v*) The performance of some transform domain feature extraction methods (such as Fourier power spectrum, shearlet transform, non-subsampled contourlet transform etc.) for diagnosis of MRD should be investigated.

# References


[1] Internal anatomy of kidney. http://slideplayer.com/slide/8509968/

[2] R. Hoffman and J. Riley, "The diagnostic approach to the parenchymal renal mass", American Journal of Roentgenology, vol. 100, no. 3, pp. 698–708, 1967.

[3] K. Fong, M. Rahmani, T. Rose, M. Skidmore, and T. Connor, "Fetal renal cystic disease: sonographic-pathologic correlation", American Journal of Roentgenology, vol. 146, no. 4, pp. 767–773, 1986.

[4] J. Tsang, and M. K. Yuen. "Sonography of Baker's cyst (popliteal cyst): the typical and atypical features", Hong Kong Journal of Radiology, vol. 14, pp. 200-206, 2011.

[5] O. Inci, M. Kaplan, O. Yalcin, I. H. Atakan, and H. Kubat, "Renal angiomyolipoma with malignant transformation, simultaneous occurrence with malignity and other complex clinical situations", International Urology and Nephrology, vol. 38, no. 3-4, pp. 417–426, 2006.

[6] M. Dickinson, H. Ruckle, M. Beaghler, and H.R. Hadley, "Renal angiomyolipoma: optimal treatment based on size and symptoms", Clinical Nephrology, vol. 49, no. 5, pp. 281-286, 1998.

[7] Sample ultrasound image of AML class. http://www.jultrasoundmed.org/content/24/6/855/F1.expansion

[8] R. J. Motzer, N. H. Bander, and D. M. Nanus, "Renal-cell carcinoma", New England Journal of Medicine, vol. 335, no. 12, pp. 865-875, 1996.

[9] H. Cohen and F. J. McGovern, "Renal-cell carcinoma", New England Journal of Medicine, vol. 353, no. 23, pp. 2477-2490, 2005.

[10] Sample ultrasound image of RCC class. http://www.jultrasoundmed.org/content/23/3/439/F1.expansion

[11] E. Quaia and M. Bertolotto, "Renal parenchymal diseases: is characterization feasible with ultrasound?", European Radiology, vol. 12, no. 8, pp. 2006–2020, 2002.

[12] D. K Huntington, S. C. Hill, and M. C. Hill, "Sonographic manifestations of medical renal disease", Seminars in Ultrasound, CT, and MR, vol. 12, no. 4, pp. 290-307, 1991.

[13] H. Zarnow, and L. R. Bigongiari, "Parenchymal diseases of the kidneys" in, E.K.Lang (ed.), Radiology of the Upper Urinary Tract, Berlin Heidelberg: Springer, 1991, pp. 71-101.

[14] M. R. Ghalib, S. Bhatnagar, S. Jayapoorani and U. Pande, "Artificial neural network based detection of renal tumors using CT scan image processing", International Journal of Engineering and Technology, vol. 6, no. 1, pp. 28-35, 2014.

[15] H. Rayner, M. Thomas, and D. Milford - *Understanding Kidney Diseases*, First edition, Springer International Publishing Switzerland, 2016.

[16] J. Page, S. Morgan, J. Eastwood, S. Smith, D. Webb, S. Dilly, J. Chow, A. Pottier, and A. Joseph, "Ultrasound findings in renal parenchymal disease: comparison with histological appearances", Clinical Radiology, vol. 49, no. 12, pp. 867–870, 1994.

[17] D. Soldo, B. Brkljacic, V. Bozikov, I. Drinkovic and M. Hauser, "Diabetic nephropathy: comparison of conventional and duplex Doppler ultrasonographic findings", Acta radiologica, vol.38, no.2, pp. 296-302, 1997.

[18] P.J. Kenney, "Imaging of chronic renal infections", American Journal Of Roentgenology, vol. 155, no.3, pp. 485-494, 1990.

[19] A.T. Rosenfield and N.J. Siegel, "Renal parenchymal disease: histopathologic-sonographic correlation", American Journal of Roentgenology, vol.137, no.4, pp.793-798, 1981.

[20] X. Chen, R. M. Summers, and J. Yao, "Kidney Tumor Growth Prediction by Coupling Reaction–Diffusion and Biomechanical Model", IEEE Transactions on Biomedical Engineering, vol. 60, no. 1, pp. 169–173, 2013.

[21] K. C. Hung, "Echocardiographic characteristics of chronic kidney disease: the Taiwanese experience", Journal of Medical Ultrasound, vol. 23, no. 1, pp. 14–16, 2015.

[22] S. Singla, S. Rakshith, M. A. Ameen, N. Kumar, and J. Siddappa, "Correlation of ultrasonographic parameters with serum creatinine in chronic kidney disease," Journal of Clinical Imaging Science, vol. 3, no. 1, pp. 28, 2013.

[23] Chen, Xinjian, R. Summers, and Y. Jianhua, "FEM-based 3-D tumor growth prediction for kidney tumor", IEEE Transactions On Biomedical Engineering, vol. 58, no. 3, pp. 463-467, 2011.

[24] S. Strauss, E. Gavish, P. Gottlieb, L. Katsnelson, "Interobserver and intraobserver variability in the sonographic assessment of fatty liver", American Journal of Roentgenology, vol. 189, no. 6, pp. W320-W323, 2007.

[25] S. İçer, A. Coşkun, and T. İkizceli, "Quantitative grading using grey relational analysis on ultrasonographic images of a fatty liver", Journal Of Medical Systems, vol. 36, no. 4, pp. 2521-2528, 2012.

[26] R. Momenan, R. F Wagner, M. H Loew, M. F Insana, and B. S Garra, "Characterization of tissue from ultrasound images", IEEE Control Systems Magazine, vol. 8, no. 3 pp. 49-53, 1988.

[27] F. Fiorini and L. Barozzi, "The role of ultrasonography in the study of medical nephropathy", Journal of Ultrasound, vol. 10, no. 4, pp. 161–167, 2007.

[28] K. Viswanath and R. Gunasundari, "Design and analysis performance of kidney stone detection from ultrasound image by level set segmentation and ANN classification", 2014 in Proceedings of International Conference on Advances in Computing, Communications and Informatics (ICACCI), pp. 407-414, 2014.

[29] N. A. Patel and P. P. Suthar, "Ultrasound appearance of congenital renal disease: p review", The Egyptian Journal of Radiology and Nuclear Medicine, vol. 45, no. 4, pp. 1255–1264, 2014.

[30] A. Kadioglu, “Renal measurements, including length, parenchymal thickness, and medullary pyramid thickness, in healthy children: what are the normative ultrasound values?”, American Journal of Roentgenology, vol. 194, no. 2, pp. 509–515, 2010.

[31] H. C. Thoeny, F. D. Keyzer, R. H. Oyen, and R. Peeters, “Diffusion-weighted MR imaging of kidneys in healthy volunteers and patients with parenchymal diseases: initial experience 1”, Radiology, vol. 325, no. 3, pp. 911-917, 2005.

[32] A. W. Leung, G. M. Bydder, R. E. Steiner, D. J. Bryant and I. R. Young, “Magnetic resonance imaging of the kidneys”, American Journal Of Roentgenology, vol. 143, no. 6, pp. 1215-27, 1984.

[33] M. Linguraru, S. Wang, F. Shah, R. Gautam, J. Peterson, W. Linehan, and R. Summers, “Computer-aided renal cancer quantification and classification from contrast-enhanced CT via histograms of curvature-related features”, in Proceedings of the Annual International Conference of the IEEE Engineering in Medicine and Biology Society, pp. 6679-6682, 2009.

[34] S. Raman, Y. Chen, J. Schroeder, P. Huang, and E. Fishman, “CT texture analysis of renal masses: pilot study using random forest classification for prediction of pathology”, Academic Radiology, vol. 21, no. 12, pp. 1587-96, 2014.

[35] K. Raja, M. Madheswaran, and K. Thyagarajah. “A general segmentation scheme for contouring kidney region in ultrasound kidney images using improved higher order spline interpolation”, Journal of Biology and Medical Science, vol. 2, no. 2, pp. 81-88, 2007.

[36] C. Loizou, C. Christodoulou, C. Pattichis, R. Istepanian, M. Pantziaris, and A. Nicolaides, “Speckle reduction in ultrasound images of atherosclerotic carotid plaque”, in Proceedings of the 14th International Conference on Digital Signal Processing, vol. 2, pp. 525-528, 2002.

[37] A. J. Ahumada, and C. H. Null, “Image quality: A multidimensional problem”, in A.B. Watson (ed.) Digital Images And Human Vision, Cambridge Mass: Bradford Press, pp.141-148, 1993.

[38] S. F. Huang, R. F. Chang, D. R. Chen, and W. Moon, “Characterization of spiculation on ultrasound lesions,” IEEE Transactions on Medical Imaging, vol. 23, no. 1, pp. 111–121, 2004.

[39] C. P. Loizou, C. S. Pattichis, M. Pantziaris, T. Tyllis, and A. Nicolaides, “Quality evaluation of ultrasound imaging in the carotid artery based on normalization and speckle reduction filtering”, Medical and Biological Engineering & Computing, vol. 44, no. 5, pp. 414–426, 2006.

[40] M. B. Subramanya, V. Kumar, S. Mukherjee, and M. Saini, “SVM-based CAC system for B-mode kidney ultrasound images”, Journal of Digital Imaging, vol. 28, no. 4, pp. 448–458, 2014.

[41] M. B Subramanya, V. Kumar, S. Mukherjee, and M. Saini, “Classification of normal and medical renal disease using B-mode ultrasound images”, in Proceedings of 2nd International Conference on Computing for Sustainable Global Development (INDIACom), IEEE, pp. 1914-1918, 2015.

[42] G. Kulanthaivel, and G. Ravindran “Web based diagnostic classifier system for kidney lesions using image texture parameters” in Proceedings of the 2005 Annual IEEE India Conference-Indicon, IEEE, pp. 220-223, 2005.

[43] J. Virmani, V. Kumar, N. Kalra, and N. Khandelwal, "A comparative study of computer-aided classification systems for focal hepatic lesions from B-mode ultrasound", Journal of Medical Engineering & Technology, vol. 37, no. 4, pp. 292–306, 2013.

[44] J. Virmani, V. Vinod, N. Kalra, and N. Khandelwa, "PCA-SVM based CAD System for focal liver lesions using B-mode ultrasound images", Defence Science Journal, vol. 63, no. 5, pp. 478–486, 2013.

[45] S. Golodetz, I. Voiculescu, and S. Cameron, "A proposed decision-support system for (renal) cancer imaging", in Proceedings of the Frontiers in the Convergence of Bioscience and Information Technologies, IEEE, pp. 361-366, 2007.

[46] K. Raja, M. Madheswaran, and K. Thyagarajah, "Ultrasound kidney image analysis for computerized disorder identification and classification using content descriptive power spectral features", Journal of MedicalSystems, vol. 31, no. 5, pp. 307–317, 2007.

[47] K. Raja and M. Madheswaran, "Determination of kidney area independent unconstrained features for automated diagnosis and classification", in Proceedings of International Conference on Intelligent and Advanced Systems (ICIAS-2007), IEEE, pp. 724-729, 2007.

[48] K. Raja, M. Madheswaran, and K. Thyagarajah, "Analysis of ultrasound kidney images using content descriptive multiple features for disorder identification and ANN based classification", in Proceedings of International Conference on Computing: Theory and Applications (ICCTA-2007), IEEE, pp. 382-388, 2007.

[49] K. Raja, M. Madheswaran, and K. Thyagarajah, "Evaluation of tissue characteristics of kidney for diagnosis and classification using first order statistics and RTS invariants", in Proceedings of 2007 International Conference on Signal Processing, Communications and Networking, IEEE, pp. 483-487, 2007.

[50] K. Raja, M. Madheswaran, and K. Thyagarajah, "A hybrid fuzzy-neural system for computer-aided diagnosis of ultrasound kidney images using prominent features", Journal of Biology and Medical Science, vol. 32, no. 1, pp. 65–83, 2007.

[51] K. Raja, M. Madheswaran, and K. Thyagarajah, "Texture pattern analysis of kidney tissues for disorder identification and classification using dominant Gabor wavelet", Machine Vision and Applications, vol. 21, no. 3, pp. 287–300, 2008.

[52] K. Dhanalakshmi and V. Rajamani, "An efficient association rule-based method for diagnosing ultrasound kidney images",in Proceedings of 2010 IEEE International Conference on Computational Intelligence and Computing Research (ICCIC-2010), pp. 1-5, 2010.

[53] J.S Jose, R. Sivakami, N.U. Maheswari and R. Venkatesh, "An efficient diagnosis of kidney images using association rules", International Journal of Computers and Technology in Electronics Engineering, vol.12, no. 2, pp.14-20, 2012

[54] K. D. Krishna, V. Akkala, R. Bharath, P. Rajalakshmi, A. Mohammed, S. Merchant, and U. Desai, "Computer aided abnormality detection for kidney on FPGA based IoT enabled portable ultrasound imaging system", IRBM, 2016.

[55] P. Akkasaligar, and S. Biradar, “Classification of medical ultrasound images of kidney”, in Proceedings on International Conference on Information and Communication Technologies, vol. 3, pp. 24-28, 2014.

[56] W. M. Hafizah, E. Supriyanto, and J. Yunus, “Feature extraction of kidney ultrasound images based on intensity histogram and gray level co-occurrence matrix”, 2012 Sixth Asia Modelling Symposium, pp. 115-120, 2012.

[57] M. Wagih, F. Abou-Chadi, H. El-Din and N. Mekky, “Classification of Ultrasound kidney images using PCA and neural networks”, International Journal of Advanced Computer Science and Applications, vol. 6, no. 4, 2015.

[58] J. Virmani, V. Kumar, N. Kalra and N. Khandelwal, “A rapid approach for prediction of liver cirrhosis based on first order statistics”, in Proceedings of International Conference on Multimedia, Signal Processing and Communication Technologies (IMPACT), pp. 212-215, IEEE, Dec 2011.

[59] J. A. Zagzebski, J. F. Chen, F. Dong and T. Wilson, “Intervening attenuation affects first-order statistical properties of ultrasound echo signals”, IEEE Transactions On Ultrasonics, Ferroelectrics, And Frequency Control, vol. 46, no. 1, pp. 35-40, 1999.

[60] J. K. Tugnait, and W. Luo, “On channel estimation using superimposed training and first-order statistics”, in Proceedings of 2003 IEEE International Conference on Acoustics, Speech and Signal Processing (ICASSP-2003), vol. 4, pp. 624-627, 2003.

[61] R.Wagner, S. Smith, F. Robert, J. Sandrik and H. Lopez, “Statistics of speckle in ultrasound B-scans”, IEEE Transactions on Sonics and Ultrasonics, vol. 30, no. 3, pp. 156-163, 1983.

[62] M. Bevk, and I. Kononenko “A statistical approach to texture description of medical images: a preliminary study”, In Proceedings of the 15th IEEE Symposium on Computer-Based Medical Systems, IEEE, pp. 239-244, 2002.

[63] J. Virmani, V. Kumar, N. Kalra and N. Khandelwal, “Neural network ensemble based CAD system for focal liver lesions from B-mode ultrasound”, Journal of Digital Imaging, vol. 27, no. 4, pp. 520-537, 2014.

[64] R. Haralick, and K. Shanmugam, “Textural features for image classification”, IEEE Transactions on Systems, Man, And Cybernetics, vol. 6, pp. 610-21, 1973.

[65] J. Virmani, V. Kumar, N. Kalra and N. Khandelwal, "SVM-based characterisation of liver cirrhosis by singular value decomposition of GLCM matrix", International Journal of Artificial Intelligence and Soft Computing, vol. 3, no. 3, pp. 276-296, 2013.

[66] J. Virmani, V. Kumar, N. Kalra, and N. Khandelwal, “Prediction of cirrhosis based on singular value decomposition of gray level co-occurrence matrix and a neural network classifier,” in Proceedings of Developments in E-systems Engineering (DeSE), IEEE, pp. 146-151, 2011.

[67] C.M. Wu, Y.C. Chen, and K.S. Hsieh, “Texture features for classification of ultrasonic liver images,” IEEE Transactions on Medical Imaging, vol. 11, no. 2, pp. 141–152, 1992.

[68] J. Virmani, V. Kumar, N. Kalra and N. Khandelwal, “Characterization of primary and secondary malignant liver lesions from B-mode ultrasound”, Journal of Digital Imaging, vol. 26, no. 6, pp. 1058-1070, 2013.

[69] D. Balasubramanian, P. Srinivasan and R. Gurupatham, “Automatic classification of focal lesions in ultrasound liver images using principal component analysis and neural networks”, in Proceedings of 29th Annual International Conference of the IEEE Engineering in Medicine and Biology Society, IEEE, pp. 2134-2137, 2007.

[70] S. Nawaz, A. Dar, “Hepatic lesions classification by ensemble of SVMs using statistical features based on co-occurrence matrix”, in Proceedings of 4th International Conference on Emerging Technologies (ICET), IEEE, pp. 21-26, 2008.

[71] M. Partio, B. Cramariuc, M. Gabbouj and A. Visa, “Rock texture retrieval using gray level co-occurrence matrix”, in Proceedings of 5th Nordic Signal Processing Symposium, vol. 75. 2002.

[72] J.R. Carr, and F. P. De Miranda “The semivariogram in comparison to the co-occurrence matrix for classification of image texture”, IEEE Transactions on Geoscience and Remote Sensing vol. 36, no. 6, pp. 1945-1952, 1998.

[73] F. Albregtsen, B. Nielsen, and H. E. Danielsen, “Adaptive gray level run length features from class distance matrices”, In Proceedings of 15th International Conference on Pattern Recognition, IEEE, vol. 3, pp. 738-741, 2000.

[74] X. Tang, “Texture information in run-length matrices”, IEEE transactions on image processing, vol. 7, no. 11, pp.1602-1609, 1998.

[75] G. Castellano, L. Bonilha, L.M. Li, and F. Cendes, “Texture analysis of medical images”, Clinical radiology, vol. 59, no. 12, pp. 1061-1069, 2004.

[76] C. Lee and S. Chen, “Gabor Wavelets and SVM Classifier for Liver Diseases Classification from CT Images”, IEEE International Conference on Systems, Man and Cybernetics, vol. 1, pp. 548-552, IEEE, 2006.

[77] A. Ben-Hur, and J. Weston. "A user’s guide to support vector machines." Data mining techniques for the life sciences, pp. 223-239, 2010.

[78] J. Virmani, V. Kumar, N. Kalra, and N. Khandelwal, “SVM-Based Characterization of Liver Ultrasound Images Using Wavelet Packet Texture Descriptors”, Journal of Digital Imaging, vol. 26, no. 3, pp. 530–543, Nov. 2012.

[79] T. S. Furey, N. Cristianini, N. Duffy, D.W. Bednarski, M. Schummer, D. Haussler, “Support vector machine classification and validation of cancer tissue samples using microarray expression data”, Bioinformatics vol. 16, no.10, pp. 906-914, 2000.

[80] S. Tong, and E. Chang “Support vector machine active learning for image retrieval”, In proceedings of the ninth ACM international conference on Multimedia. ACM, pp. 107-118, 2001.

[81] C. Chang and C.J. Lin, “LIBSVM: a library for support vector machines,” ACM Transactions on Intelligent Systems and Technology (TIST), vol. 2, no. 3, pp. 1–27, Jan. 2011.

[82] R. Shenbagavalli, K. Ramar, "Classification of Soil Textures Based on Laws' Features Extracted from Preprocessing Images on Sequential and Random Windows", Bonfring International Journal of Advances in Image Processing, vol. 1, no. 1, pp. 15-18, 2011.

[83] Kriti, and J. Virmani, "Breast density classification using Laws' mask texture features" International Journal of Biomedical Engineering and Technology, vol. 19, no. 3, pp. 279-302, 2015.

[84] J. Virmani, N. Dey, and V. Kumar. "PCA-PNN and PCA-SVM based CAD systems for breast density classification", Applications of Intelligent Optimization in Biology and Medicine, Springer International Publishing, pp. 159-180, 2016.

[85] H. Elnemr, "Statistical analysis of law's mask texture features for cancer and water lung detection" International Journal of Computer Science Issues, vol. 10, no.6, 2013.

[86] A. Setiawan, Elysia, J. Wesley and Y. Purnama, "Mammogram Classification using Law's Texture Energy Measure and Neural Networks", Procedia Computer Science, vol. 59, pp. 92-97, 2015.

[87] J. Virmani, V. Kumar, N. Kalra, and N. Khandelwal, "Prediction of cirrhosis from liver ultrasound B-mode images based on Laws' masks analysis", International Conference on Image Information Processing (ICIIP),IEEE, pp. 1-5, 2011.

[88] O.F. Ertugrul, "Adaptive texture energy measure method", International journal of intelligent information systems, vol. 3, no. 2, pp. 13-18, Jun 2014.

[89] R. Yoshikawa, A. Teramoto, T. Matsubara, and H. Fujita, "Automated detection of architectural distortion using improved adaptive Gabor filter", International Workshop on Digital Mammography, Springer International Publishing, pp. 606-611, June 2014.

[90] Shantanu, Banik and R. Rangayyan, "Correction to Detection of architectural distortion in prior mammograms using Gabor filters, phase portraits, fractal dimension, and texture analysis [1]", International journal of computer assisted radiology and surgery, vol. 5, no. 4, pp. 421-423, 2010.

[91] V. V. Raad, "Design of Gabor wavelets for analysis of texture features in cervical images", Proceedings of the 25th Annual International Conference of the IEEE Engineering in Medicine and Biology Society, vol. 1, pp. 806-809, 2003.

[92] R. J. Ferrari, RM. Rangayyan, JL. Desautels, AF. Frere, "Analysis of asymmetry in mammograms via directional filtering with Gabor wavelets", IEEE Transactions on Medical Imaging, vol. 20, no. 9, pp. 953-964, 2001.

[93] R. Rangayyan and F. Ayres, "Gabor filters and phase portraits for the detection of architectural distortion in mammograms", Medical & Biological Engineering and Computing, vol. 44, no. 10, pp. 883-894, 2006.

[94] S. Lahmiri and M. Boukadoum, "Hybrid discrete wavelet transform and Gabor filter banks processing for features extraction from biomedical images", Journal of medical engineering, 2013.

[95] M. Hussain, S. Khan, G. Muhammad, M. Berbar, and G. Bebis, “Mass detection in digital mammograms using gabor filter bank”, In IET Conference on Image Processing (IPR 2012), pp. 1-5, 2012.

[96] J. Virmani, V. Kumar, N. Kalra and N. Khandelwal, “Prediction of liver cirrhosis based on multiresolution texture descriptors from B-mode ultrasound”, International Journal of Convergence Computing, vol. 1, no. 1, p. 19, 2013.

[97] D. Dunn, W. Higgins and J. Wakeley, “Texture segmentation using 2-D Gabor elementary functions", IEEE Transactions on Pattern Analysis and Machine Intelligence, vol. 16, no. 2, pp. 130-149, 1994.

[98] L. Wang, G. Xu, J. Wang, S. Yang, L. Guo, and W. Yan, “GA-SVM based feature selection and parameters optimization for BCI research,” 2011 Seventh International Conference on Natural Computation, vol 1, pp. 580-583, 2011.

[99] C.L. Huang and C.J. Wang, “A GA-based feature selection and parameters optimization for support vector machines”, Expert Systems with Applications, vol. 31, no. 2, pp. 231–240, 2006.

[100] Y. Xie, L. Setia, and H. Burkhardt, “Block DCT vectors construction for face retrieval based on genetic algorithm”, in Proceedings of Third International Conference on Natural Computation (ICNC 2007), IEEE, vol. 3, pp. 770-775, 2007.

[101] A. Aouatif, M. Rziza, and D. Aboutajdine. “SVM-based face recognition using genetic search for frequency-feature subset selection” , in Proceedings of International Conference on Image and Signal Processing, Springer Berlin Heidelberg, pp. 321-328, 2008.

[102] B. Cetisli, “Development of an adaptive neuro-fuzzy classifier using linguistic hedges: Part 1” Expert Systems with Applications, vol. 37, no. 8, pp. 6093-6101, 2010.

[103] B. Cetisli, “The effect of linguistic hedges on feature selection: Part 2” Expert Systems with Applications, vol. 37, no. 8, pp. 6102-6108, 2010.

[104] R. Kher, T. Pawar, V. Thakar and H. Shah, “Physical activities recognition from ambulatory ECG signals using neuro-fuzzy classifiers and support vector machines”, Journal of Medical Engineering & Technology, vol. 39, no. 2, pp. 138-152, 2015.

[105] B.D. Liu, C.Y. Chen, and J.Y. Tsao, “Design of adaptive fuzzy logic controller based on linguistic-hedge concepts and genetic algorithms”, IEEE Transactions on Systems, Man, and Cybernetics, Part B, vol. 31, no. 1, pp. 32–53, 2001.

[106] Q. H. Do and J.F. Chen, “A neuro-fuzzy approach in the classification of students’ academic performance”, Computational Intelligence and Neuroscience, vol. 2013, pp. 1–7, 2013.

[107] C.T. Sun, and J.S. Jang. “A neuro-fuzzy classifier and its applications”, in Proceedings of Second IEEE International Conference on Fuzzy Systems, IEEE, pp. 94-98, 1993.

[108] A.T Azar, and A.E Hassanien, “Dimensionality reduction of medical big data using neural-fuzzy classifier”, Soft Computing, vol. 19, no. 4, pp. 1115-1127, 2015.

[109] H. Tonekabonipour, A. Emam, M. Teshnelab, and M. A. Shoorehdeli, "Comparison of neuro-fuzzy approaches with artificial neural networks for the detection of Ischemia in ECG signals", in Proceedings of 2010 IEEE International Conference on Systems, Man and Cybernetics, IEEE, pp. 4045-4048, 2010.

[110] J. Vieira, F.M. Dias, and A. Mota. "Neuro-fuzzy systems: a survey" in Proceedings of 5th WSEAS NNA International Conference, 2004.

[111] J. S. Jang, "ANFIS: adaptive-network-based fuzzy inference system", IEEE Transactions on Systems, Man, and Cybernetics, vol. 23, no. 3, pp. 665–685, 1993.

[112] S. S. Ahmed, N. Dey, A. Ashour, D. Sifaki-Pistolla, D. Bălas-Timar, V. Balas, and J. Tavares "Effect of fuzzy partitioning in Crohn's disease classification: a neuro-fuzzy-based approach", Medical and Biological Engineering and Computing, pp.1-15, 2016.

[113] N. Andrei, "Scaled conjugate gradient algorithms for unconstrained optimization", Computational Optimization and Applications, vol. 38, no. 3, pp. 401-416, 2007.

[114] C. K. Seong, J. S. Lee, K. H. Kim, J. S. Sim and K.H. Chang, "Hypoechoic normal renal sinus and renal pelvis tumors sonographic differentiation", Journal Of Ultrasound In Medicine, vol. 21, no. 9, pp. 993-999, 2002.

[115] J. Radermacher, "Ultrasonography of the kidney and the renal vessels: part I: normal findings, inherited and renoparenchymatous diseases", Internist Berlin, vol. 44, no.10, pp. 1283-1297, 2003.

[116] A. T. Rosenfield, KJ. Taylor, AG. Dembner and P. Jacobson, "Ultrasound of renal sinus: new observations", American Journal of Roentgenology, vol. 133, no. 3, pp. 441-448, 1979.

[117] J. F. Platt, J. H. Ellis, J. M. Rubin, M. A. DiPietro, and A. B. Sedman, "Intrarenal arterial Doppler sonography in patients with nonobstructive renal disease: correlation of resistive index with biopsy findings", American Journal Of Roentgenology, vol. 154, no. 6, pp.1223-1227, 1990.

# Appendix A

## List of Publication

[1] K. Sharma and J. Virmani "Classification of Renal Diseases using First Order and Higher Order Statistics", In Proceedings of 10th Indiacom IEEE International Conference on Computing for Sustainable Global Development, March 2016, BVICAM, New Delhi. [Status: Accepted]

[2] K. Sharma and J. Virmani, "A Decision Support System for Classification of Normal and Medical Renal Disease using Ultrasound Images: A DSS for Medical Renal Diseases", International Journal of Ambient Computing and Intelligence, 2016. [Status: Accepted]

[3] K. Sharma and J. Virmani, "Haralick's Texture Descriptors for Classification of Renal Ultrasound Images", Hybrid Intelligent Techniques for Pattern Analysis and Understanding, Eds. S. Bhattacharya et. al. [to be published by CRC Press]. [Status: Accepted]

# Appendix B

## Originality Report

ORIGINALITY REPORT

| 18% | 3% | 15% | 7% |
|---|---|---|---|
| SIMILARITY INDEX | INTERNET SOURCES | PUBLICATIONS | STUDENT PAPERS |

PRIMARY SOURCES

| | | |
|---|---|---|
| 1 | Studies in Computational Intelligence, 2016.<br>Publication | 6% |
| 2 | Submitted to Indian Institute of Technology Roorkee<br>Student Paper | 5% |
| 3 | Kriti, N.A., and Jitendra Virmani. "Breast density classification using Laws' mask texture features", International Journal of Biomedical Engineering and Technology, 2015.<br>Publication | 1% |
| 4 | Subramanya, M. B., Vinod Kumar, Shaktidev Mukherjee, and Manju Saini. "SVM-Based CAC System for B-Mode Kidney Ultrasound Images", Journal of Digital Imaging, 2015.<br>Publication | 1% |
| 5 | Virmani, Jitendra, Vinod Kumar, Naveen Kalra, and Niranjan Khandelwal. "SVM-based characterisation of liver cirrhosis by singular value decomposition of GLCM matrix", International Journal of Artificial Intelligence and Soft Computing, 2013.<br>Publication | 1% |